The Philosophical Magazine

FIRST PUBLISHED IN 1798

A Journal of Theoretical Experimental and Applied Physics

Vol. 5 July 1960 No. 55
Eighth Series

25s. 0d., plus postage
Annual Subscription £13 10s. 0d., payable in advance

Printed and Published by
TAYLOR & FRANCIS LTD
RED LION COURT, FLEET STREET, LONDON, E.C.4

THE PHILOSOPHICAL MAGAZINE

Authors wishing to submit papers for publication in the Journal should send manuscripts directly to the Publishers.

Manuscripts should be typed in *double* spacing on one side of quarto (8×10 in.) paper, and authors are urged to aim at absolute clarity of meaning and an attractive presentation of their texts.

References should be listed at the end in alphabetical order of authors and should be cited in the text in terms of author's name and date. Diagrams should normally be in Indian ink on white card, with lettering in soft pencil, the captions being typed on a separate sheet.

A leaflet giving detailed instructions to authors on the preparation of papers is available on request from the Publishers.

Authors are entitled to receive 25 offprints of a paper in the Journal free of charge, and additional offprints can be obtained from the Publishers.

The *Philosophical Magazine* and its companion journal, *Advances in Physics*, will accept papers for publication in experimental and theoretical physics. The *Philosophical Magazine* publishes contributions describing new results, letters to the editor and book reviews. *Advances in Physics* publishes articles surveying the present state of knowledge in any branch of the science in which recent progress has been made. The editors welcome contributions from overseas as well as from the United Kingdom, and papers may be published in English, French and German.

Creep in Face-centred Metals and Solid Solutions with special reference to α-brasses†

By P. Feltham and G. J. Copley
The University, Leeds

[Received June 24, 1959; and in revised form August 29, 1959]

Abstract

The creep of α-brasses containing 10–35% Zn was studied in the range 350–650°c. The equilibrium creep rate satisfied the relation $\dot{\epsilon}=A_0(T)\exp(-H/kT)\sinh(q\sigma/kT)$, but two sets of the parameters A_0, H and of the activation volume q associated with the tensile stress σ were required, one above and one below a critical stress $\sigma_c'(T)$ above which Cottrell–Lomer locking appeared to become a less effective impediment to slip than at lower stresses. A peak in the activation energy H' (below σ_c') close to the composition represented by Cu_3Zn is interpreted in terms of local order near dislocation cores. This affects the migration of jogs and hence recovery by climb. Below σ_c', H is equal to 1·6 times the activation energy for grain boundary self-diffusion. Two models are proposed in which the climb of dislocations over intragranular obstacles or within grain boundaries are rate determining, depending on whether $\sigma<\sigma_c'$ or $\sigma>\sigma_c'$. The temperature dependence of A_0', A_0, q' and q is explained on the basis of the assumption that the dimensions of the intragranular substructure developing during creep attain lower limiting values which, at any given temperature, depend only on σ_c'.

§ 1. Introduction

In their recent paper on the creep of face-centred cubic metals Feltham and Meakin (1959) showed that the steady, equilibrium, creep rate of oxygen-free high-conductivity copper (99·99%) of constant grain size could be represented by the relation

$$\dot{\epsilon}=A_0(T)\exp(-H/kT)\sinh(q\sigma/kT), \quad . \ . \ . \ . \quad (1)$$

but that at any given temperature within the range 400–700°c used by them two sets of the parameters A_0, H, as well as of the activation volume q associated with the applied tensile stress σ had to be used, one below and one above a critical value of the applied stress $\sigma_c'(T)$ above which Cottrell–Lomer locking appeared to become a less effective impediment to slip than at lower stresses. While they could account quite well for the observed orders of magnitude of these parameters in terms of a model involving recovery facilitated by the climb of edge dislocations, they felt unable to advance an explanation of the pronounced temperature dependence of A_0 with the limited experimental data, relating in particular to the effect of intragranular substructures on the creep rate, then at their disposal.

† Communicated by the Authors.

The main object of the present work was to extend their research to alpha-brasses, utilizing the zinc content as a new variable which, through its effect on the creep rate, was expected to make a further development of the theory possible.

§ 2. Materials and Method

The equipment and the experimental methods were as described for copper (Feltham and Meakin 1959). Creep took place under constant stress in a vacuum better than $1\,\mu$ Hg. Rod-shaped specimens with a 10 cm gauge length and of 0·17 cm diameter were used. These were annealed *in situ* prior to creep, as in the case of copper, until a mean grain diameter $D = 3 \times 10^{-3}$ cm was obtained. During annealing and creep each specimen was enveloped in thin foil rolled from the same type of brass from which the specimen had been drawn, and this was found to reduce zinc losses to a level at which no significant change was detectable after creep either gravimetrically or by microscopy.

The brasses used came from the same stock as those employed by Feltham and Copley (1958) in their study of grain-growth, and contained nominally 10, 20 30 and 35% of zinc by weight†.

Table 1

Brass	Cu%	Zn%	Fe%	Ni%	Sn%	Pb%	Bi%
90/10	89·68	10·29	0·030	0·000	—	0·000	0·0006
80/20	80·88	19·11	0·006	0·000	—	0·000	0·0006
70/30	71·13	28·85	0·004	0·000	0·003	0·009	0·0004
65/35	65·04	34·93	0·008	0·000	0·002	0·021	0·0003

Table 2

Brass	Annealing time (min)	Annealing temperature (°c)
90/10	20	650
80/20	20	600
70/30	20	550
65/35	15	550

Analyses of the brasses, and the annealing times and temperatures which were used to obtain the standard grain size are shown in tables 1 and 2. X-ray back-reflection photographs and electrolytic etching techniques (Jacquet 1954) showed the annealed brasses to be polygonized.

† As the atomic weight copper differs from that of zinc by less than 3% weight percentages are virtually equal to the corresponding atomic percentages.

The sub-grains appeared to be of the type observed by Young (1958) in copper, and by Hibbard and Dunn (1957) in silicon iron. The mutual inclination between sub-grains was of the order of $\frac{1}{2}°$ (fig. 1, Pl. 77).

§ 3. Experimental Results

The creep of the brasses was similar in essence to that found in copper†, as may be seen from the recurrence of the following features, previously observed and discussed by Feltham and Meakin (1959):

(*a*) The instantaneous strain ϵ_0, measured within the first 1–2 sec after the application of the load to the specimen, obeyed the 'parabolic' work-hardening law

$$\sigma^2 = \chi_p(\epsilon_0 - \epsilon_c), \quad \ldots\ldots\ldots \quad (2)$$

where $\chi_p(T)$ is the coefficient of work-hardening, and ϵ_c a small strain‡ (fig. 2).

Fig. 2

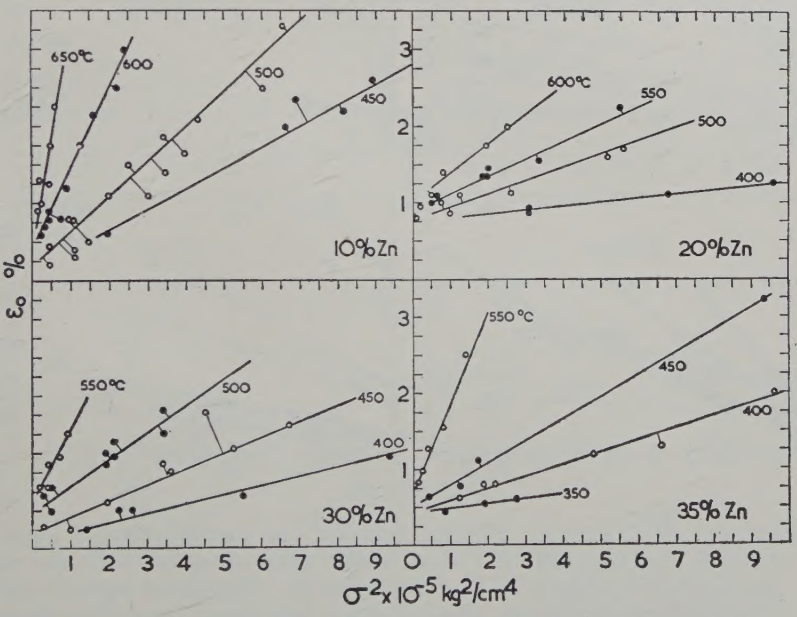

The initial strain as function of the applied stress (eqn. (2)).

(*b*) The transient stage, which follows the initial extension, consisted of two parts, the first obeying the Andrade equation

$$\epsilon_{tr} = \beta(\sigma, T)t^{1/3}, \quad \ldots\ldots\ldots \quad (3)$$

† All data on copper referred to in the text or diagrams are taken from the paper by Feltham and Meakin (1959). A full documentation of the experimental work discussed in the present paper has been given by Copley (1959).

‡ That the lines do not pass through the origin is probably due to the fact that the hardening is linear at low strains.

the second, subsequent, part showing a 'flattening out' with a creep rate much smaller than predicted by eqn. (3). No definite evidence of the existence of the $t^{1/3}$ stage was however obtained with the brasses containing 20, 30 and 35% of zinc, in which the whole transient stage was rather 'flat', as may be seen from the characteristic creep curves shown in fig. 3. Similarities between the transient creep of copper and the 90/10 brass are apparent from the validity of the relation

$$(\epsilon_{tr})_{max} - \epsilon_0 = \lambda(T), \quad \sigma > \sigma_c' \quad . \quad . \quad . \quad . \quad . \quad . \quad . \quad (4)$$

indicated by the horizontal parts of the curves in fig. 4. Here $\lambda(T)$ is constant at any given temperature; $(\epsilon_{tr})_{max}$ is the strain at the onset of

Fig. 3

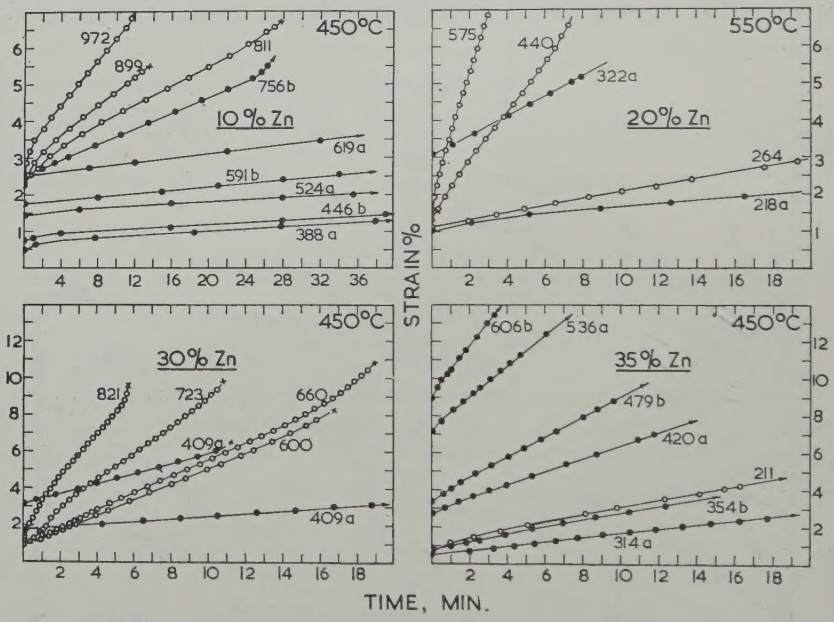

Characteristic creep curves. Figures indicate the applied tensile stress in kg/cm². Curves with the same suffix were obtained with the same specimen by changing the load during creep. The initial part of curves *a* for 35% Zn is not shown. An incubation period was sometimes observed, e.g. an almost horizontal part of curve 600 for 30% Zn. For curve 211 (35% Zn) multiply time-scale by 10.

the steady stage of creep, and ϵ_0 the initial instantaneous strain referred to in equation (2). While the stress dependence of the strain $(\epsilon_{tr})_{max}$ is similar in all the brasses (fig. 5), the relation given by eqn. (4) does not seem to be applicable to all of them.

(*c*) The equilibrium, steady, tensile strain rate could be expressed by the relation.

$$\dot{\epsilon} = \tfrac{1}{2}A_0(T)\exp\left[-(H - q\sigma)/kT\right], \quad . \quad . \quad . \quad . \quad . \quad . \quad (5)$$

Fig. 4

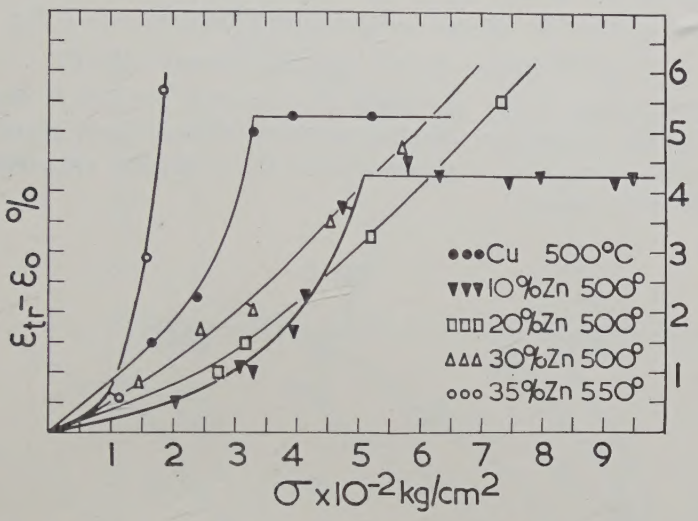

The difference between the maximum of the transient strain and the initial strain as function of the applied stress (eqn. (4)).

Fig. 5

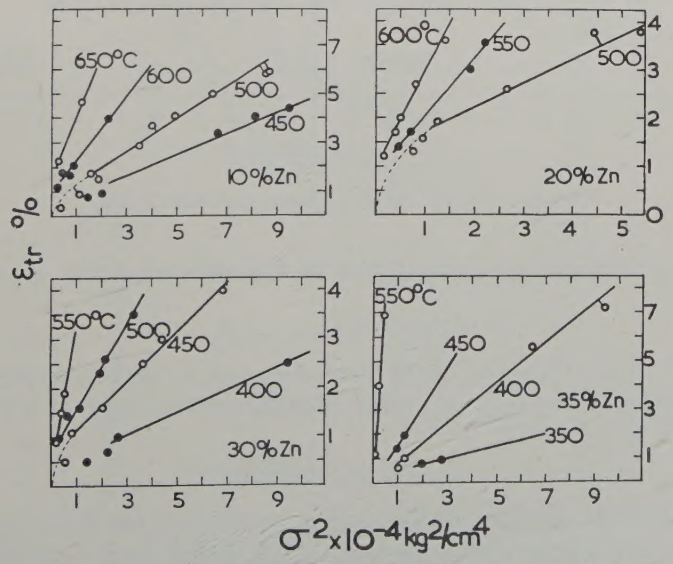

The stress dependence of the total transient strain

and again two sets of the parameters were required, i.e. A_0', H' and q' below a critical tensile stress σ_c', corresponding to the breaks in the isotherms in fig. 6, and A_0, H and q above σ_c'. The values of H' and H, q' and q, and the virtual temperature independence of the products

$$A_0'(T)\exp(-H'/kT) \text{ and } A_0(T)\exp(-H/kT) \quad . \quad . \quad . \quad (6)$$

are shown in figs. 7–10; the heats of activation H' and H were determined by the temperature-cycling method (Feltham and Meakin 1959). (In the log $\dot{\epsilon}$ versus log σ representation the isotherms are cusp shaped, with the nodes at σ_c'.)

Fig. 6

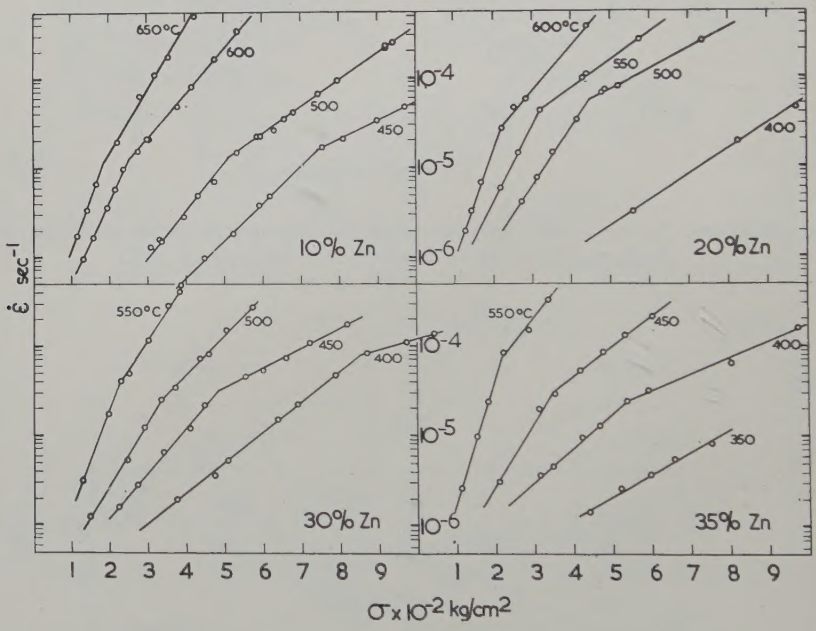

Stress versus steady strain rate isotherms.

(*d*) The temperature dependence of the critical stress σ_c' was again given by

$$\log(\sigma_c'/G) \simeq c_1 - c_2 T, \quad . \quad . \quad . \quad . \quad . \quad . \quad . \quad . \quad (7)$$

(fig. 11), where G is the shear modulus, and c_1 and c_2 constants. An equally satisfactory representation over the entire range of temperatures used was found to be

$$\sigma_c' = (\sigma_c')_0 \exp(Q/kT), \quad . \quad . \quad . \quad . \quad . \quad . \quad . \quad . \quad (8)$$

the 'activation energy' Q depending somewhat on the zinc content. Equation (8) will be used at a later stage, being more convenient than eqn. (7) (see eqn. (11) and fig. 14).

Fig. 7

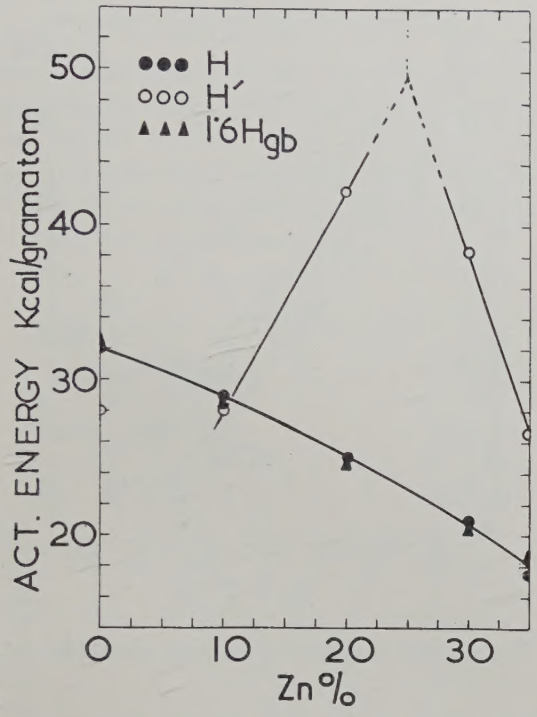

The activation energies H' and H below and above σ_c' respectively.

Fig. 8

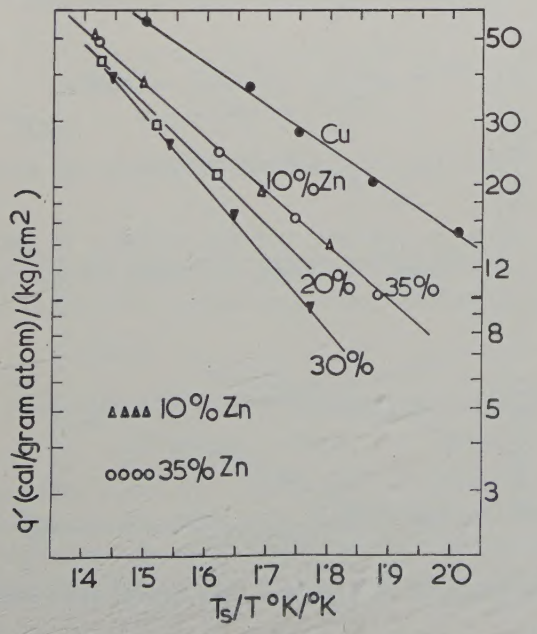

The activation volume q' obtained from fig. 6. The solidus temperatures are, with ascending zinc contents, 1356, 1305, 1253, 1191 and 1175°K.

Fig. 9

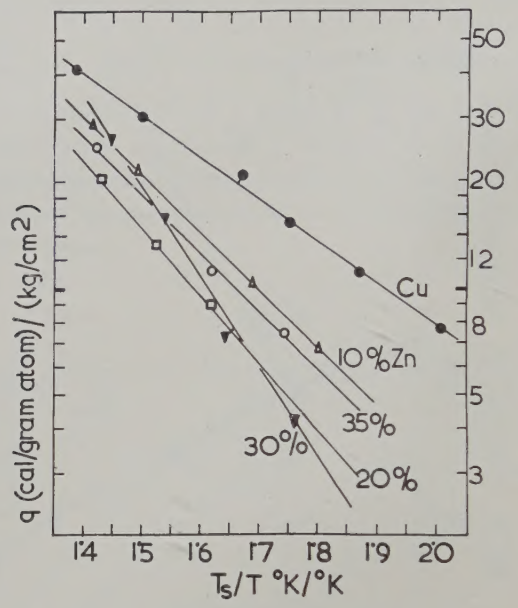

The activation volume q at stress exceeding σ_c'.

Fig. 10

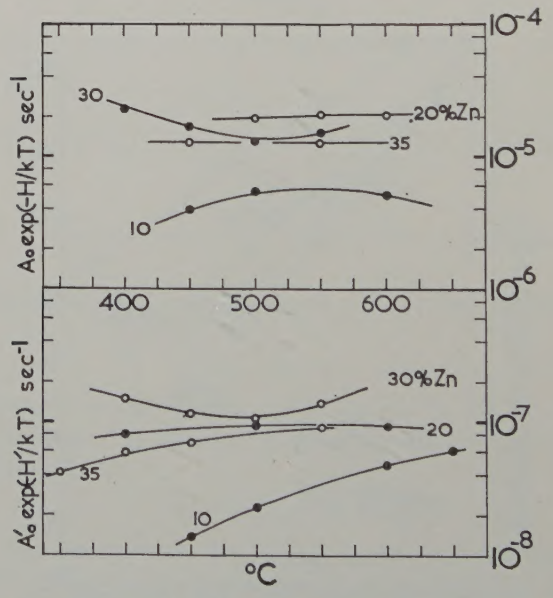

The products A_0' exp $(-H'/kT)$ and A_0 exp $(-H/kT)$.

(*e*) The time to fracture, t_f, can be expressed in terms of the equilibrium creep rate:

$$t_f=(K/\dot{\epsilon})^m, \quad . \quad . \quad . \quad . \quad . \quad . \quad . \quad . \quad . \quad (9)$$

where K and m are constants, and $m \simeq 1{\cdot}0$ (fig. 12).

(*f*) The formation of slip-bands was observed to take place in creep at stresses above σ_c' (fig. 13, Pl. 78); below σ_c' slip was not resolvable by optical microscopy. Intragranular cavitation, sometimes in the form of discrete adjacent voids of the string-of-beads type previously reported by Greenwood *et al.* (1954), was also observed.

Fig. 11

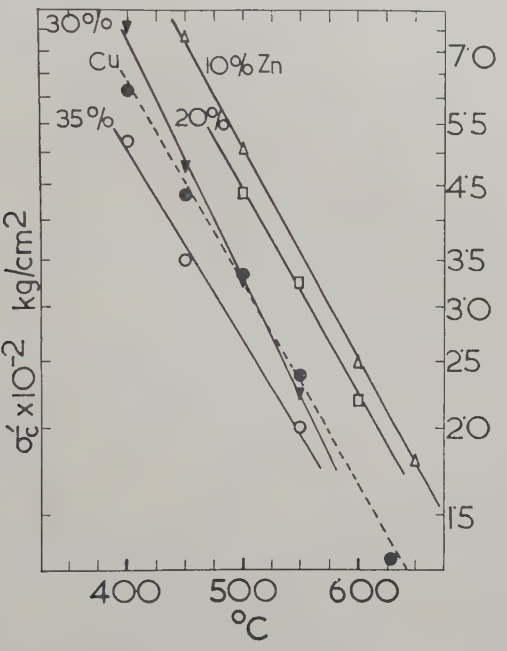

Temperature dependence of the critical tensile stress σ_c'.

(*g*) The existence of a linear relation between χ_p (eqn. (2)) and σ_c' was again confirmed, as may be inferred from the constancy of the products $\sigma_c'q'$ and $\chi_p q$ (figs. 14 and 15), and the experimentally established relation (figs. 8 and 9):

$$q' \simeq 2q. \quad . \quad . \quad . \quad . \quad . \quad . \quad . \quad . \quad . \quad (10)$$

The temperature dependence of q', and hence of q, was of the form

$$q'=q_0' \exp(-Q/kT) \quad . \quad . \quad . \quad . \quad . \quad . \quad . \quad (11)$$

as is apparent from figs. 8 and 9. Values of Q are given in table 3.

(*h*) The equilibrium strain rate was independent of the grain size below σ_c', above this stress it was a linear function of the square of the mean grain diameter (fig. 16).

(*i*) The value of H' obtained at 450°c by the thermal cycling method with a single crystal, which had been grown in an evacuated silica tube from a rod of the 65/35 brass by Bridgman's method, was found to be 45 kcal/gram atom, i.e. close or equal to the activation energy of chemical self-diffusion, and appreciably higher than H' as observed in polycrystals of the same brass.

Table 3

Brass	Cu	90/10	80/20	70/30	65/35
H' kcal/g atom	28	28	42	38·5	26·5
Q kcal/g atom	7·1	9·8	10·9	13·8	12·5
H'/Q	3·9	2·9	3·8	2·8	2·1

Fig. 12

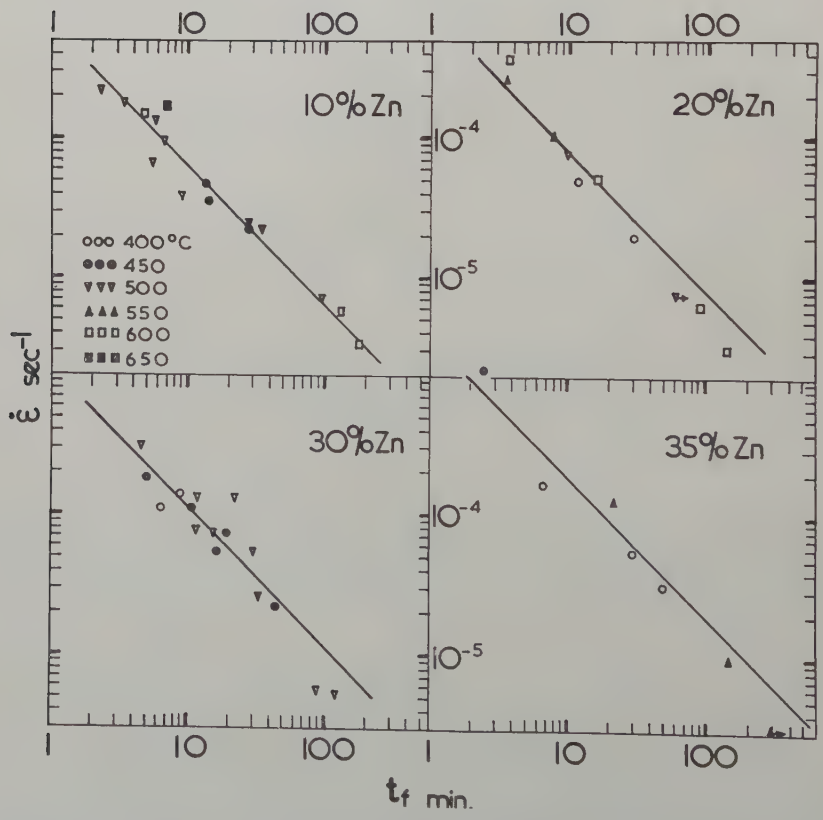

The time to fracture as function of the equilibrium creep rate. The lines correspond to $m=1$ in eqn. (9).

Of the observations which cannot be correlated with similar ones made on copper two are of particular interest. First, with the exception of the 90/10 brass, the difference between H' and H was much greater than in copper (fig. 7). While H' (below σ_c') was found to be independent of temperature it changed significantly with the zinc content, particularly at concentrations approaching the composition Cu_3Zn. Second, H (at stresses exceeding σ_c') did not show a similar maximum, but decreased uniformly with increasing zinc contents. As may be seen from fig. 7,

$$H \simeq 1{\cdot}6\, H_{gb}, \quad . \quad . \quad . \quad . \quad . \quad . \quad . \quad . \quad . \quad (12)$$

where H_{gb} is the heat of activation of grain boundary self-diffusion as determined by Feltham and Copley (1958) from grain-growth data.

Fig. 14

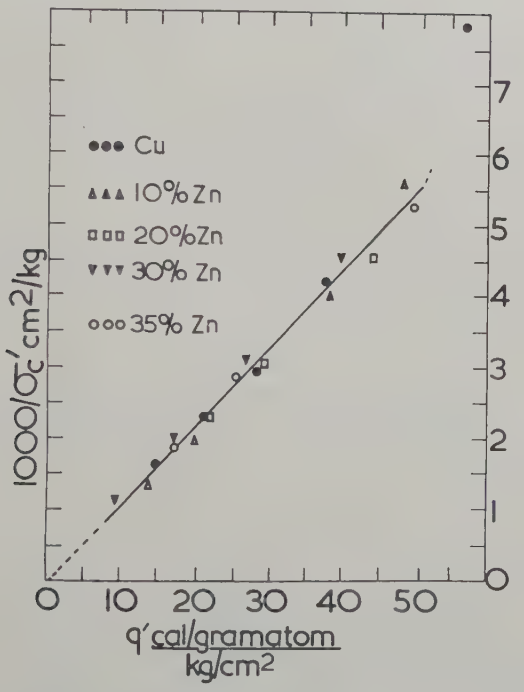

The relation between the critical stress σ_c' and q'.

A correlation of $(\epsilon_{tr})_{max}$ with σ^2, not previously attempted for copper, shows a parabolic law of the same form as eqn. (2) to be again applicable (fig. 5). The coefficients of work-hardening are generally lower (dotted lines in fig. 17) than the corresponding ones (full lines) derived from the initial extension (fig. 2).

The qualitative similarities between the characteristics of the creep of alpha-brasses and copper, indicated by the above points, suggest that the mechanisms of creep are essentially the same in polycrystals of the

Fig. 15

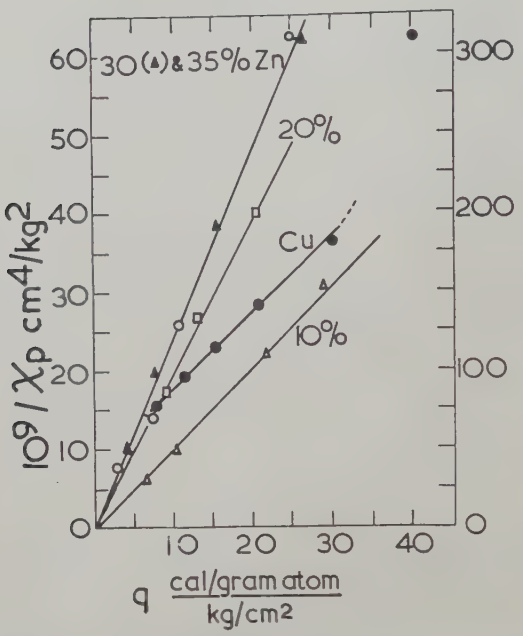

The coefficient of parabolic work-hardening (eqn. (2)) as function of the activation volume q. The right hand scale is for copper and the 90/10 brass only.

Fig. 16

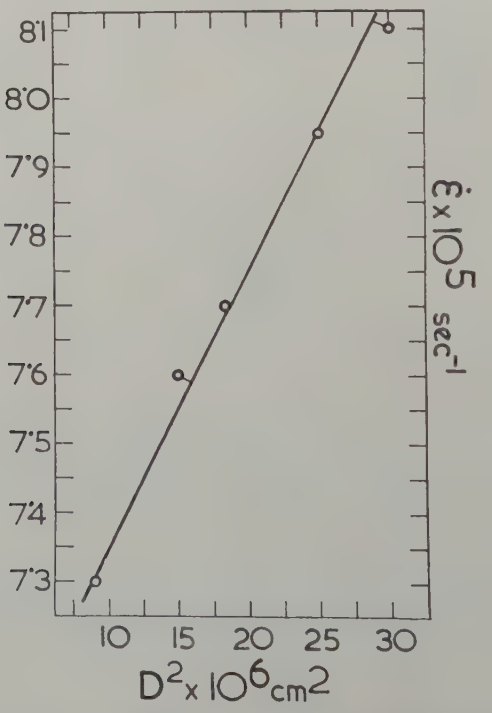

The effect of grain size on the creep rate at 500°c in 70/30 brass. The various grain sizes were obtained by annealing at 600°c for periods up to 45 min.

brasses and copper; a similar inference appears to be justified for single crystals also (point (*i*)). We shall therefore attempt to correlate the observations in terms of a model similar to that employed by Feltham and Meakin (1959) in describing the creep of copper, first however developing the model in the light of the results obtained in the present work, particularly those arising from the use of the alloy composition as a variable.

Fig. 17

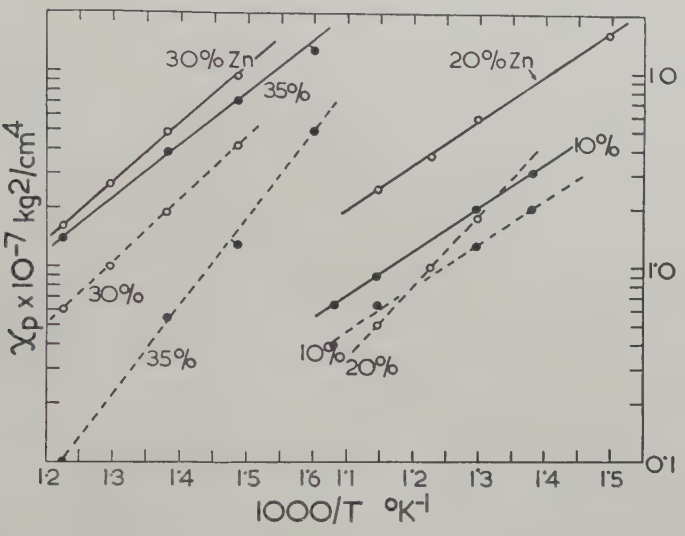

The coefficients of parabolic work-hardening obtained from fig. 2 (full line) and fig. 5 (broken line) for the initial extension and the total transient strain respectively.

§ 4. Discussion

4.1. *Dislocation Climb and Ordering*

Basing ourselves on the reasoning of Feltham and Meakin (1959) we therefore assume that the rate determining mechanism, i.e. the slowest recovery mechanism, is the climb of edge dislocations over obstacles, both above as well as below σ_c', and that the dislocations are lost mainly at sinks within the grains below σ_c', while the grain size dependence of $\dot{\epsilon}$, as well as micrography suggest that above σ_c' intergranular recovery is rate determining, the grain boundary being less permeable to the propagation of slip than the intragranular obstacles.

Of the features due to alloying the composition dependence of H' is indicative of a tendency to superlattice formation which, in view of the high temperatures, cannot be general throughout the lattice (Masumoto *et al.* 1952), but is probably located in the immediate vicinity of the dislocation cores. If the rate determining mode of recovery occurs at grain boundaries then superlattice formation would be expected to be of

little consequence in view of the non-crystallographic structure of the grain interfaces, and effects due to ordering should not affect the activation energy of creep significantly. The observation that H (above σ_c') is in fact a monotone function of the zinc content thus further supports the view that the rate controlling recovery process at stresses exceeding σ_c' occurs at grain boundaries.

We shall assume that in polycrystalline brasses, as in copper, climb takes place through the migration of jogs in edge dislocations in which the jogs are due to intersection of the climbing dislocation with 'forest' dislocations, and that the applied stress assists the migration of the jog by reducing the activation energy from H' (or H) to $H' - q'\sigma$ (or $H - q\sigma$) by a mechanism of the type described by Feltham and Meakin (1959). In their work H' was identified with the activation energy for the non-conservative migration of a jog in the presence of a vacancy adjacent to it; $H(\sigma > \sigma_c')$, given by them as 32 kcal/gram atom, is close to the activation energy for grain boundary slip (33 kcal/gram atom) as found in copper by Rotherham and Pearson (1956).

The assumption that climb occurs by the migration of jogs in the presence of vacancies does not imply that the process is equally simple in copper and in the brasses; the appreciable variation of H' with zinc concentration suggests a greater complexity in the brasses than in copper, involving, in particular, disordering of the superlattice in a small volume surrounding the jog. We shall therefore write for the free energy of activation of the process:

$$E' = H_j' + zH_0'\left(1 - \frac{T}{T_s}\right) = H' - zH_0'\frac{T}{T_s} \quad . \quad . \quad . \quad . \quad (13)$$

where H_j' is about 27 kcal/gram atom, i.e. corresponding to the line which may be drawn through the values of H' for copper, and the 90/10 and 65/35 brasses for which ordering makes no or only a negligible contribution (fig. 7), T_s the solidus temperature, and z an ordering parameter with values between 0 (Cu) and 1 (for approximately 25% Zn). The second term in the bracket in eqn. (13) represents the entropy of the disordering process.

4.2. *Creep Below* σ_c'

Now if, in general, a jog has to migrate a distance l_j', i.e. l_j'/b times before the dislocation containing it (among others) has climbed by one lattice spacing b, and if this dislocation has to climb $\frac{1}{2}l_s'/b$ times before escaping over an obstacle having a stress field of wavelength l_s', then the time of escape will be given by

$$t' \simeq (1/\nu)(\tfrac{1}{2}l_j'l_s'/b^2)\exp[(E' - q'\sigma)/kT], \quad . \quad . \quad . \quad . \quad (14)$$

where ν is of order of $10^{12}\,\mathrm{sec}^{-1}$, and (Feltham and Meakin 1959):

$$q' = l_j'b^2/4 = fl_s'b^2/4 \quad . \quad . \quad . \quad . \quad . \quad . \quad . \quad (15)$$

where f is a real fraction which, in correlating the experimental results we shall later take to be equal to 1/70.

We have written σ instead of $\sigma-\sigma_y$ in eqn. (14), because the tensile yield stress σ_y (which may be defined as the stress to give a tensile creep rate of, say $10^{-8}\,\mathrm{sec}^{-1}$) is negligible in comparison with the values of σ which have here been used, as may be seen from a rough extrapolation of the isotherms (fig. 6) to such low strain rates.

If the mean spacing of the intragranular slip zones is l_h', then the creep rate in shear is $(b/l_h')/t'$, assuming that the dislocations climb over barriers singly. On taking the tensile strain rate to be half the shear rate one obtains on substituting for t from eqn. (14):

$$\dot{\epsilon}=\tfrac{1}{2}A_0'\exp\left[-(H'-q'\sigma)/kT\right] \quad . \quad . \quad . \quad . \quad . \quad (16)$$

with

$$A_0'=2(vb^3/v')\exp\left(zH_0'/kT_s\right), \quad . \quad . \quad . \quad . \quad . \quad . \quad (17)$$

where we have written

$$v'=l_h'l_j'l_s'. \quad . \quad . \quad . \quad . \quad . \quad . \quad . \quad . \quad . \quad (18)$$

We shall revert to the discussion of eqn. (17) after having considered the equilibrium creep rate above σ_c'.

4.3. *The Equilibrium Creep Rate above* σ_c'

In view of the grain size effects discussed above we shall assume, following Feltham and Meakin (1959), that at stresses above σ_c' the active slip zones generally extend across the entire grain, the grain boundary now being the strongest obstacle to the propagation of slip. Transgranular slip bands as are observed above σ_c' in copper and in the brasses (fig. 13) will then be regarded as having resulted from the propagation of slip initiated by the failure of intragranular obstacles† to contain dislocations within the small glide zones active below σ_c'.

Now, if we imagine slip to spread from one such small zone across the grain it will induce the spreading of slip from similar zones situated within a volume of the grain equal to about $\bar{D}^2l_h$ where, as before, l_h is the mean distance between small slip zones, and is thus of the same order of magnitude as l_h'. We shall take the area $\bar{D}^2$ equal to aD^2-L^2, with $a\simeq\frac{1}{2}$, D the mean grain diameter, and L the length of the initial slip zone. We would therefore observe the formation of a slip band comprising on the average $N(\bar{D}^2l_h)$ active slip planes, N being the density of active slip zones per unit volume prior to the onset of band formation, i.e. below σ_c'. If, now, the average slip distance at stresses below σ_c' is L then we may write.

$$N=C/L^2l_h \quad . \quad . \quad . \quad . \quad . \quad . \quad . \quad . \quad (19)$$

† The role of sessile dislocations of the Cottrell–Lomer type in providing or stabilizing obstacles in face-centred metals has been discussed by Feltham and Meakin (1959). In body-centred metal sessile dislocations may form through the reaction $\frac{1}{2}a[\bar{1}\bar{1}1]+\frac{1}{2}a[11\bar{1}]=a[001]$, proposed by Cottrell (1958).

where C is a numerical constant of order unity The shear strain induced in the grain by the loss of one dislocation per active slip plane, assuming adjacent bands to be $2l_h$ apart, is then given by $N(\bar{D}^2 l_h)(b/l_h)$; the corresponding tensile strain may therefore be written, on substituting for N from eqn (19):

$$\epsilon = Cb\bar{D}^2/l_h L^2. \quad . \quad . \quad . \quad . \quad . \quad . \quad . \quad . \quad (20)$$

The formation of bands on one slip system only has been considered in deriving eqn. (20), it being assumed that the effect of the more complex geometry of deformation of actual grains would also find expression through C.

We shall assume the climb in the grain boundary to be akin to that within the grain, so that the life-time, t, of a dislocation will again be given by an equation of the same form as (14), omitting dashes from the parameters, and where now also

$$E = H + (34C_{\mathrm{Zn}})T. \quad . \quad . \quad . \quad . \quad . \quad . \quad . \quad . \quad (21)$$

The reason for using eqn. (21) is as follows:

As is apparent from fig. 7, the measured value of H is equal to 1·6 times the heat of activation of grain boundary self-diffusion in the brasses. The free energy of grain boundary self-diffusion in the brasses contains however a composition dependent entropy term (Feltham and Copley 1958):

$$E_{\mathrm{gb}} = H_{\mathrm{gb}} + (21{\cdot}2C_{\mathrm{Zn}})T \text{ kcal/gram atom}, \quad . \quad . \quad . \quad . \quad (22)$$

which leads to the corresponding entropy term in eqn. (21) on multiplying by 1·6, the observed ratio H/H_{gb}. The strain rate ϵ/t is therefore (using eqns. (14), (20) and (21)):

$$\dot{\epsilon} = \tfrac{1}{2}A_0 \exp\left[-(H - q\sigma)/kT\right], \quad . \quad . \quad . \quad . \quad . \quad (23)$$

where now

$$A_0 = 2(Cb^3\nu\bar{D}^2/L^2 v)\exp(-17C_{\mathrm{Zn}}), \quad . \quad . \quad . \quad . \quad . \quad (24)$$

with C_{Zn} expressed as a proper fraction, and

$$v = l_h l_j l_s. \quad . \quad . \quad . \quad . \quad . \quad . \quad . \quad . \quad . \quad (25)$$

From eqns. (17) and (24) one obtains

$$A_0/A_0' = C(\bar{D}/L)^2(v'/v)\exp\left[-17C_{\mathrm{Zn}} - (zH_0'/kT_s)\right]. \quad . \quad . \quad (26)$$

It is clear from eqns. (17) and (24) that the pronounced temperature dependence of A_0' and, by implication, that of A_0 (eqn. (26)), must be ascribed to v' and v respectively. This we shall now consider.

4.4. *The Temperature Dependence of* A_0', A_0, q' *and* q

In discussing the temperature dependence of these parameters we shall make the basic assumption that in the transient stage of creep the

intragranular substructure developing by glide and polygonization finally attains a lower limiting size beyond which no further fragmentation takes place. A sub-structure with a characteristic dimension l_s' then persists throughout the steady stage of creep, l_s' being a measure of the wavelength of the intragranular stress fields. We shall also assume that the mean spacing between adjacent jogs on dislocations l_j' is given by

$$l_j' = f l_s' \text{ and } l_j = f l_s, \quad . \quad . \quad . \quad . \quad . \quad . \quad (27)$$

as in eqn. (15), and that we may write

$$l_s' = \alpha G b / \tau_c', \quad . \quad . \quad . \quad . \quad . \quad . \quad . \quad . \quad (28)$$

where the shear stress

$$\tau_c' \propto \sigma_c', \quad . \quad . \quad . \quad . \quad . \quad . \quad . \quad . \quad . \quad (29)$$

and α a dimensionless constant of order 0·1, the exact value of which is determined by the specific arrangement of the dislocations characteristic of the steady stage. As, according to Feltham and Meakin (1959), σ_c' appears to be determined by the magnitude of the stacking-fault energy†, so is then the characteristic length l_s'.

If now we take the spacing between slip zones ($\sigma < \sigma_c'$) to be of the same magnitude as the wavelength of the intragranular stress field, i.e.

$$l_h' = l_s', \quad (\text{and } l_h = l_s), \quad . \quad . \quad . \quad . \quad . \quad . \quad . \quad (30)$$

then eqn. (17) yields, on using eqns. (18), (27) and (28),

$$A_0' = (2f^2 \nu b^3 / l_s'^3) \exp(z H_0' / k T_s), \quad . \quad . \quad . \quad . \quad . \quad (31)$$

or

$$A_0' = (2\nu f^2 / \alpha^3 G^3) \tau_c'^3 \exp(z H_0' / k T_s). \quad . \quad . \quad . \quad . \quad . \quad (32)$$

On taking $\nu = 10^{12}\,\text{sec}^{-1}$, $G = 4 \times 10^5\,\text{kg/cm}^2$, $\alpha^3/f^2 = 2{\cdot}2$, one obtains for copper ($z = 0$):

$$A_0' = (\tau_c'/70)^3\,\text{sec}^{-1},$$

and on taking

$$\sigma_c' = 3\tau_c', \quad . \quad . \quad . \quad . \quad . \quad . \quad . \quad . \quad . \quad (33)$$

$$A_0' = (\sigma_c'/210)^3\,\text{sec}^{-1}, \quad . \quad . \quad . \quad . \quad . \quad . \quad . \quad (34)$$

σ_c' and τ_c' being expressed throughout in kg/cm^2. The values of A_0' obtained from eqn. (34) compare well with those obtained by Feltham and Meakin (1959) experimentally (table 4).

On substituting for l_s' from eqn. (15) into eqn. (31) one obtains for copper:

$$A_0' = \nu f^2 b^2 / 32 q'^3 \quad . \quad . \quad . \quad . \quad . \quad . \quad . \quad . \quad (35)$$

which, with $f = 1/70$, yields

$$A_0' \simeq 10^5 / q'^3\,\text{sec}^{-1}, \quad . \quad . \quad . \quad . \quad . \quad . \quad . \quad (36)$$

q' being given in (cal/gram atom)/(kg/cm^2). Values of A_0' obtained by means of eqn. (36) are also shown in table 4. With the above value of f, α in eqn. (32) assumes the value 0·077.

† Feltham and Meakin found that the stress $\sigma_c'(T)$ at which linear hardening terminates in copper in the range 77–293° K did not extrapolate well to the values of $\sigma_c'(T)$ obtained in creep between 400 and 700° C. This was confirmed with brasses, using σ_c values obtained by Feltham and Copley (1960); extrapolation was not possible.

As to A_0, we observe that on taking the slip distance to be $L=5\mu$ in eqn. (26), the ratio $(\bar{D}/L)^2$ is equal to about 18, so that for copper, for which $q'/q=2$ and hence $v'/v=8$,

$$A_0/A_0'=130C,$$

which, remembering that C was assumed to be of order 1, is in fair agreement with the values of this ratio in table 4.

Table 4

Brass		Temperature (°C)					
		400	450	500	550	600	650
Cu	A_0' eqn. (34)	25	8·9	2·9	1·3	0·8‡	—
	A_0' eqn. (36)	36	13·5	4·5	2·0	0·6‡	—
	A_0' (expt.)†	26 (*a*)	8·9	3·3	1·2	0·6‡	—
	A_0	$1·6\times10^4$	2900	660	140	33‡	—
	A_0/A_0'	390	325	200	116	55	—
90/10	A_0'	—	16	3·8	—	0·3	0·056
	A_0	—	2000	730	—	82	—
	A_0/A_0'	—	125	191	—	366	—
80/20	A_0'	$3·0\times10^6$	—	$6·6\times10^4$	—	2600	—
	A_0	—	—	180	84	24	—
	A_0/A_0'	—	—	$2·7\times10^2$	—	$9·3\times10^{-3}$	—
70/30	A_0'	$2·7\times10^5$	$3·3\times10^4$	$4·5\times10^3$	$1·4\times10^3$	—	—
	A_0	140	34	12	5·6	—	—
	A_0/A_0'	52×10^{-3}	0·012	0·0027	0·004	—	—
65/35	A_0'	78 (*b*)	21	7·0	0·99	—	—
	A_0	—	97	—	0·72	—	—
	A_0/A_0'	—	0·46	—	0·73	—	—

† All remaining A_0' and A_0 are experimental values expressed in sec^{-1}.
‡ 630°C. (*a*) Previously erroneously given as 41. (*b*) 350°C.

4.5. *The Effect of Alloying on A_0' and A_0*

Assuming that the effect of alloying is expressed only through the exponential terms in eqns. (24) and (26), we find that in a 65/35 brass, in which z may be assumed to be 0, (eqn. (13)) A_0 should be approximately 365 times smaller than A_0 in copper, i.e. by $\exp(-17\times0·35)$, on using eqn. (24). This overestimates the ratio obtained at 550°C (194) by a factor of about 2, with a bigger error at lower temperatures, presumably because of the simplifying assumption made in deriving the theoretical ratio.

In order to investigate the effect of the local ordering we shall compare the ratio A_0/A_0' for copper with that of the 70/30 brass, taking zH_0 in eqn. (26) to be equal to 11·5 kcal/gram atom (i.e. 38·5 − 28; table 3, eqn. (13)). With $T_s = 1191°$K for 70/30 brass the ratio should be $1{\cdot}4 \times 10^4$ times greater in copper than in the brass. This compares very well with the average value of the experimentally determined ratio obtained from values given in table 4, namely $1{\cdot}8 \times 10^4$.

The treatment also accounts for the virtual temperature independence of the products $A_0'(T)\exp(-H'/kT)$ and $A_0(T)\exp(-H/kT)$, also observed in copper and other metals (Fastov 1950), for the temperature dependence of A_0' and A_0 is of the form $\exp(3Q/kT)$, (eqns. (10), (11), (26) and (35)), and this largely cancels the effect of the Boltzmann term containing the activation energies H' and H respectively. Further, the observation (Feltham 1957) that at temperatures corresponding to the same fraction of the melting point large values of q' are associated with metals having large stacking-fault energies can be explained if a significant part of the stress defining l_s' (eqn. 28) is due to chemical interaction of the stacking-fault region of extended dislocations with solute atoms or vacancies. For then the proportionality between σ_c' and $1/q'$ (eqns. (15), (28) and (29)), arising if α is assumed constant, shows that an increase of τ_c' with zinc content would result in a decrease in q'. The assumed constancy of α in eqn. (28) also implies invariance of the product $q'\sigma_c'$. This is born out by the data in fig. 14; it is however only approximate, as may be seen from the relation between the two parameters obtainable on equating strain rates in eqns. (5) and (16).

Allowing for the various simplifying assumptions made in developing the models of the creep mechanisms the agreement obtained with experiment may be considered satisfactory. The treatment also clearly shows, however, that further detailed studies of the modes of deformation and of the effect of intragranular substructures in creep are necessary before truly quantitative laws of the high-temperature deformation of metals can be advanced.

References

Copley, G. J., 1959, Ph.D. Thesis, The University, Leeds.

Cottrell, A. H., 1958, *Trans. met. Soc. Amer. Inst. mech. Engrs*, **212**, 192.

Fastov, N. S., 1950, *Zhur. Tekh. Eksp. Fiz.*, **20**, 543.

Feltham, P., 1957, *Phil. Mag.*, **2**, 584.

Feltham, P., and Copley, G. J., 1958, *Acta Met.*, **6**, 539; 1960, *Ibid.* (to be published).

Feltham, P., and Meakin, J. D., 1959, *Acta Met.*, **7**, 614.

Greenwood, J. N., Miller, D. R., and Suiter, J. W., 1954, *Acta Met.*, **2**, 250.

Hibbard, W. R., and Dunn, C. G., 1957, *Creep and Recovery* (Cleveland: Amer. Soc. Metals.)

Jacquet, P., 1954, *Acta. Met.*, **2**, 752.

Masumoto, H., Saito, H., and Sugihara, M., 1952, *Sci. Rep. res. Inst. Tohôku Univ.* A, **4**, 480.

Rotherham, L. R., and Pearson, G. S., 1956, *Trans. Amer. Inst. met. Engrs*, **206**, 881.

Young, F. W., 1958, *J. appl. Phys.*, **29**, 760.

On Dislocations Formed by the Collapse of Vacancy Discs†

By C. Elbaum
Physics Department, Metals Research Laboratory, Brown University, Providence, Rhode Island

[Received February 15, 1960]

Abstract

The formation of dislocations by the collapsing vacancy disc mechanism is examined for aluminium, copper, silicon and germanium. It is shown that this mechanism can be important in the case of metals. In the case of silicon and germanium dislocation loops produced by the above mechanism, during usual crystal growth from the melt, will not reach sizes detectable by means of the optical microscope.

§ 1. Introduction

The problem of the origin of dislocations in crystals in general, and in crystals grown from the melt, in particular, has been the object of considerable speculation in recent years. Among other possible mechanisms, it has been suggested that dislocations in crystals grown from the melt are likely to originate from the collapse of vacancy discs formed by the precipitation of these imperfections. This precipitation takes place under conditions of supersaturation during cooling of the crystal. (For a summary see Kuhlmann-Wilsdorf 1958.) In the following, some remarks are made concerning the likelihood of this mechanism operating in the case of metals and of silicon and germanium.

A dislocation loop may be expected to nucleate by the above mechanism when the free energy associated with this dislocation loop is equal to or smaller than the free energy associated with a vacancy disc. Collapse of the disc will occur when it reaches a size for which the above condition is satisfied. Subsequent growth of the dislocation loop thus formed can take place by climb, through the addition of vacancies from the surrounding volume. This process increases the size of the loop and thus the free energy associated with it. Growth will therefore occur only if there is a supersaturation of vacancies with respect to the dislocation loop. In order to make numerical estimates of the necessary supersaturation, the free energy associated with a dislocation loop must be examined. It should also be emphasized that the collapsing vacancy disc mechanism and subsequent growth of the dislocation loop are confined to temperatures at which the vacancy mobility is sufficient for appreciable growth of the loop to occur. Consideration must, therefore, be given to the temperature dependence of the free energy associated with a dislocation.

† Communicated by the Authors. This research was supported by the Office of Naval Research under Contract Nonr 562 (27).

§ 2. Temperature Dependence of the Dislocation Energy

By far the major part of the free energy associated with a dislocation comes from the elastic energy of the strain field around a dislocation and, for practical purposes, the free energy and the elastic energy may be considered numerically equal (Cottrell 1953). This energy, per atomic plane, is approximately proportional to $\mu\mathbf{b}^3$, where μ is the appropriate shear modulus and $\mathbf{b}$ is the Burgers vector. The temperature variation of the above product will be:

$$\frac{1}{\mu\mathbf{b}^3}\frac{d(\mu\mathbf{b}^3)}{dT} = \frac{1}{\mu}\frac{d\mu}{dT} + \frac{3}{\mathbf{b}}\frac{d\mathbf{b}}{dT} = \beta + 3\alpha \quad . \quad . \quad . \quad (1)$$

where β is the temperature coefficient of the shear modulus (in all cases considered, the shear modulus increases with increasing temperature) and α is the linear coefficient of thermal expansion. If we call $W_{T_0} = (\mu\mathbf{b}^3)_{T_0}$ this energy at some arbitrary temperature, say room temperature, then W_T at some other temperature will be:

$$W_T + W_{T_0}[1 + (\beta + 3\alpha)(T - T_0)]. \quad . \quad . \quad . \quad . \quad (2)$$

Table 1 gives the values of W_{T_0} (at room temperature) and the ratios W_T/W_{T_0} at $T = 0{\cdot}9T_M$ (where T_M denotes the melting temperature), for aluminium, copper, silicon and germanium. In these calculations

Table 1

Element	$T = 0{\cdot}9T_M$ (°K)	$\alpha \times 10^6$ (per °C)	$\beta \times 10^6$ (per °C)	$(\mu\mathbf{b}^3)_{300°K}$ (ev)	$\frac{(\mu\mathbf{b}^3)_T}{(\mu\mathbf{b}^3)_{300°K}}$
Al	840	28·7	510	3·94	0·75
Cu	1220	20·3	380	5·02	0·706
Si	1517	3·3	44	28·1	0·955
Ge	1091	7·0	90	27·2	0·95

average values of α, in the temperature range considered, were taken from the Handbook of the American Institute of Physics (1957) and values of β from the references quoted by Huntington (1958). It was assumed that β was constant in the temperature range considered, since these temperatures are well above $\theta_D/3$, where θ_D is the Debye temperature; a linear variation of the elastic constants with temperature may, therefore, be expected.

Two points are immediately apparent: (*a*) the well-known fact that the elastic energy of a dislocation is considerably lower in aluminium and in copper than in silicon and germanium; (*b*) the ratio W_T/W_{T_0} is much smaller for aluminium and copper than for silicon and germanium. This leads to the qualitative conclusion, that in the case of a metal the generation of dislocations, by any mechanism, becomes considerably

easier as the temperature increases. This does not apply to the same extent in the case of silicon and germanium.

§ 3. Dislocations Formed by the Collapse of Vacancy Discs

Special consideration will now be given to dislocations forming by the collapsing vacancy disc mechanism in the case of crystal growth from the melt. Schoeck and Tiller (1960) recently calculated the supersaturation of vacancies necessary for the growth of a dislocation loop formed by the above mechanism. Their expression is of the form:

$$\ln \frac{C}{C_0} = P \frac{\mu \mathbf{b}^4}{T}. \qquad \ldots\ldots (3)$$

Here C denotes the actual concentration of vacancies in the lattice at the temperature T and C_0 is the concentration of vacancies at T corresponding to equilibrium with respect to an external surface. P is a proportionality factor, which for a given material is a function only of the dislocation loop radius:

$$P = \frac{1}{4\pi(1-\nu)rk}\left[\ln\left(\frac{r}{\mathbf{b}} + 1{\cdot}6\right) + \frac{1}{1+1{\cdot}6\mathbf{b}/r}\right]$$

where ν is Poisson's ratio (assumed to be $\frac{1}{3}$ for numerical estimates), k is Boltzmann's constant, r is the loop radius and $\mathbf{b}$ is the Burgers vector. Writing

$$\frac{C}{C_0} = \exp\left[-\frac{U_f}{R}\left(\frac{1}{T_M} - \frac{1}{T}\right)\right]$$

these authors derive from eqn. (3) the expression

$$\frac{\Delta T}{T_M} = \frac{3\mu\mathbf{b}^3}{8\pi U_f}\frac{\mathbf{b}}{r}\left[\ln\left(\frac{r}{\mathbf{b}} + 1{\cdot}6\right) + \frac{1}{1+1{\cdot}6\mathbf{b}/r}\right] \qquad \ldots (4)$$

where $\Delta T = T_M - T_C$ defines the temperature drop from the melting temperature, at which a sufficient supersaturation is reached for a dislocation loop of a given radius r to form; U_f is the energy of formation of a single vacancy.

If the radius r is expressed in Burgers vectors and the temperature variation of $\mu\mathbf{b}^3$ (eqn. (2)) is taken into account, expression (4) can be rewritten in the form:

$$T_c = \frac{1 - A(\mu\mathbf{b}^3)_{T_0}[1+300(\beta+3\alpha)]}{\frac{1}{T_M} + A\frac{(\mu\mathbf{b}^3)_{T_0}}{U_f}(\beta+3\alpha)} \qquad \ldots\ldots (5)$$

where A is a numerical factor which depends on the value chosen for r and $(\mu\mathbf{b}^3)_{T_0}$ is taken at 300°K. T_c is the temperature at which a sufficient vacancy supersaturation is reached to form a dislocation loop of a given radius r_c.

Calculations by Schoeck and Tiller show that a vacancy disc of a radius 5**b** or more may be considered to have collapsed and formed a dislocation loop. Assuming this to be valid, the temperatures T_c were calculated for the four elements under consideration, for $r_c = 5\mathbf{b}$ and $r_c = 10\mathbf{b}$, and are given in table 2. In all the calculations experimental values of U_f and U_m

Table 2

Element	U_f (ev)	U_m (ev)	T_c (°K)	$\frac{\Delta T}{T_M}$	$\frac{dr}{dt}$ (cm/sec)	$r_{\max}$ (cm)
Al $r_c = 5\mathbf{b}$	0·76	0·43	778	0·166	4·6	$2{\cdot}76 \times 10^{4}$
Al $r_c = 10\mathbf{b}$			835	0·105	64·5	$3{\cdot}7 \times 10^{4}$
Cu $r_c = 5\mathbf{b}$	0·9	1·1	1103	0·186	0·108	10^{3}
Cu $r_c = 10\mathbf{b}$			1200	0·115	0·575	$3{\cdot}2 \times 10^{3}$
Si $r_c = 5\mathbf{b}$	2·6	1·3	645	0·616	$3{\cdot}76 \times 10^{-11}$	$2{\cdot}1 \times 10^{-7}$
Si $r_c = 10\mathbf{b}$			995	0·412	$1{\cdot}16 \times 10^{-7}$	$1{\cdot}45 \times 10^{-4}$
Ge $r_c = 5\mathbf{b}$†	2	0·97	282	0·76	10^{-17}	—
Ge $r_c = 10\mathbf{b}$			600	0·5	$1{\cdot}57 \times 10^{-9}$	$2{\cdot}75 \times 10^{-6}$

† Here T_c is below room temperature, hence no value for $r_{\max}$ is given.

(U_m is the activation energy for migration of vacancies) are used, except in the case of silicon, for which no such values are available. It is assumed instead, by comparison with germanium, that the activation energy U_{SD} for self-diffusion in silicon is at least equal to the highest values of activation energy for diffusion of substitutional impurities, such as boron, gallium, indium and thallium (Fuller and Ditzenberger 1956). This activation energy is approximately 90 000 cal/mol. Again by analogy with germanium (Letaw *et al.* 1956) it is assumed that for silicon a vacancy self-diffusion mechanism is valid and that $U_f \cong \frac{2}{3}U_{SD} = 60\,000$ cal/mol and $U_m \cong \frac{1}{3}U_{SD} = 30\,000$ cal/mol. It should also be pointed out that the chosen value of U_f for silicon satisfies the empirical relation

$$(U_f/T_M)_{\text{silicon}} \cong (U_f/T_M)_{\text{germanium}}.$$

The values of $\Delta T/T_M$ for the four elements are also given in table 2. It is seen that this ratio is much higher for silicon and germanium than for aluminium and copper. The question thus arises whether dislocation loops forming at these values of $\Delta T/T_M$ can grow to measurable sizes in the time available during crystal growth, for a temperature drop from T_C to room temperature.

An estimate will now be made of the maximum size that a dislocation loop thus formed can reach in each of the four elements. The maximum rate of growth of a circular dislocation loop, at a given temperature T, is derived as follows. When the ring grows from radius r to $r+dr$ it absorbs a volume of vacancies given by $a2\pi r\,dr$, where a is the lattice parameter. The maximum rate of growth will be achieved when this volume of vacancies will be supplied by the diffusion to the dislocation ring of all the available excess vacancies from an appropriately expressed volume element dV. Here dV is an increment in the volume of a torus of average principal radius r and of cross-sectional radius s, where $s=D_v^{1/2}t^{1/2}$ (D_v is the vacancy diffusion coefficient and t is time), i.e.

$$dV=(2\pi r)2\pi s\,ds.$$

The volume of vacancies in dV is obtained by multiplying dV by the concentration of excess vacancies $(C-C_0)$. It is assumed here that the actual vacancy concentration is given by the concentration corresponding to equilibrium with respect to an external surface at the melting temperature, thus

$$C\cong\exp(-U_f/RT_M)\quad\text{and}\quad C_0\cong\exp(-U_f/RT).$$

By equating the two volumes of vacancies we obtain:

$$a2\pi r\,dr=(C-C_0)(2\pi r)2\pi s\,ds.$$

Finally, the rate of growth is given by:

$$\frac{dr}{dt}=\frac{dr}{ds}\frac{ds}{dt}=\frac{\pi}{a}D_v(C-C_0). \qquad \ldots\ (7)$$

In the following it is assumed that the dislocation loop under consideration is the only available sink for vacancies in the crystal. Thus the maximum loop radius attainable in a time t_1, during which the temperature of the crystal drops from T_c to room temperature, will be given by

$$r_{\max}=r_c+\frac{\pi}{a}(C-C_0)\int_0^{t_1}D_v\,dt \qquad \ldots\ (8)$$

where $T=T_c$ at $t=0$.

We will now evaluate $r_{\max}$ in the case of crystal growth from the melt. Under typical laboratory conditions crystals are grown from the melt at rates v of approximately 10^{-3} cm/sec and with a temperature gradient G (along the growth direction of the crystal) of about 20°c/cm. Thus the rate of temperature decrease along the crystal will be given by $w=dT/dt=vG=2\times10^{-2}$ degrees/sec. The integral on the right-hand side of expression (8) can now be evaluated as follows:

$$D_v(T)=D_0\exp(-U_m/RT)\quad\text{and}\quad T=T_c-wt;$$

hence

$$\int_0^{t_1}D_v\,dt=D_0\int_0^{t_1}\exp\left[-\frac{U_m}{RT_c\left(1-\dfrac{wt}{T_c}\right)}\right]dt;$$

by expanding $(1-wt/T_c)^{-1}$ and retaining the first two terms, we obtain:

$$\int_0^{t_1}D_v\,dt=D_v(T_c)\frac{RT_c^{\,2}}{U_m w}\left[1-\exp\left(-\frac{wU_m t_1}{RT_c^{\,2}}\right)\right].$$

Hence: $$r_{\max}=r_c+\frac{\pi}{a}(C-C_0)D_v(T_c)\frac{RT_c^2}{wU_m}\left[1-\exp\left(-\frac{wU_m t_1}{RT_c^2}\right)\right]. \quad (9)$$

Assuming $D_0=1$, values of $r_{\max}$ (eqn. (9)), starting from $r_c=5\mathbf{b}$ and $r_c=10\mathbf{b}$, and of dr/dt (eqn. (7)), at T_c for $r_c=5\mathbf{b}$ and $r_c=10\mathbf{b}$, are given in table 2.

§ 4. Discussion and Conclusions

It appears from the values of $r_{\max}$ that in the case of aluminium and copper, the actual size of loops originating from collapsed discs will not be determined by $r_{\max}$. This size will probably depend on the presence of other vacancy sinks in the crystal, in particular on the presence of other dislocations. It should also be pointed out that for aluminium and copper, the rate dr/dt at T_c is well in excess of the usual crystal growth rate. Dislocation loops can, therefore, grow into regions where the temperature is above T_c. The rate dr/dt can thus increase until the loop reaches a region at temperature $T_{\max}$ (near T_M) at which $dr/dt(T)$ goes through a maximum, after which it drops rapidly, reaching zero at $T=T_M$. This again suggests that in aluminium and copper $r_{\max}$ is neither the limiting nor necessarily the determining factor in the ultimate size of the loops.

For silicon and germanium the values of $r_{\max}$ indicate that dislocations produced by the collapsing vacancy disc mechanism will not attain sizes visible in an optical microscope. Moreover, for these elements dr/dt is several orders of magnitude smaller than the crystal growth rate. The dislocation loops are, therefore, always in a region whose temperature decreases at the rate given by the product vG. Thus $r_{\max}$, determined from eqn. (9) appears to give an upper limit of loop size.

It is suggested that the above conclusions explain why crystals essentially free of dislocations detectable by means of the optical microscope (Dash 1959) can be produced by growth from the melt in the case of silicon and germanium. Such crystals are grown under very carefully controlled conditions, from materials of very high purity. All major known dislocation-producing mechanisms, except collapsing vacancy discs, are thus essentially eliminated, whereas the latter is not capable of producing dislocations of detectable size. It appears that for metals, even when purity and solidification conditions are similar to those of silicon and germanium, the prevention of dislocation growth from collapsed vacancy discs will be more difficult.

References

American Institute of Physics, 1957, *Handbook* (McGraw-Hill Co.), pp. 4–51.

Cottrell, A. H., 1953, *Dislocations and Plastic Flow in Crystals* (Clarendon Press), p. 39.

Dash, W. C., 1959, *J. appl. Phys.*, **30**, 459.

Fuller, C. S., and Ditzenberger, J. A., 1956, *J. appl. Phys.*, **27**, 544.

Huntington, H. B., 1958, *Solid State Physics*, **7**, 322, Editors F. Seitz and D. Turnbull.

Kuhlmann-Wilsdorf, D., 1958, *Phil. Mag.*, **3**, 125.

Letaw, H. J., Parotnoy, W. M., and Slifkin, L., 1956, *Phys. Rev.*, **102**, 636.

Schoeck, G., and Tiller, W. A., 1960, *Phil. Mag.*, **5**, 43.

Palaeomagnetism of the British Carboniferous System†

By C. W. F. Everitt
Imperial College, London

and J. C. Belshé
Department of Geodesy and Geophysics, Cambridge

[Received May 23, 1960]

Abstract

Superficially conflicting evidence has been found concerning the direction and sense of the earth's magnetic field in carboniferous times. Various explanations of the results are considered here. We conclude that the discrepancies in direction occur because some sites underwent secondary remagnetization during the Triassic period. If this hypothesis is correct, the mean direction for the Carboniferous period was 200° east of true north and 27° down; placing Britain 15° south of the equator. As regards the sense of the field we conclude that it probably underwent a rapid series of inversions in the early part of the Carboniferous period and then remained reversed for a considerable time.

§ 1. Introduction

We have been independently engaged on palaeomagnetic studies of rocks from the British Carboniferous system. The investigations revealed systematic discrepancies of about 70° between the axes of magnetization in different formations, and provided strongly conflicting evidence concerning reversal of the earth's magnetic field. In the present account we propose to summarize the results and examine the discrepancies.

A map of the areas examined is given in fig. 1. They may conveniently be divided as follows : first, sedimentary formations in Derbyshire, Lancashire, Staffordshire, and South Wales ; second, baked and igneous formations in the English Midlands including Derbyshire ; third, baked and igneous formations in Scotland.

The sedimentary formations cover almost the complete Carboniferous period. In Derbyshire, the geological succession comprised about 14 000 ft of sediments extending from the Carboniferous limestone to the Coal Measures ; the estimated time-span being about 220–280 million years. In the Lancashire Coalfield there are 20 000 ft of sediments, and in the South Wales Coalfield 15 000 ft of sediments, covering approximately the same period. Samples were taken from 46 sites in these areas, and from one site in the late Carboniferous Keele beds of Staffordshire. Further details are given in the table.

† Communicated by the Authors.

Fig. 1

Distribution of sites.
● Baked and igneous formations.
○ Sedimentary formations.

Summary of Results

Region	Description	Material examined		Material accepted		Declination	Inclination	Period	Approximate age
		Sites	Samples	Sites	Samples	Degrees east of true north			Millions of years
Derbyshire	Sedimentary	22	84	3	13	37°	39° down	Carboniferous Limestone to Millstone Grit	230–280
				3	11	197°	37° down		
Lancashire	Sedimentary	12	49	4	14	24°	22° down		
				3	10	184°	23° down		
Staffordshire	Sedimentary	1	7	1	7	199°	34° down	Late Carboniferous	270
South Wales	Sedimentary	12	79	2	18	205°	49° down		
English Midlands	Baked Sills	6	11	6	11	202°	17° down	Late Carboniferous	280
			12		12	196°	13° down		
	Baked Lava	1	2	1	2	349°	1° down	Carboniferous Limestone	240
			5		3	357°	14° down		
Derbyshire	Baked Sill (1)	1	6	1	6	221°	34° down	Middle Carboniferous?	260?
			7		7	218°	36° down		
	Lava (2)	1	3	1	3	48°	45° up	Carboniferous Limestone	240
	Lavas (2)	2	3	2	3	200°	29° down		
Scotland (Kinghorn) (2) (3)	Beds 9–15	4	7	2	5	12°	18° up	Calciferous Sandstone	230
	Beds 16–20	4	11	3	8	170°	24° down		
	Bed 21	1	3	1	2	55°	19° down		
	Beds 25–48	13	25	10	20	13°	35° up		
	Beds 50–55	5	8	4	6	205°	41° down		
	Bed 65	1	2	1	2	15°	14° down		
	Bed 69 (4)	1	2	1	2	15°	35° up	Late Calciferous Sandstone?	240?

(1) The origin of this formation at Tideswelldale is not certain. It may be lava.
(2) The directions for two of the Derbyshire lavas and in beds 12, 15, 19, 20, 31, 32, 38, 48 from Kinghorn are values after thermal or alternating field cleaning (see text).
(3) All the results are from igneous rocks except beds 25, 45, 54 which were baked sandstones.
(4) This formation is a sill of uncertain age.

The English baked and igneous rocks were from two areas. In the first, near Birmingham, there were six late Carboniferous sills and one lava of Carboniferous Limestone age. In the second area, in Derbyshire, there were three lavas also of Carboniferous Limestone age, and one Middle or Late Carboniferous Sill.

The Scottish baked and igneous rocks were a series of lavas and interbedded sediments from Kinghorn, Fife, covering a few million years in the Calciferous Sandstone period. In the table the beds are numbered consecutively from the bottom upwards, irrespective of their nature, in accordance with the notation of Geikie (1900).

Fig. 2

Results from sedimentary formations (lower hemisphere of Schmidt projection).

Some details of the sampling are included in the table. Several oriented blocks were collected at each site. As a rule, three to six discs $1\frac{3}{8}$ in. diameter $\frac{1}{4}$ in.–$\frac{1}{2}$ in. thick were cut from each block and measured on a Blackett magnetometer. The mean directions and, where necessary, the standard deviations were calculated by the methods given by Wilson (1959). Certain other measurements were also carried out as described in the following sections.

§ 2. Results

2.1. *Directions of Magnetization*

The main results are set out in the table and plotted on figs. 2–4. The directions are all given relative to the original bedding and flow-planes. They have been plotted on the lower hemisphere of a Schmidt projection, the sense of the magnetization being reversed for the upward dips.

Fig. 3

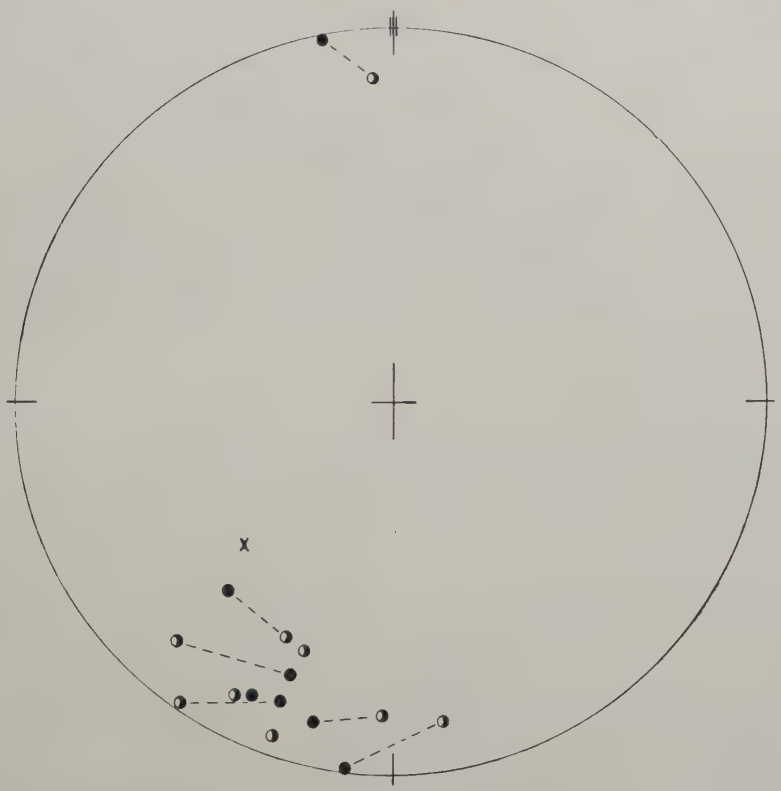

Results from English baked and igneous formations (lower hemisphere of Schmidt projection).

● Baked rocks.
◑ Igneous rocks (north magnetic pole).
× Igneous rocks (south magnetic pole).
– – – Joins results from same site.

In the sedimentary rocks the magnetization was often extremely weak and sometimes widely scattered ; but at some sites there was good agreement between the mean directions of different blocks. As a first step in analysis, only the sites for which the standard deviations between individual blocks was less than 20° were accepted. Out of 47 sites, 16 fall within this category. Their directions, which are plotted in fig. 2,

fall in two well-defined groups ; one with a mean azimuth 34° east of true north and a mean dip of 31° down, and the other 195° east and 35° down. The smaller angle between these two mean axes is about 70°. On the sites with scattered directions, the results still showed some tendency to group about the same two axes. Sometimes the two directions even occurred at the same site ; the most striking example being the Union Strip Mine, Derbyshire, where three blocks agreed closely at 25° east, 33° down and three others agreed at 213° east and 31° down.

Fig. 4

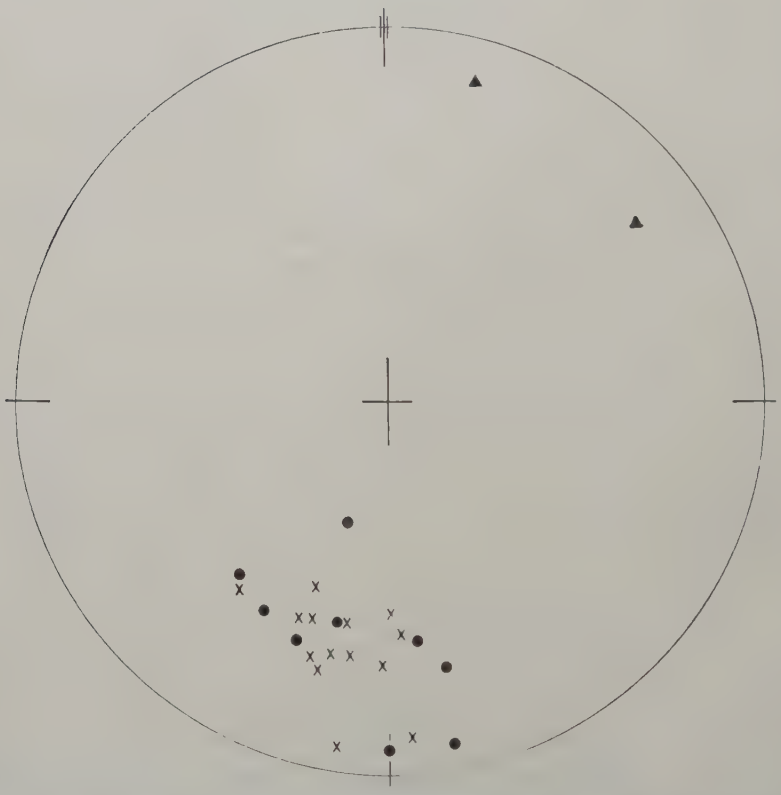

Results from Scottish baked and igneous formations (lower hemisphere of Schmidt projection).

● North pole.
× South pole.
△ Discordant directions (north pole).

Figure 3 shows the directions in the English baked and igneous rocks. In the sills and associated baked sediments the mean direction was 202° east and 19° down ; while of the lavas from Derbyshire, one was magnetized 46° east, 45° up, and two showed initial north-east downwards directions, which changed on heating to within 100°c of the Curie

temperature and gave a final mean direction of 200° east and 20° down. The remaining lava, near Birmingham, gave a mean 357° east and 7° down ; but since the scatter of directions was large (standard deviation 14°), this probably only represented a reversal of the south-west downward axis.

The directions for the baked and igneous formations in Scotland contrast with the preceding data. They are given in fig. 4. The mean axis was 193° east 33° down. Along this axis, magnetizations existed in either sense ; there being successive groups of normal and reversed lavas. In two lavas (numbers 25 and 65) lying between normal and reversed groups there were discordant directions which are differently designated in fig. 4. Apart from these, which may represent an intermediate direction during the course of an earth's field reversal, there was no sign of the north-east/downwards magnetization.

The results as a whole, then, show two distinct directions ; 40 sites being magnetized along south-east/downwards axes, and 7 along a north-east/downwards axis. The angle between these two axes is about 70°. It should be remarked that some measurements by Clegg *et al.* (1954) on sediments at Frampton Cotterill Gloucestershire, also gave a north-east/downwards direction (44° east, 35° down).

2.2. *Stability*

In assessing the significance of the magnetizations we must consider not only their stability (that is whether they represent a unique direction of the earth's magnetic field) but also their age : for a stable magnetization may easily have been acquired long after the rocks were formed.

The stability of the south-west/downwards direction is demonstrated by four lines of evidence, as follows :

(1) There was close agreement in direction between igneous and sedimentary rocks of widely different type.

(2) Exact 180° reversals occurred ; showing that there had not been any secondary magnetization sufficient to disalign the two directions.

(3) The directions for the Scottish beds (which are tilted 30° eastwards) agreed with the English ones more closely relative to the bedding planes than the present horizontal. This indicates that the magnetization was acquired before tilting.

(4) There was good agreement between the directions in associated baked and igneous rocks. This line of evidence seems especially convincing since the intrinsic scatter of the baked rocks was only 2–3°.

The measurements on baked rocks also provided a test of the date of magnetization. At several sites there was a large and systematic decrease of intensity and increase of scatter with distance from the contact (Everitt and Clegg 1960), which strongly suggests that the baked material became magnetized when the igneous bodies cooled, and therefore that the magnetizations were of Carboniferous age.

Several of the Scottish lavas had widely scattered natural magnetizations. Laboratory heating experiments were carried out on six of these by Mr. R. L. Wilson. In each case, he found that the directions came into line with the mean values for adjacent beds, on heating to within 100°C of the Curie temperature. For two lavas a similar effect was achieved by alternating field demagnetization. The sites treated in this way are distinguished in a note to the table.

The stability of the north-east/downwards magnetization is not so well attested. However, there is some field evidence from measurements on two limbs of the Pendle monocline, which agreed more closely relative to the bedding-planes than to the present horizontal ; although since the direction of magnetization was only a few degrees from the strike axis, this test is not absolutely decisive. In addition, there was some laboratory evidence for stability, since the directions of magnetization showed no appreciable change on heating in zero field to 200°C.

2.3. *Age of the Magnetizations*

The evidence from baked rocks, outlined in the preceding section, strongly suggests that the south-west/downwards magnetizations were acquired at the time of formation of the igneous rocks, which—for the Kinghorn lavas at least—can confidently be assigned to the Carboniferous period.

The north-west/downwards magnetization on the other hand occurs only in the sedimentary rocks and may be assigned to any period before the folding of the Pendle monocline. The mean direction was 39° east and 35° down, which is remarkably near the figure of 34° east, 28° down given by Clegg *et al.* (1954) for the Triassic period. It is therefore conceivable that the magnetization was acquired by a secondary process during Triassic times.

There is some geological evidence to support this view. Many of the Carboniferous formations underlying the Permo-Triassic strata on either side of the Pennines are markedly reddened to depths of 1000 ft or so. According to Trotter (1953), the reddening was due to weathering of the iron minerals to hematite while the overlying strata were being formed. The beds examined here did not belong to the most severely weathered series but, as we have seen, the magnetic material in them was hematite. Although it has not been possible to relate in detail their position to the Permo-Triassic erosion surface, there does seem to be a definite connection. This may be illustrated conveniently by results from three sites in the Coal Measures of Derbyshire–Yorkshire border. At Sheffield Brick Pit, which is some way from the erosion surface, the mean direction was 207° east, 36° down ; at Hardwick Hall, which is very near the erosion surface, the direction was 50° west and 33° down ; while at Union Strip Mine, which was slightly further away than Hardwick Hall, three blocks agreed at 25° east, 33° down, and three others agreed at 213° east,

31° down. Much the simplest explanation of these results is in terms of local re-magnetization during Triassic times.

A second line of evidence is provided by the Keele beds of Staffordshire, in which the hematite is thought to be primary and should therefore retain the original Carboniferous magnetization. Their direction was indeed 199° east and 34° down.

The most obvious objection to the interpretation in terms of remagnetization is that the beds of the Pendle monocline appear to have acquired their north-east magnetization before being folded in the Hercynian orogeny, which occurred during early Permo-Triassic times. As mentioned above, the evidence is not absolutely decisive. But even if the beds were magnetized before folding, that only proves that the north-east downwards direction appeared fairly early in Permo-Triassic times : it may still have been a considerable time after the Carboniferous period ended.

2.4. *Reversals*

We have seen that at Kinghorn the normal and reversed magnetizations occur in separate groups of five or more lavas. This suggests that the earth's field underwent inversions : a view which is supported by the conjunction of concordantly magnetized baked sediments with both normal and reversed groups : and also by the absence of any positive evidence from the heating experiments for physico-chemical reversals. If so, inversions of the field occurred at the rate of about one per million years—that is, at about the same rate as found by Hospers (1953) for the Tertiary period.

If this interpretation is correct, it is puzzling that all the lavas and baked sediments showing these periodic inversions were formed during a relatively small part of the early Carboniferous, while all the later sediments and intrusions (which extend over the major part of the period) are reversed.

In assessing these results, we distinguished two questions. The first is whether the earth's field reversed at all, the second whether it underwent a rapid sequence of inversions from normal to reversed and back. There seem to be four possibilities :

(i) All the sedimentary and some igneous rocks were self-reversed.

(ii) All rocks were magnetized in a reversed field, and some early lavas and associated baked sediments underwent physico-chemical reversal to the normal direction.

(iii) Inversions of the earth's field occurred frequently throughout the period, but the sediments and intrusions by chance only became magnetized during periods of reversed field.

(iv) Inversions occurred frequently during early Carboniferous times, but afterwards the field remained continuously reversed for a considerable period.

The first explanation would require a great exercise of special pleading. Of the remaining explanations the second is the least satisfying because once the possibility of a reversed field is admitted, the main ground for believing that self-obliterating physico-chemical reversals have occurred commonly in rocks disappears. The third hypothesis is excluded, because it seems inconceivable that all the sediments became magnetized in less than a million years. Hence it is best to accept tentatively the fourth hypothesis that the earth's field underwent several inversions during the early part of the period and afterwards remained reversed.

§ 3. Conclusion

Our conclusions may be summarized as follows :

1. The results in the south-west/downwards group give a mean axis of magnetization for the Carboniferous period (age about 250 million years) of 200° east and 27° down. The standard deviation was 20°. These figures are consistent with the directions of 200° east and 35° down given by Nairn (private communication) for the continent of Europe, and 189° east and 9° up given by Creer (1957) for the early Permian in Britain (age about 200 million years).

Some of our results have already been quoted by Irving (1959) and by Blackett, Clegg and Stubbs (1960). The present results are based on more complete and accurate data, and must be regarded as superseding their figures. Broadly they confirm the picture presented by these workers but place Britain about 20° further south. and thus, for example, considerably reduce the relative displacement between England and Australia from that originally claimed by Irving.

Our final mean values for the four quantities ΔI, ϕ, ψ and λ_m defined by Blackett *et al.* (1960) are ΔI, 92° ; ϕ, 87° ; ψ, 23° ; and λ_m, 22° S.

2. Some of the sediments were probably remagnetized during Triassic times. This suggests that the effects of Permo-Triassic weathering extended to a considerably greater depth than has usually been supposed. Palaeomagnetic measurements obviously provide a powerful method of investigating such phenomena.

3. The earth's field seems to have undergone a rapid series of inversions in early Carboniferous times and afterwards to have remained reversed for a considerable period.

Acknowledgments

We wish to thank Professor P. M. S. Blackett, Dr. J. A. Clegg, and Professor S. K. Runcorn for their interest in this work.

In collecting we were helped by Dr. P. H. S. Stubbs, Mr. G. Turnbull, and Mr. M. Andrew ; and we are also especially indebted to Mr. G. W. Masse for his help in collecting and in many other ways.

C. W. F. E. is indebted to the D.S.I.R. for a Research Studentship, and J. C. B. to the U.S. Educational Commission for a Fulbright Fellowship. The work was supported by grants from D.S.I.R.

References

Blackett, P. M. S., Clegg, J. A., and Stubbs, P. H. S., 1960, *Proc. roy. Soc.* A (in the press).
Clegg, J. A., Almond, M., and Stubbs, P. H. S., 1954, *Phil. Mag.*, **45,** 583.
Creer, K. M., 1957, *Phil. Trans.*, **250,** 111.
Everitt, C. W. F., and Clegg, J. A., 1960, (to be published).
Geikie, Sir A., 1900, Geological Survey Memoir for Central Western Fife
Hospers, J., 1953, *Kon. Ned. Acad. Wet.*, **56,** 477.
Irving, E., 1959, *Geophys. J., R.A.S.*, **2,** 51.
Trotter, F. M., 1953, *Proc. York. geol. Soc.*, **29,** 1.
Wilson, R. L., 1959, *Phil. Mag.*, **4,** 750.

Recovery of Quenched-in Resistivity at High Temperatures in Gold†

By M. Meshii and J. W. Kauffman
Materials Science Department, Northwestern University
Evanston, Illinois, U.S.A.

[Received September 15, 1959]

Abstract

For quenches made from 1000°c, 90% of the quenched-in resistivity anneals out in the vicinity of room temperature leaving 10% which subsequently recovers only at much higher temperatures. This remaining resistivity is associated with configurations which are formed from the quenched-in vacancies. The recovery of this remaining resistivity was studied. Two recovery regions were defined: The first region was found within a wide temperature range, 200°c to 600°c; the second region was observed within a very narrow temperature range about 630°c. Complete recovery occurred during this stage. The recovery in the temperature range 200°c to 600°c had no observable effect on the yield stress. However, the second step of the resistivity recovery observed in a narrow temperature range above 600°c corresponds to the resoftening of quench-hardening.

§ 1. Introduction

Previous studies of the annealing out of quenched-in resistivity have been confined to annealing temperatures in the neighbourhood of room temperature. However, there is a portion of the quenched-in resistivity which does not recover at these temperatures. A much higher temperature is necessary for its recovery. It is now well accepted that the room temperature recovery of quenched-in resistivity is associated with the migration of essentially random vacancies and vacancy complexes either to sinks, where they disappear, or else they migrate, finally forming stable configurations which are less effective in scattering electrons and hence contribute a smaller amount of electrical resistivity. Some of these configurations of lower electrical resistivity and lower lattice energy are responsible for quench-hardening. The purpose of the present work is to investigate the nature of this remaining resistivity and to study the correlation of this to the quench-hardening mechanism.

§ 2. Experimental Procedure

The quenching methods have been described in a previous publication (Meshii and Kauffman 1959a). All quenches were made from 1000°c ± 10°c with a rate of 30 000°c/sec. The samples used were gold wire 0·016 in. in

† Communicated by the Authors. This investigation was performed with the support of the Office of Naval Research of the United States Government.

diameter. The purity was 99·999%. Subsequent to the quench the specimens were annealed in a furnace kept within ± 1°C. The resistivity measurements were then made at 4·2°K, using standard potentiometric methods.

Fig. 1

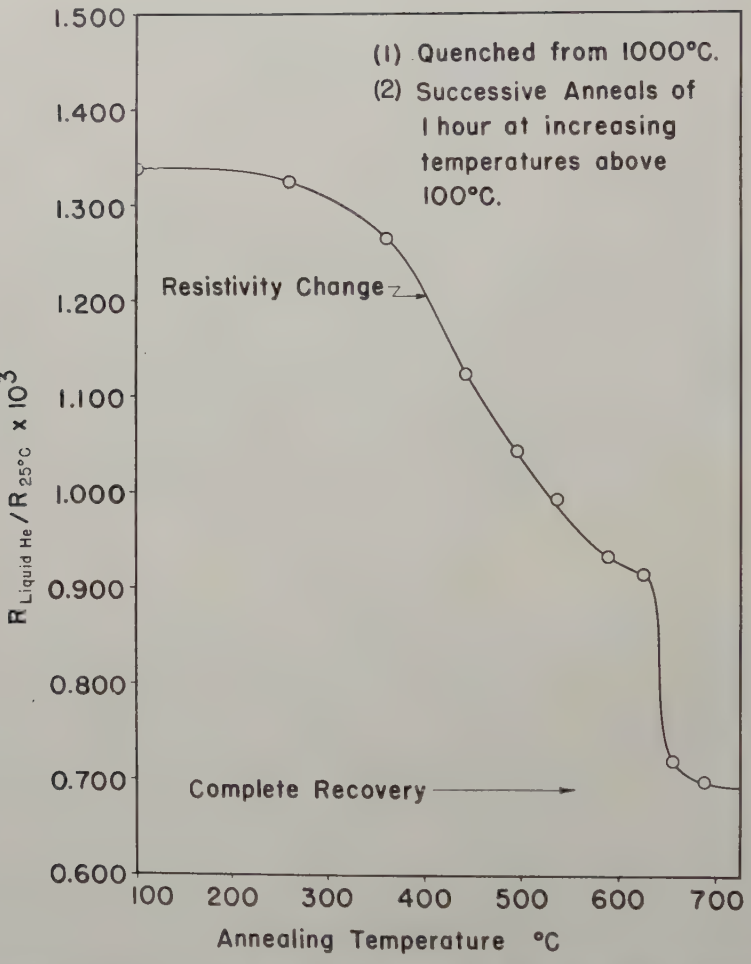

Resistivity recovery during successive isochronal annealings after complete ageing.

§ 3. Experimental Results

The recovery of the electrical resistivity upon one hour annealings at fixed temperatures is shown in fig. 1. The rate of recovery as a function of annealing temperature is shown in fig. 2. These curves do not correspond to the recovery of the yield stress of quenched gold (Meshii and Kauffman 1959b, 1960), except for the last recovery stage above 600°C. One hour annealings below 500°C produce a considerable recovery of resistivity,

while they do not affect mechanical properties. It is also seen from figs. 1 and 2 that there are at least two stages in the resistivity recovery below 600°C. About two-thirds of the quenched-in resistivity remaining after the room temperature recovery anneals out below 600°C.

Fig. 2

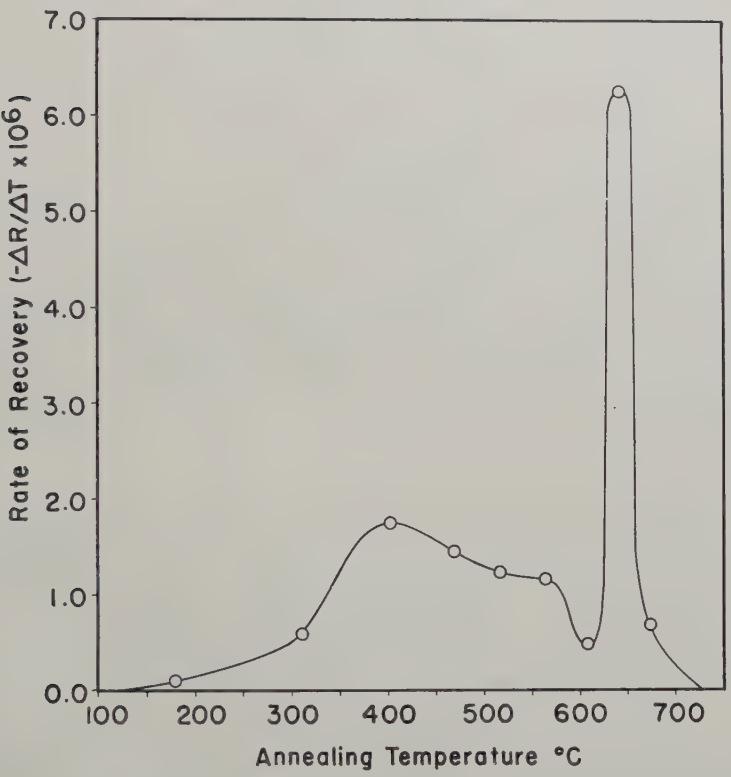

Average rate of recovery between two adjacent points in fig. 1 is plotted against average temperature.

The activation energy for the recovery of this resistivity was difficult to determine accurately, first, because the change in resistivity is small and therefore difficult to measure, and secondly, it appears that more than one process is operating and therefore a unique activation energy would not be expected. An example of the data is shown in fig. 3. From these data, using the slope intersection method, a value of $1{\cdot}2 \pm 0{\cdot}1$ ev was obtained for temperatures between 415°C and 440°C. A value of $1{\cdot}5 \pm 0{\cdot}3$ ev was found between 440°C and 484°C. These results indicate that the processes occurring below 600°C have a much lower activation energy than that associated with resoftening, where 4·7 ev was found (Meshii and Kauffman 1959 b, 1960). The recovery stage above 600°C is seen to be highly dependent on temperature. Complete recovery had occurred after a narrow temperature range. This behaviour is similar

to that found for the recovery of the yield stress, both in regard to the temperature range and the apparent dependence on temperature.

Fig. 3

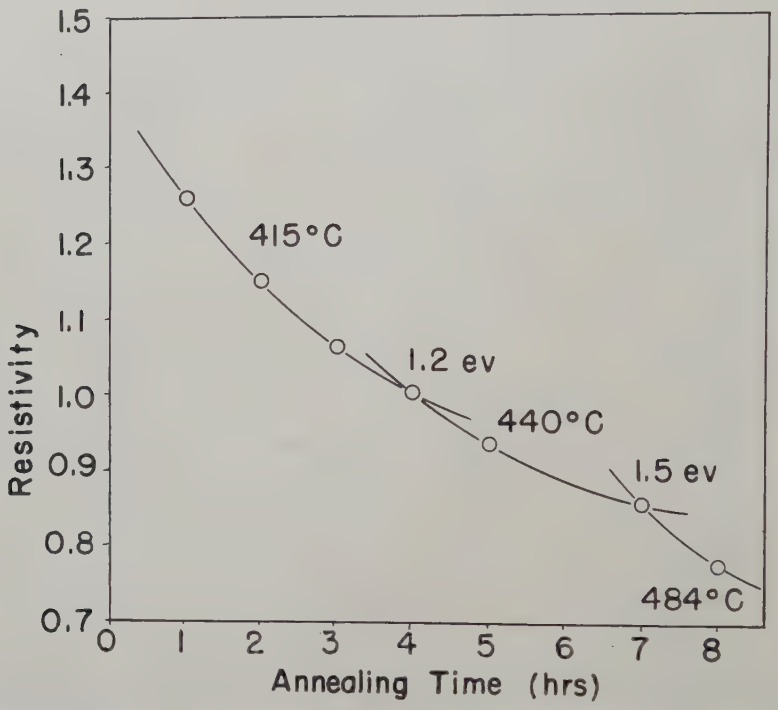

Activation energy determinations in the first stage of resistivity recovery.

§ 4. Discussion

Quench-hardening has not been found immediately after quenching, the hardening only occurs upon ageing at room temperature. Resoftening of the quench-hardening is found to occur only above 600°C. Therefore, as concluded (Meshii and Kauffman 1959 b, 1960) configurations which give rise to hardening are formed as a result of vacancy and vacancy complex migration near room temperature. The recovery of the quenched-in resistivity beteen 200°C and 600°C then has little effect on the yield stress. However, the recovery occurring about 650°C apparently corresponds to the recovery of quench-hardening.

Acknowledgment

The authors wish to thank Mr. R. Kloske for assistance in making some of the measurements.

References

Meshii, M., and Kauffman, J. W., 1959 a, *Acta Met.*, **7**, 180 ; 1959 b, *Bull. Amer. phys. Soc.*, **4**, 172 ; 1960 *Phil. Mag.*, **5** (to be published).

Localized Modes in Crystals and Sharp Details of the Optical Absorption Spectra†

By Robert Englman
Department of Physics, Israel Institute of Technology, Haifa, Israel

[Received April 12, 1960]

Abstract

A theory is put forward in qualitative terms to account for the sharp nibs frequently observed at the long wavelength end of the spectral lines of ionic crystals, in which optical absorption by a cation has taken place. The broad band is primarily due to excitation of the vibrational modes of the crystal by the Franck–Condon strain; nibs are supposed to be caused by localized modes introduced in the crystal either by the differing mass or by a change in the force constants of the absorbing ion. Experimental evidence in rocksalt-type crystal indicates the presence of T_{2g}-modes of localized vibrations.

§ 1

The shape of the absorption spectra of paramagnetic ions in crystals is not particularly well understood today. The lack of thoroughgoing research in this field results in a situation that, while the assignment of bands can be made with confidence on the basis of crystal field theory, the fine details of the absorption line (sometimes also called *structure*) are explained in an *ad hoc* manner and without relation to the broader problems involved. The questions are sharpened by recent works with paramagnetic ions in ionic crystals, appearing either substitutionally as impurities or as the host ion, and mainly for two reasons:

First, because in at least the simplest cases investigated, crystals with the NaCl structure, we should have quite a good working knowledge of the dynamical behaviour of the crystal; in contrast to ligand coordinated complexes (which historically take precedence), whose interaction with their immediate neighbours is as yet a matter of speculation. Secondly, while the numerous discrete vibrational modes of the latter can accommodate the interpretation of practically any 'structure' of the line, in a crystal, where there exist continua of vibrational modes, the very existence of discrete peaks is puzzling.

In figs. 1 and 2 we show two optical absorption lines which are typical of their kind and which exhibit sharp nibs superimposed on the broad bands. The lines are due to chromium ion in magnesium oxide (at 77°K) and chromium ion in Al_2O_3 (77°K). Both host crystals are predominantly cubic (Stahl-Brada and Low 1959)

† Communicated by the Author.

In the writer's view two aspects of the bands, the band-breadth and the nibs, should be distinguished. In fact, it is argued that the broadening is due to what Brillouin (1953) calls passing bands and the nibs to stopping

Fig. 1

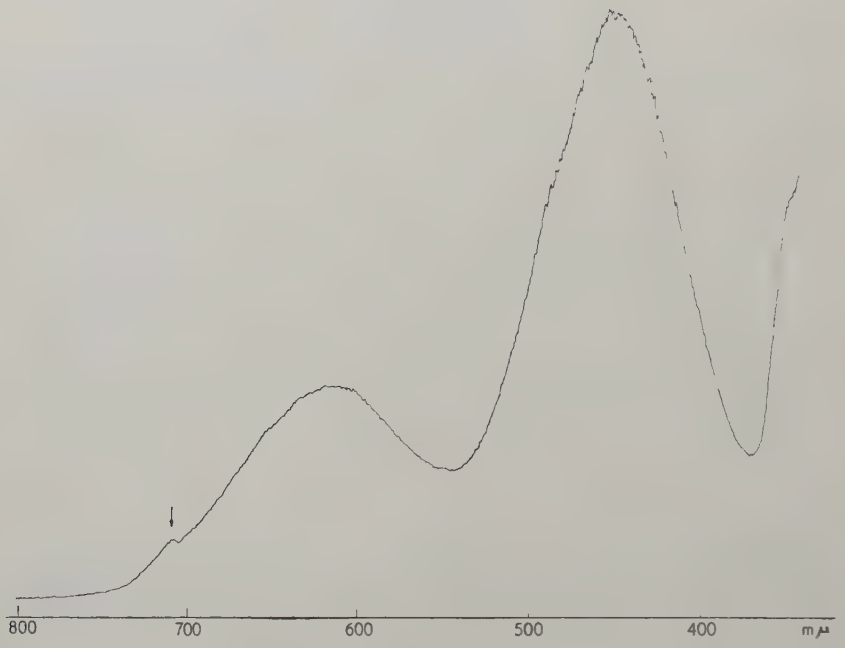

Fig. 2

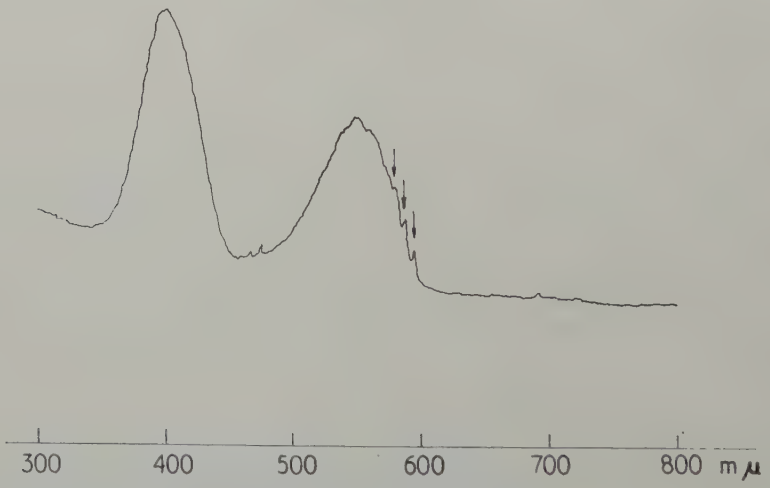

bands. The theory of the line shape should of course be put quantitatively. Nonetheless, even before this (formidable) task is achieved, good purpose is served by formulating the ideas qualitatively. Some of the conclusions are by no means trivial.

§ 2

It is well known that the optical absorption by the ion will in general leave the crystal strained, since different equilibrium dispositions will correspond to the excited and to the ground states. In a crystal this change in the equilibrium configuration will in general affect all the modes in what is presumably a continuous manner. (We expect that the relative change in the configuration on going from one mode to another of adjacent energy will tend to zero as the number of crystal points goes to infinity.) Consequently, various harmonics of each mode will be simultaneously excited with varying probabilities; the variation of the totality of probabilities will produce the rise and fall of the intensity curve. We wish now to emphasize that because of the smooth variation (throughout the continuum of modes) of the equilibrium configurations and of the excitation probabilities a smooth absorption line must result.

We have so far considered the continua, both acoustic and optic, of vibrational modes, called also passing modes, since an excitation in this mode will pass through the whole lattice. It is, however, easy to convince ourselves that other modes may also exist. For this purpose, consider the chromium ion in the MgO lattice. The chromium ($Z=24$) is just about twice as heavy as its host, Mg($Z=12$), and will not, even with the same force constant, fit in with any existing vibrational mode. It has in fact been shown (Maradudin *et al* 1958) that, while the frequencies of the continua are slightly shifted, there will now appear new frequencies spaced apart from the continua of frequencies. The modes corresponding to these frequencies will be localized round the impurity; necessarily so, since the regular lattice cannot 'pass' vibrations of such modes. The number of such *stopping* modes per impurity atom is at most six (Ledermann 1944). It is clear that the excitation of these localized modes by the local strain will be relatively highly likely.

It is also known that on introducing an atom heavier than the host the stopping mode will recede from the bottom of the optic branch, while for a lighter atom the stopping mode will emerge from the top of the acoustic (or optic) branch. We shall now consider the possible energies of these modes.

§ 3

Magnesium oxide forms a rocksalt-like structure. The six branches of such a crystal are shown in fig. 3. (Two–two transverse branches coalesce by symmetry.)

The curves are the results of Kellerman's classic calculations (Kellerman 1940) on NaCl. For our purposes there is no difference between these curves and the refined and more recent results of Cochran (1959). We shall use these curves for MgO by adjusting the vertical scale so as to fit the observed circular dispersion frequency $\omega_0 = 10{\cdot}9 \times 10^{13}\,\mathrm{sec}^{-1}$ for MgO (Born and Huang 1956). For NaCl, $\omega_0 = 3{\cdot}09 \times 10^{13}\,\mathrm{sec}^{-1}$.

Then the positions of stopping bands are as follows:

Longitudinal mode: 580–770 cm^{-1}; Transverse mode: 382–540 cm^{-1}.

A careful reference to fig. 1 gives a value of 500 cm^{-1} for the position of the nib from the beginning of the band. This puts the energy of this mode clearly into the upper half of the transverse stopping band. What is the nature of such a mode?

Fig. 3

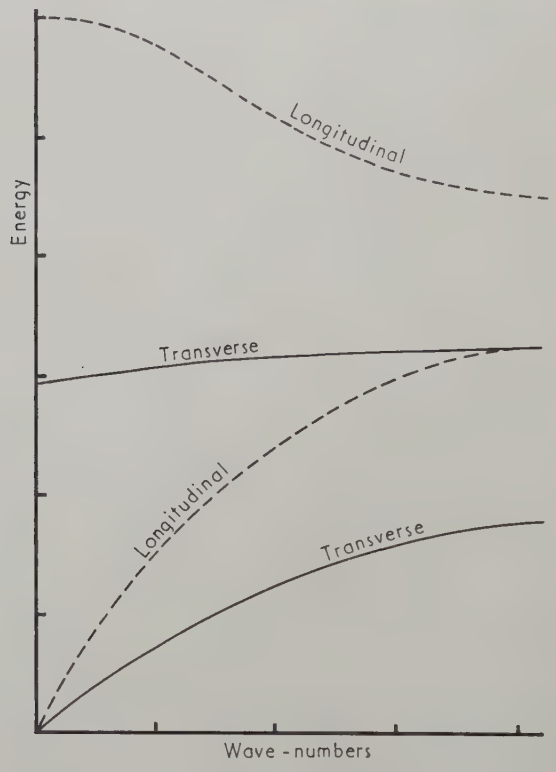

Fig. 4

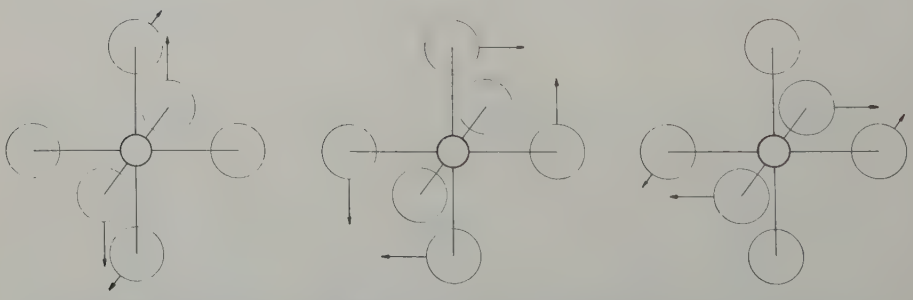

It is known (Brillouin 1953) that in a diatomic chain at the bottom of the optic band the heavy atom is stationary and the light atoms vibrate 180° out of phase. It is very plausible that the character of vibration persists also for a localized mode emerging from the bottom of the optic band. In

terms of the classification (Öpik and Pryce 1957) of *localized* octahedral modes this is a T_{2g} (Q_4, Q_5, Q_6) mode. (We recall that transverse vibrations are considered.)

Now, such modes are related to trigonal distortion of the complex. It follows that these modes may be expected to be prominent whenever either the ground state or the excited state is associated with sizeable trigonal distortion. Professor Low has informed me that there is indeed a strong correlation between the appearance of the nib and a trigonal distortion of the lattice in the ground state.

§ 4

We shall end with a few brief remarks.

The absence of further nibs in fig. 1, cannot be construed as though no further stopping modes are excited, but rather that the rapid rise of the main band obscures any satellite peak. Accordingly the nibs will be most apparent whenever their energy, or that of their overtones, reaches the beginning, top or end of the band.

The three nibs of fig. 2 are probably not successive overtones, since their separation $\sim 130\,\mathrm{cm}^{-1}$ is too small to be fitted into the stopping band. (We assume for Al_2O_3 a roughly similar vibrational structure to that for MgO.) The first nib appears at 480–$500\,\mathrm{cm}^{-1}$.

When the absorption is on the host cation, no localized modes exist due to differences in mass. But there will be localized modes due to changes in the force constants of the absorbing ion (Englman 1960). These changes may be at the same time a decrease in one direction and increase in another, giving rise to localized modes arising both from the optical and from the acoustic branches. Thus, nibs of lower frequencies may also make their appearance.

Acknowledgment

My thanks are due to Professor W. Low for showing me the spectra in figs. 1 and 2.

References

Born, M., and Huang, K., 1956, *Dynamical Theory of Crystal Lattices* (Oxford: The Clarendon Press).

Brillouin, L., 1953, *Wave Propagation in Periodic Structures* (New York: Dover Publications, Inc.).

Cochran, W., 1959, *Phil. Mag.*, **4,** 1082.

Englman, R., 1960, *Mol. Phys.*, **3,** 23.

Kellerman, E. W., 1940, *Phil. Trans. roy. Soc.*, **238,** 513.

Ledermann, W., 1944, *Proc. roy. Soc.* A, **182,** 362.

Maradudin, A. A., Mazur, P., Montroll, E. W., and Weiss, G. H., 1958, *Rev. mod. Phys.*, **30,** 175.

Öpik, V., and Pryce, M. H. L., 1957, *Proc. roy. Soc.* A, **238,** 425.

Stahl-Brada, R., and Low, W., 1959, *Phys. Rev.*, **113,** 775.

Micro-cracks and their Relation to Flow and Fracture in Single Crystals of Magnesium Oxide†

By F. J. P. Clarke and R. A. J. Sambell
Atomic Energy Research Establishment, Harwell, Berks

[Received December 4, 1959]

Abstract

Evidence on mechanisms of fracture in magnesium oxide single crystals subjected to tensile loading is given. As-cleaved crystals contain micro-cracks typically 10^{-4} in. long and slip originating from near these cracks occurs during deformation. At a later stage the cracks grow gradually until they increase to a critical size when catastrophic propagation occurs. If the cracks are removed by polishing ductility is enhanced five to ten times Some crystals were reactor irradiated to doses in the range 10^{14}–10^{19} n.v t. (epithermal) and the effects of this treatment on flow and fracture are described and discussed.

§ 1. Introduction

Cleaved single crystals of magnesium oxide are generally more ductile if chemically polished prior to stressing. The mechanisms of fracture in the polished state have been investigated by Stokes *et al.* (1959 a, b, c) and in the unpolished state by Gorum *et al.* (1958) and Washburn *et al.* (1959). The factors leading to fracture in the unpolished state are not clearly defined at present and it is the purpose of this paper to aid an understanding of the processes involved.

Reactor irradiation has been used as a means of varying the amount of slip preceding fracture, and the fracture characteristics have been examined at six different doses in the range 10^{14} to 10^{19} n.v.t. (epithermal).

§ 2. Experimental Method

Crystals of magnesium oxide were obtained from the Norton Company, Niagara Falls, and the purity of two crystals from which the specimens were cleaved is given in table 1.

All tests reported here are tensile tests made on a Hounsfield tensometer. The load was estimated by measuring the movement of the load beam with a micrometer dial gauge; the figure thus obtained gave the tensile force measurement to about 0·1 lb wt. Another dial gauge was used to measure the combined extension of the beam, specimen and specimen grips. By calibrating the apparatus initially specimen extensions alone down to 10^{-4} in. could be deduced. The rate of loading was kept constant at about 1 lb wt min^{-1}.

† Communicated by the Authors.

The grip part of the apparatus is shown schematically in fig. 1. Axial holes of diameter to suit each specimen, were drilled into the ends of two stainless steel rods 0·25 in. diameter and 2–3 in. long. The rod radius was reduced near these ends to allow a 4 mm microscope objective to approach the specimen. The crystal test bar typically 0·02 in. square by 1 in. long was araldited into these holes and the whole placed into a stainless steel guide collar. This collar had slots milled near the specimen to allow transmitted light microscopic examination to be made during the testing. The other ends of these rods were mounted into small brass collars soldered into Meccano universal couplings. These couplings were fixed to the load grips of the tensometer. By careful machining of the rods and collar

Table 1. Analysis of impurity content of crystals used

Impurity	Be	Al	Fe	Ca	Si	Ni	Mn	Ba	Crystal
Concentration (p.p.m.)	70	100	100	500	100	10	10	—	A
	—	300	600	1500	700	200	—	100	B

Fig. 1

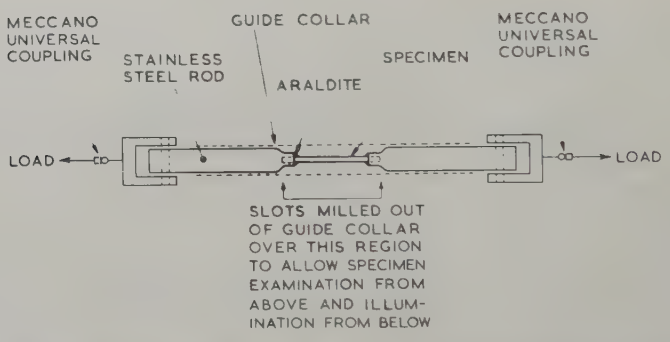

Schematic representation of load grips and associated apparatus (not to scale).

non-axial stresses could be reduced sufficiently to prevent any preferential slip at the test piece ends for most tests and the position of fracture occurred randomly. However, in some tests on very brittle specimens there was evidence (given in the text) that non-axial loading was sufficient to give rise to special effects.

Etching and polishing were carried out in two solutions:

Solution A. Equal parts of saturated ammonium chloride and concentrated sulphuric acid.

Solution B. 88% orthophosphoric acid.

Solution A was used to etch dislocation positions, and solution B as a polishing solution. A detailed study of the action of these solutions has already been described (Ghosh and Clarke 1959).

§ 3. Experimental Results

3.1. *Unirradiated Crystal*

Figure 2 (*a*)† illustrates typical irregularities seen at the edges of a crystal after cleaving. At these high magnifications ($\times 2000$) it is difficult to know exactly what the irregularities represent. Small lines may be revealed by etching solution A, also at the edge, as shown in fig. 2 (*b*) (typical one arrowed); these are not necessarily associated with the pre-etching irregularities. The lines are typically $\sim 10^{-4}$ in. in length and may occur as close together as 10^{-4} in. It will be argued later that these lines are etched micro-cracks and we shall call them cracks in the following description. It has not so far been found possible to control the occurrence of these cracks, but edges have been cleaved along which none has been observed. It is likely that such cracks are present in the as-cleaved and unstrained condition because dislocations, which might produce a crack nucleus, are not invariably found near them; however etching usually reveals a few dislocation loops apparently arising from near the crack tip as shown in fig. 2 (*b*). Such loops may be on one or all possible (110) slip planes, though more often slip is restricted to one such plane at this stage. If a crystal which has been etched is subsequently subjected to tensile stress (to about $0{\cdot}6 \times$ fracture stress, σ_f), any dislocation loops formed prior to etching may expand but an appreciable increase in the number of loops is not observed. If a crystal be stressed to this value *prior* to etching, however, there is an appreciable increase in the number of dislocations arising at or near a crack tip (fig. 2 (*c*)). As before these are revealed by etching, and the etching operation tends to inhibit the production by stress increase of further loops. It is not possible therefore to follow with etching techniques the changes produced in a particular slip band and associated with a particular crack, as a function of change in stress level, because the etching interferes with the mechanisms at work. It *is* possible to carry out a number of experiments on different specimens and to look for a pattern in development and this has been done.

As the crystal is further strained the amount of slip increases and new dislocation loops are activated at the edges of planes already populated, thus forming slip bands. The cracks may grow at these higher stresses but some increase in the amount of slip associated with the crack always precedes the growth of the crack in unirradiated crystals. By the time this stage is reached slip is, more often than not, occurring on orthogonal systems converging on the crack, but sometimes is still restricted to one system as shown in fig. 3 (*a*). At this stage the crack grows along (100) cleavage planes and the largest crack length obtainable prior to fracture varies with the impurity content; for a crystal of analysis B it was typically 5×10^{-3} in. At this size the crack can clearly be seen as such by examination with light reflected off its face.

---

† Figures 2 to 6 and fig. 8 are shown as plates.

While only the slip arising from a single crack has so far been mentioned, in practice several cracks grouped together are often responsible for the pattern observed especially where it occurs on orthogonal systems as fig. 3 (*b*). The cracks themselves cannot clearly be seen in this photograph but it has been confirmed that each slip system has originated at a crack tip of the type already discussed. The cracks described above lie in (100) planes. Crack configurations have been observed in which the crack lies in both (100) and (110) planes as shown in fig. 6. A suggested diagrammatic representation of the crack geometry is also given and this will be discussed in § 4.2.

A typical fracture surface is shown in fig. 4 (*a*) and is similar to those already reported (Stokes *et al.* 1959 c, Clarke 1959); the crack has spread out from the quadrant-shaped plane ABC, which has a radius between 5×10^{-3} and 8×10^{-3} in. long. This photograph was taken from a specimen from crystal B, and in a purer crystal (analysis A) the crack may spread

Table 2. Comparison of fracture data for unirradiated crystals (analysis A) and those given reactor irradiation to the dose range 10^{14}–10^{16} n.v.t. (epithermal)

Specimen number	Irradiation dose (n.v.t.)	Treatment	Fracture stress (10^4 lb wt in.$^{-2}$)	Strain (10^{-4})	Comments on type of fracture
36	None	None	0·67	6·7	Line + corner
35	None	Polished	1·0	42·2	Line
37	None	Etched	0·60	24·3	Line
38	10^{14}	None	1·0	1·3	Corner
39	10^{14}	Polished	1·6	7·1	Line
40	10^{15}	None	1·3	2·8	Corner
41	10^{15}	Polished	1·7	1·8	Line + corner
42	10^{16}	None	1·5	0·35	Corner
43	10^{16}	Polished	1·9	2·5	Line

out from a line or from a line + corner as shown in figs. 4 (*b*) and (*c*) respectively. An important feature of this quadrant-shaped area is the distribution of slip bands revealed by etching. Figure 5 photographed at the corner of the quadrant shaped area shows that these are along the crack front of increasingly large quadrant shaped areas, similar to those which can be formed by gradual cleaving (Gilman 1958).

If after cleaving, the crystal edges be polished away using orthophosphoric acid as for the experiments recently reported by Stokes *et al.* (1959 a, b, c), to a depth sufficient to remove the initially present crack nuclei, the crystal exhibits considerably more ductility prior to fracture, and the fracture stress is raised (table 2). It has been shown (Stokes *et al.* 1958, Clarke 1959) that cracks may then form as a result of dislocation interaction by both the mechanism due to Cottrell (1958) and Stroh (1954).

Table 3. Comparison of fracture data for crystals (analysis A) given reactor irradiation to the dose range 10^{17}–10^{19} n.v.t. (epithermal) and unirradiated crystals (analysis B)

Specimen number	Irradiation dose (n.v.t.)	Treatment	Fracture stress (10^4 lb wt in.$^{-2}$)	Strain (10^{-4})	Comments on type of fracture
50	10^{17}	None	2·3	5·3	Line + corner
51	10^{17}	Polished	2·2	4·5	Line
52	10^{17}	None	1·9	0·47	Point away from edge
53	10^{17}	Polished	2·3	2·8	Point away from edge
48	3×10^{18}	None	4·1	Some but none measurable	Point away from edge
49	3×10^{18}	Polished	5·0	ditto	Point away from edge
58	3×10^{18}	None	4·2	ditto	Corner
45	10^{19}	None	4·2	None	Corner
47	10^{19}	Polished	7·1	Some but none measurable	Corner + line
54	10^{19}	None	4·0	None	Point away from edge
55	10^{19}	Polished	4·7	1·2	Point away from edge
56	None: impure crystal	None	1·7	0·4	Corner
57	None: impure crystal	Polished	2·0	41	Point away from edge

3.2. *Irradiated Crystal*

Irradiation increases the fracture stress; it also decreases the amount of ductility obtained before fracture (tables 2 and 3). Other characteristics of the fracture vary with the dose range and so the effects will be

considered in this way. All the specimens for these results were taken from crystal A.

3.2.1. 10^{14}–10^{16} *n.v.t.*.

Unpolished specimens usually fracture from a corner and the characteristic cleavage quadrant may be seen at that corner; the radius of this quadrant is decreased as the irradiation dose, and hence the fracture stress, is increased. The change of quadrant radius, c, with fracture stress, σ_f, is such that a plot of σ_f against $c^{-1/2}$ is linear (fig. 7). Orthogonal slip systems acting on {110} planes often intersect at the edge from which the catastrophic crack propagation has originated, in a manner similar to that observed by Washburn *et al.* (1959) and observed in unirradiated specimens. However, more rarely the crack origin corresponds to the position where only one active slip band meets the crystal edge, as in fig. 3 (*a*).

Fig. 7

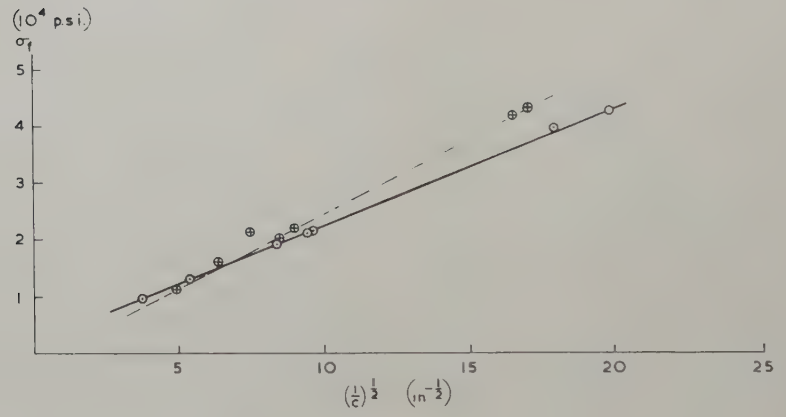

Plot of σ_f against $c^{-1/2}$ to demonstrate agreement with Griffith relation c = radius of quadrant region (ABC of fig. 4 (*a*) for example). ○, A series of measurements taken from photographs; ⊕, a series using a microscope graticule.

The amount of ductility is decreased as the irradiation dose is increased (table 2) and this is reflected in the distribution of slip bands in two ways; the bands are less numerous and they are much narrower. Irradiation seems to inhibit nucleation of new dislocation loops at the edge of existing bands.

Polished specimens usually fracture from a line as shown in fig. 4 (*b*), where the fracture has spread out catastrophically from AB. Sometimes however, (fig. 4 (*c*)) the fracture spreads out from both a line (CD) and a corner (E). The line is that of intersection of orthogonal slip systems which is generally away from the crystal edge and such specimens show the

fracture characteristics reported by Stokes *et al.* (1959 a, b, c). For specimens which clearly fracture from a line across the crystal face, both the ductility and fracture stress have been increased by polishing. A specimen which fractures as fig. 4 (*c*) may show a slightly decreased ductility as compared with one fracturing as fig. 4 (*b*). This difference in ductility is small however compared with the differences observed between pure corner and pure line-originating cracks (table 2). Polishing generally raises the fracture stress by an appreciable amount.

Typical experimental figures illustrating these various features are shown in table 2. Important features include:

(i) With the exception of specimen 41 the polished specimens are five to seven times more ductile than untreated ones, the slip being more evenly distributed along the whole length of the crystal.

(ii) There is an increase in the fracture stress with irradiation.

(iii) Polished specimens fracture at a higher stress than unpolished ones.

(iv) Etching (specimen 37) gives enhanced ductility, but less than polishing. The specimen corners were not detectably rounded by the etching treatment.

(v) For irradiations in this range the occurrence of a combined corner + line originating fracture (as specimen 41) is the exception rather than the rule.

3.2.2. 10^{17}–10^{19} *n.v.t.*

In this range the occurrence of an unambiguous corner or line originating fracture is now the exception, and in addition a new fracture configuration is observed occurring from a surface point near the centre of the face in question. A typical case is illustrated in fig. 4 (*d*).

The strains observed at 10^{18} n.v.t. were usually below 10^{-4} but at 10^{17} n.v.t. they were just measurable. Unpolished specimens invariably show that the crack origin has been at a line + point (fig. 4 (*c*)) or at a point (fig. 4 (*a*)). This point may be at the crystal edge or away from it, but always at a surface. Polished specimens, on the other hand, have the crack origin coming from either a point or a line or both. If from a point then the point is at the crystal surface and if from a line then the line is within the crystal.

At 10^{19} n.v.t. much the same pattern of crack characteristics is observed, but for unpolished specimens there is usually no plastic deformation; none is measurable, and in addition no slip lines are revealed by etching for cases of corner-originating fracture. A polished specimen by comparison fractures at a very much higher stress and shows signs of slip.

Some typical experimental results are given in table 3. Rather more examples are given for each dose than before to demonstrate the variation due to the extra fracture characteristics. The pattern of behaviour is not

nearly so clear here, but attention is drawn to these aspects:

(i) Polishing generally increases ductility if the comparison is made between corner and line-originating fracture, or between specimens both of which show point-away-from-edge originating fracture.

(ii) The general increase in fracture stress with increase in irradiation dose is maintained.

Micro-cracks have been observed along a face (fig. 8) away from an edge and it is probable that they are responsible for some of the slip and the fracture in, for example, the cases of specimens 52, 53, 54 and 55 of table 3. It has been noticed however that such cracks tend to occur nearer the araldited ends and so may be associated with stress concentrations due to non-axial loading. This defect would show up more in irradiated (and hence more brittle) specimens.

3.3. *Less Pure Crystal*

It has been shown (Anderson and Clarke 1959 a, b) that impurities increase the fracture stress but do not change the ductility. This is in contrast to the effect of irradiation which raises the fracture stress and decreases the ductility. We include some comparative results on these effects in table 3.

§ 4. Discussion

4.1. *Unirradiated Crystal*

We have suggested previously (Clarke 1959) that micro-cracks may be responsible for the orthogonal slip so often associated with fracture and this is the basis of the present interpretation. Whether these micro-cracks are present before cleaving and are opened up by cleaving, or are formed during the cleaving is not certain. They cannot be detected prior to etching; the crystal edges are so imperfect when viewed at a magnification of around $\times 2000$ however, that it would be difficult to distinguish small cracks from cleavage steps, etc. (see fig. 2 (*a*)). Etching might be expected to reveal cracks more clearly however and it is believed that the black lines at right angles to the crystal edge in fig. 2 (*b*) are cracks revealed in this way. This interpretation is consistent with:

(i) The dislocation loops originating near the line end (fig. 2 (*b*)). If the line were a crack as suggested, the tip would act as a stress concentrator and hence as a preferential source of slip. Small dislocation loops can be created by a slowly propagating cleavage crack (Gilman 1957) but the dislocations typified in fig. 2 (*b*) are not correctly oriented with respect to the crack to be related to these.

(ii) Stressing prior to etching increases the number of loops present near such black lines (fig. 2 (*c*)).

(iii) The lines continue unbroken across both faces forming the edge (see both the long and the shorter lines of fig. 3 (*a*)).

(iv) Some of the lines observed are longer after stressing at near the fracture stress (fig. 3 (*a*)). These longer lines are unambiguously cracks, since they may be seen in the unetched condition by light reflected off the crack faces.

(v) After etching, the production of more dislocations near the line end is inhibited. This could be because the etchant tends to round off the crack tip and so reduce the stress concentration there.

These cracks are initially too small to propagate as Griffith cracks, for taking

Surface energy per face, $S = 1{\cdot}5 \times 10^{-2}$ lb wt in.$^{-1}$ (2700 ergs cm^{-2}: Gilman 1959).

Young's modulus, $E = 4{\cdot}4 \times 10^{7}$ lb wt in.$^{-2}$ (3×10^{12} dyn cm^{-2}: Gilman 1959).

Fracture stress, $\sigma_f = 10^{4}$ lb wt in.$^{-2}$, a typical value for an unirradiated crystal of analysis B. Then if we take the form of Griffith equation to be $\sigma_f = (2ES/\pi c)^{1/2}$

(e.g. Petch 1954) the critical crack length, c, turns out to be about 4×10^{-3} in. compared with a typical initial size of 10^{-4} in.

However, it is noted that the maximum crack size seen on unirradiated crystals after stressing (5×10^{-3} in.) is close to that calculated from the Griffith equation. This suggests that the crack may propagate catastrophically as a Griffith crack when it grows to a critical size, and more evidence will be given later to support this.

The dislocation pattern of fig. 5 is similar to that reported by Gilman (1958) and would seem to indicate that at the beginning of its growth the quadrant shaped area grows in radial bursts of about 10^{-4} in. As the crack opens up, the driving force must decrease and so the crack slows down; a crack velocity is thus reached at which dislocation loops can be nucleated (Gilman 1957–1958) and the remaining crack energy is absorbed in this way. As the external stress is further increased the crack energy is again raised and the process is repeated. In fig. 3 (*a*) there is a forked dislocation pattern ahead of the crack tip. This is interpreted as representing the lines of intersection of these loops with the crystal surface; a similar pattern has been fully discussed by Washburn *et al.* (1959). At this crack size the crack front below the surface must, on this interpretation, be bowing out ahead of the surface crack. The closeness in the size of the largest cracks seen prior to fracture and the radius of a quadrant shaped area (§ 3.1) suggests that the quadrant represents the crack area prior to catastrophic propagation. The change in the size of this area as the fracture stress is raised by irradiation is consistent with this interpretation and this will be discussed more fully in § 4.2.

So far we have discussed the presence of (100) micro-cracks. It is fairly easy to cleave magnesium oxide along {110} though it is difficult to obtain large areas in this way. However, it would seem reasonable for whatever mechanism gives rise to (100) cracks to give rise also to (110) cracks and we

interpret the photograph of fig. 6 in this way. Referring to the diagram of fig. 6, it is suggested that the original crack occurs over the adjacent {100} faces containing AB and BC, and occupies the quadrant-shaped area ABC in (110). At C the crack end changes from (110) to (100) and we assume for the sake of illustration that the length AC also changes as it reaches the line CD perpendicular to the face containing BCE. Then as the crack front AC sweeps out to some point such as D, the end A must also change direction across the face containing AB towards the general direction of D, if the crack plane is to be continuous and eventually complete. The line ABCE of the diagram represents the corresponding line in the photograph and it is suggested that the final part of the line in the photograph, corresponding to the continuation of the crack line BA, may be explained in this way.

4.2. *Irradiated Crystal*

It has been observed that the initial cracks present in a crystal do not normally propagate until some slip has occurred. There are two consequences of this. The first is that reactor irradiation should increase the fracture stress because the electronic re-distribution or the displaced atoms it produces might be expected to pin dislocations. This would increase the stress required to move dislocations and hence the fracture stress. The second is that it should, in principle, be possible to reach a stress below that required to move dislocations but sufficient to propagate the micro-crack as a Griffith crack without any growth having to take place. Both of these conditions are realized in practice. It is quite clear from table 3 that the fracture stress is raised by irradiation and at a dose of 10^{19} n.v.t. the crack propagates catastrophically without any detectable slip (cf. specimens 45 and 47). A corollary of this interpretation is that the length of the micro-crack prior to catastrophic crack propagation should be related to the fracture stress by the usual Griffith-type equation. More particularly a plot of fracture stress σ_f, against $c^{-1/2}$, where c is the crack length, should be linear; fig. 7, which includes data from irradiated and unirradiated specimens, shows that it is.

If dislocations are not able to move at the fracture stress for an unpolished crystal irradiated at 10^{19} n.v.t., then a polished crystal given this dose should fracture at a higher stress, above that necessary to operate dislocation sources, because dislocation interactions are now necessary to *form* crack nuclei. This would explain the unusually large differences in fracture stress between the polished and unpolished crystal results of specimens 45 and 47. However, the crack size is critical here because the fracture stress would vary with it in the case of unpolished crystals.

§ 5. Conclusions

Microcracks typically 10^{-4} in. long present after cleaving may be responsible for the fracture characteristics of as-cleaved magnesium oxide single crystals. At this size the cracks are too small to propagate as

Griffith cracks; nevertheless they do propagate and the following stages are involved:

(i) At about $0{\cdot}6\sigma_f$ slip arising from the microcrack tip begins to spread across the crystal.

(ii) The crack grows gradually as the applied stress is further raised.

(iii) When the crack reaches a critical size it propagates catastrophically, probably as a Griffith crack.

If the edges of the crystal be removed by chemically polishing to a depth sufficient to remove the micro-crack, crack nucleation then has to take place by dislocation interaction and there is an increase in the amount of slip preceding fracture; hence polished crystals exhibit greater ductility than unpolished ones.

Reactor irradiation affects the crystal in several ways:

(*a*) The fracture stress is raised.

(*b*) The amount of slip preceding fracture is decreased.

(*c*) Any slip bands produced are narrower.

(*d*) The area over which micro-cracks have to grow to cause fracture is reduced to conform to a Griffith-type relation between fracture stress and crack length.

At irradiation doses of 10^{19} n.v.t. micro-cracks can grow catastrophically in unpolished specimens at stresses below those required to operate dislocation sources.

Acknowledgments

We would like to thank various of our colleagues for discussions on the subject matter of this paper. We are also grateful to Dr. P. Murray and Mr. J. Williams for their encouraging interest during the period of research.

References

Anderson, P. J., and Clarke, F. J. P., 1959 a, U.K.A.E.A. Report AERE M.491; 1959 b, E.A.E.S. Symposium on Reactor Materials, Stockholm, U.K. 6.

Clarke, F. J. P., 1959, *Special Ceramics*: Proceedings of a Symposium held at the British Ceramic Research Association, July (London: Heywood & Co.).

Cottrell, A. H., 1958, *Trans. Amer. Inst. min. (metall.) Engrs*, **212,** 192.

Ghosh, T. K., and Clarke, F. J. P., 1959, U.K.A.E.A. Report AERE R.3182.

Gilman, J. J., 1957, *Trans. Amer. Inst. min. (metall.) Engrs*, **209,** 450; 1958, *Ibid.*, **212,** 310; 1959, Fracture Conference, Swampscott, U.S.A.

Gorum, A. E., Parker, E. R., and Pask, J. A., 1958, *J. Amer. ceram. Soc.*, **41,** 5.

Petch, N. J., 1954, *Progr. Met. Phys.*, **5,** 1.

Stokes, R. J., Johnston, J. L., and Li, C. H., 1958, *Phil. Mag.*, **3,** 718; 1959 a, *Ibid.*, **4,** 137; 1959 b, *Trans. Amer. Inst. min. (metall.) Engrs*, **215,** 437; 1959 c, *Phil. Mag.*, **4,** 920.

Stroh, A. N., 1954, *Proc. roy. Soc.* A, **223,** 404; 1955, *Ibid.*, **232,** 548.

Washburn, J., Gorum, A. E., and Parker, E. R., 1959. *Trans. Amer. Inst. min. (metall.) Engrs*, **215,** 230.

Etching of Strained Aluminium†

By G. A. Bassett and C. Edeleanu
Tube Investments Research Laboratories, Cambridge

[Received February 15, 1960]

Abstract

The initiation of etch attack of strained aluminium has been studied by optical and electron microscopy. It is concluded that an important factor is rupture of the protective natural oxide film and its subsequent failure to repair completely in a short time. Slip, in a direction closely parallel to the specimen surface, or a deformation in compression appears to damage the oxide film more severely than deformation in tension. No correlation between etch pits and the end of dislocation lines has been found.

§ 1. Introduction

Amelinckx (1953) showed that it was possible to etch slip lines in aluminium using a HNO_3/HCl/HF mixture and suggested that dislocations were being etched. Forsyth (1954) however showed that if the specimen was electropolished after straining it no longer was possible to etch the slip lines and he therefore suggested that the attack observed by Amelinckx was due to the initiation of the corrosion reaction at the steps left by the slip process. Lacombe (1947) and Lacombe and Beaugard (1948) and many others have shown that it was possible to obtain pits so distributed on the surface of aluminium that it was reasonable to assume them to indicate the position of dislocations. It seems however that such etching is only possible if the metal has impurities present and it has been suitably heat treated to allow the condensation of such impurities on the dislocations (Wyon and Crussard 1951, Forty and Frank 1955). More recently Braun *et al.* (1958) reviewed some of the earlier work and demonstrated that they could only obtain pits at grain boundaries after a period of room temperature ageing during which they suggested impurities diffused through the boundaries and into the oxide film.

Somewhat similar results have been obtained on various other metal systems and there is a fair amount of evidence that, at least in metals, dislocations are not easy to etch unless some impurity is associated with them. On the other hand many alloys tend to suffer a type of failure known as stress corrosion. The detailed mechanism of this is far from understood. One school has held that failure was due to highly enhanced

† Communicated by the Authors.

corrosion due to the high stresses or strain at the tip of a crack and this view is particularly favoured by Hoar and Hines (1956) and Hoar and West (1958) whose interpretation of their electrochemical measurements is consistent with such a theory. There are however various difficulties in accepting this theory, one of which is that if strain or stress had a really marked effect on corrosion reactions the art of etching clean dislocations would presumably be well established by now. In view of this and of the fact that there are other corrosion phenomena such as the 'tunnelling' which occurs in aluminium (see for example Pearson *et al.* 1952), it was considered worth re-examining the etching of aluminium to see whether the reasons for pit localization could be established.

§ 2. Experimental

Two grades of aluminium have been used in the work; $\frac{1}{4}$ in. square bar in 99·99% Al and British Aluminium super purity sheet containing the following impurities:

Fe %	Si %	Cu %	Zn %
0·0010	0·0030	0·0015	0·0003

A few other batches of material including some zone-refined aluminium were used but no differences in behaviour were observed.

The specimens were annealed for at least $\frac{1}{2}$ hour at 600°C and air cooled. Electropolishing, whether for micro-examination or for thinning, was carried out in the usual 1–5 perchloric–alcohol bath at about 20 v.

Etching was carried out in freshly made up 47% HNO_3, 3% HF, 50% HCl solution (often used for this type of experiment) or in 3% NaCl at 1·5 v anodic to platinum. Unless otherwise stated it was carried out soon after stressing to avoid ageing effects of the Braun type.

Anodizing, for replica work, was carried out in a solution of 12 g disodium hydrogen phosphate 0·4 ml H_2SO_4 made up to 100 ml and at 30 v. For the optical work the anodizing was carried out in a 10% H_2SO_4 solution at various voltages up to 15 v.

2.1. *Etching in HNO_3–HCl–HF*

The initial experiments confirmed the finding of Amelinckx and Forsyth, and fig. 1† is a low magnification light micrograph showing the attack at slip lines on a specimen previously strained. Figure 2 shows a higher magnification micrograph of a less severely etched grain and in this it can be seen that the pits tend to bunch in a way which could be taken to be due to pile-ups of dislocations.

The initial experiments were carried out on bent specimens and it was very noticeable that by no means all slip lines etched up, that by far the

† All figures are shown as plates.

greater number of those that did were on the compression side of the specimen and that virtually none was on the tension side. This observation was subsequently confirmed by etching specimens strained in tension and in compression. In addition specimens were strained in torsion and with these there was, if anything, a greater tendency for pitting at slip lines than in the compression specimens.

Examination of the pits with the electron microscope using the oxide replica technique confirmed the light microscope observations. In addition it has been frequently found that the pitting was greatest at those slip lines which showed no, or only very small, steps at the surface (i.e. slip direction was approximately in the plane of the surface). This is shown in fig. 3 in which case it is easy to appreciate that the surface was very nearly parallel to a (110) face (the etching reagent develops (100) facets) and on such a surface slip can occur making virtually no step as indeed the micrograph shows. Figure 4 shows a different example in which etching has again occurred on a slip system making a small surface step but the important thing to note is that larger slip steps are plainly visible in a different system which have not been etched at all.

Pits were sometimes observed at visible slip steps especially in the compression specimens and fig. 5 shows an example chosen since it shows stages in the development of pits at such slip traces. In this case it seems that the upper side of the slip line is high relative to the other side and that the slip has occurred in such a way that the new surface makes an acute angle with the original surface and there is an 'overhang'. At stage one, only the high side has been attacked, at two attack is starting on the lower side and this is better seen at stage three. It is interesting to note that at stage four a fifth face has started developing on the high side of the step. This development of a fifth (and sometimes of even a sixth face) is fairly frequent.

In an attempt to correlate slip direction with tendency to pit a specimen was etched in the usual way, then strained and re-etched in the hope that a few 'old' etch pits would identify the slip direction but generally the second etch destroyed the evidence and only a few cases have been found. The available evidence indicates that where steps are present pitting is more prone to occur when the step makes acute angles with the surface than when it makes an obtuse angle and this presumably explains the observed difference between compression and tension.

The observation of Braun *et al.* that a few weeks' ageing at room temperature caused the grain boundaries to etch up was confirmed. It was found in addition that a specimen strained and then allowed to age, etched only at the grain boundaries, the slip lines being ignored whether or not the specimen was polished after straining. The materials now being used are not pure enough to recrystallize at room temperature and there must be many dislocations left on slip planes so that it seems that room temperature ageing does not make dislocations prone to etching. Similar ageing experiments were then repeated but the specimens were stored

in well-pumped down ampoules and in this case the strained specimen showed both grain boundary and slip line etching if no polishing was done after straining, fig. 6, but not otherwise. Again it will be noticed that not all slip bands etch up equally, presumably slip direction being important in this case also.

2.2. *Etching of Anodized Specimens*

The results on strained specimens seemed to be most easily explained by assuming that the localization of the pits was due to the rupturing of the natural oxide film on the aluminium by the slip process and that the repairing process of the cracks in the film left a local weakness. The film on aluminium is known to be highly inert even in acid and once it is 'punctured' because of some defect the attack on the metal is likely to be very rapid locally, and cause pitting before the reaction starts elsewhere. The pits therefore denote locations where the film happens to have been weak and has been punctured by the etching solution rather than where the metal is particularly reactive. Whilst it is easy to see how the incorporation of impurities in the film can cause the necessary type of weakness it is not so easy to see why a film broken mechanically should not repair effectively.

The natural film on aluminium is very thin and, at present, there seems to be no suitable technique for studying directly the manner in which it breaks. For this reason the film was thickened by anodizing in sulphuric acid and it was examined after the metal had been strained. It was found that thick films obtained by anodizing at 15 v cracked at right angles to the tensional direction and that the cracks ran with little deviation from grain to grain, fig. 7. In compression specimens the cracking occurred as a result of secondary tensional stresses and ran parallel to the compression direction showing that at least the thick films can accommodate some strain. The overall appearance was very similar to that of the cracks in the brittle lacquers sometimes used in stress analysis. With thinner films however the cracking was influenced by the slip process and with a 7 v film the cracking, as can be seen in fig. 8, occurred at slip lines. It seems reasonable to assume that the even thinner natural film breaks at slip lines by a mechanism similar to that proposed by Brame and Evans (1958) and Evans and Schwarzenberger (1959).

Etching experiments carried out on the strained anodized specimens, as might have been expected, confirmed that pits formed at cracks in the film whether or not these were at slip lines, and with the thicker films it was often possible to see the film left in position above the pits particularly if the etching were done in the sodium chloride solution as in the case shown in fig. 7. Naturally the anodized films cannot be repaired without further anodizing and these experiments only show that films can break but not show directly why the damage is not healed properly in all cases unless one makes the somewhat bold assumption that in tension the break

is a clean one and is easily repaired, but when shear or compression is present the break may be less clean; portions of the film may be left under strain and that it is this debris that forms the local weakness in the film.

2.3. *Etching in NaCl*

The above experiments are somewhat far removed from stress corrosion since the reagent used would not produce this type of failure even in a susceptible alloy. To get a step nearer, etching experiments were also carried out in NaCl. In this case the etching was normally random and it was found that pitting could not be produced at the slip lines of strained specimens except as stated above when these were lightly anodized. Even in these by no means all the cracks in the film etched up. This was not entirely surprising taking account of the chemistry of the process. The NaCl solution is not a particularly reactive reagent until such time as the reaction starts when, because of a hydrolysis reaction, it becomes locally highly acid and the reaction is therefore autocatalytic (Edeleanu and Evans 1951). Because of this the first few pits which form take all the available current and no fresh pits can start.

It was considered that a way to counter the autocatalytic mechanism would be to strain a specimen by bending whilst under the solution, the etching current only being applied for the period of straining. Under such conditions metal would be immediately exposed to etching conditions where the oxide film was ruptured and there would be a minimum opportunity for the film to repair. The extensive pitting at slip lines on an electropolished specimen produced by such an experiment is shown in fig. 9. It will be noted that cross slip occurred frequently in the neighbourhood of pits presumably because of local stress raising effects.

2.4. *Transmission Electron Microscopy*

The most satisfactory manner in which to study the relation between pits and dislocations is to use transmission electron microscopy and the results so far obtained using this technique are consistent with the view expressed above that pits are formed mainly because of weaknesses in the oxide films. No evidence has so far been found to indicate that dislocations in the metal play a direct part in initiating the etching process. Figure 10 for instance shows a strained specimen prepared by thinning from both sides and etching the thin film so produced. Networks of dislocations are observed but not in any marked association with etch pits. Examples have been found where interactions between pits and dislocations have occurred and fig. 11 shows two pits in which dislocations, almost in the plane of the foil, 'outcrop'. The dislocation pattern, appears distorted in the neighbourhood of pits. It should be noted however that the 'outcrop' of dislocations in pits as in fig. 11 is a reasonably unusual occurrence and seems to be no more frequent than might be expected

taking into consideration the density of dislocations. Figure 12 is more typical of unstrained material in which only two dislocations are visible. One of them does not seem to have initiated a pit whilst the other is near a pit but unlikely to have initiated it.

Dislocations in aluminium may be moved under the influence of the beam so that it is never absolutely certain that the pattern is exactly as it was whilst the etching was carried out, but the pictures were taken quickly and are thought to represent reasonably accurately the state of the original specimen. What may be significant is that the outcropping dislocation finds no difficulty in moving eventually and those in fig. 11 were seen to do so indicating that they were not anchored by 'hollowing out' on a scale smaller than could be distinguished in the micrograph.

§ 3. Discussion

For most metals the anodic reaction, that is the removal of atoms from the metals and their solvation as ions into the solution, requires a very small energy of activation (i.e. it is not highly polarized) unless oxides are present. This is presumably due to the fact that on normal surfaces there must always be frequent steps and the reaction can occur in stages as suggested by Conway and Bockris (1958). The most important surface steps are presumably those due to the emergence of dislocations since these are indestructible and under suitable conditions it should be possible to locate clean dislocations by etching but this does not appear to be at all easy, at least in the case of metals. One probable reason is that one requirement for etching dislocations is that the reaction be carried out under near equilibrium conditions which, with reactive metals such as aluminium in aqueous electrolytes is impossible. For this reason it is not considered entirely surprising that in the present case the pits have not been proved to locate dislocations but have occurred at places where the oxide film, the more important factor in controlling the anodic reaction, has been damaged.

As already stated it is not clear why air formed films do not readily repair after being damaged. They seem to do so eventually (a few weeks) if the specimen is not stored in vacuum, but a few minutes, certainly an hour or two in air, ought to be sufficient, which does not seem to be the case. The only explanation seems to be that it is the strain in the oxide debris. That such strain exists has not been possible to demonstrate in the present case but fig. 13 shows a thin tarnish film on brass broken as a result of slip. In this case the optical properties are such that an interference pattern can be seen from the light reflected from the metal and the oxide surface and it seems that the film has to some extent lifted and must have distorted and strained considerably. Damage of this type would not presumably be completely repairable by exposure to the conditions which first caused the film.

The etching of dislocations in impure metals is presumably due to a local increase in the reactivity of the oxide resulting from the incorporation

of impurities in the film but it is not easy to see how this occurs in the room temperature ageing experiments leading to grain boundary etching. In this case the film grows for all intents and purposes to its maximum thickness during the first few hours and it is not easy to visualize how it subsequently becomes contaminated.

From a corrosion point of view, apart from the pit initiation, it is at least as important to consider what is likely to occur once a pit has started no matter what the reason may have been. Under normal circumstances the metal surface will not be a cube face, so that whether or not there are dislocations there will be steps present and a pit will be able to form and grow by layers of atoms 'peeling off' from the outside edges of the pit. It is relevant to consider what will happen when the pit eventually meets a dislocation (e.g. as in fig. 11).

In such cases the face on which the dislocation emerges may contain a greater length of step per unit area than other faces and might then be expected to corrode faster than the other faces. Moreover such a face would no longer require to extend to the outer surfaces since steps would now be present and the pit may elongate in the direction of the dislocation. This presumably explains the observed formation of a fifth and sixth face in certain cases. Generally the dislocation would not however be in a [100] direction so that as the pit grows the face following a dislocation would change to an alternative cube face and the growth direction of the pit would also alter through right angles. Such pits sometimes called tunnels are in fact found in aluminium as a result of corrosion in tap waters (Pearson *et al.* 1952), or by anodic attack in chlorides (Burger *et al.* 1955). The formation of tunnels of the type found in practice probably requires something more than dislocations to be present since it is difficult to explain otherwise why they remain so narrow. Up to now they have been found in solutions in which it is reasonable to expect that the autocatalytic process mentioned above is likely to be operative. In such solutions, since the overall amount of corrosion which occurs is controlled by some outside factor such as the amount of oxygen available or the current supplied, the reaction will always tend to be concentrated at only a few points and especially at any point where there is a slight advantage. At other points the reaction would halt so that once a pit has 'found' a dislocation the reaction on the faces not containing dislocations may cease entirely. Since from both the stress corrosion and tunnelling corrosion point of view the manner in which pits extend rather than how they initiate seems more important, it may still be that even though it is difficult to 'etch' clean dislocations these may play an important part in the corrosion process.

Acknowledgments

We thank several laboratory colleagues for helpful discussions, Mr. T. Law for his able experimental assistance, and the Chairman of Tube Investments Ltd. for permission to publish this paper.

References

Amelinckx, S., 1953, *Phil. Mag.*, **44,** 1048.
Brame, D. R., and Evans, T., 1958, *Phil. Mag.*, **3,** 971.
Braun, I., Frank, F. C., and Meyrick, G., 1958, *Phil. Mag.*, **35,** 1312.
Burger, F. J., Full, F. V. G., and Harris, P. H., 1955, *Bull. Inst. Metals*, September, p. 6.
Conway, B. E., and Bockris, J. O'M., 1958, *Proc. roy. Soc.* A, **248,** 394.
Edeleanu, C., and Evans, U. R., 1951, *Trans. Faraday Soc.*, **47,** 1121.
Evans, T., and Schwarzenberger, D., 1959, *Phil. Mag.*, **4,** 889.
Forsyth, P. J. E., 1954, *Phil. Mag.*, **45,** 344.
Forty, A. J., and Frank, F. C., 1955, *J. phys. Soc., Japan*, **10,** 656.
Hoar, T. P., and Hines, J. G., 1956, *J. Iron St. Inst.*, **182,** 124.
Hoar, T. P., and West, J. M., 1958, *Nature, Lond.*, **181,** 835.
Lacombe, P., 1947, *Strength of Solids*, Report on Bristol Conference (London : The Physical Society).
Lacombe, P., and Beaugard, L., 1948, *J. Inst. Metals*, **78,** 7.
Pearson, E. C., Huff, H. J., and Hay, R. H., 1952, *Canad. J. Tech.*, **30,** 311.
Wyon, G., and Crussard, C., 1951, *Rev. Metall.*, **48,** 121.

The Anhysteretic Remanence of Magnetic Recording Tapes†

By E. P. Wohlfarth
Department of Mathematics, Imperial College, London

[Received March 24, 1960]

Abstract

The anhysteretic properties of magnetic tapes are discussed by introducing the idea of internal demagnetization spectra.

§ 1. Introduction

Recent discussions (Schwantke 1958, Woodward and Della Torre 1960, Daniel and Levine 1960) of the physics of the process of magnetic tape recording with high-frequency bias have emphasized again (Greiner 1953, Westmijze 1953, Wohlfarth 1960) the close correspondence between this process and that of the acquisition of the anhysteretic remanent magnetization (Wohlfarth 1957). The initial slope s of a curve relating this magnetization $I_{ar}(H)$ with direct field H (reduced to zero after the previous application and slow reduction of an alternating field of high initial amplitude) gives to some extent (Daniel and Levine 1960) a measure of the sensitivity of the tape under recording conditions. However, the $I_{ar}(H)$ curves of actual tape materials are only linear in H up to certain field strengths H_0, where

$$sH_0/I_{ar}(\infty)=I_{ar}(H_0)/I_{ar}(\infty)=j_b<1, \quad . \quad . \quad . \quad . \quad . \quad (1)$$

say, and where $I_{ar}(\infty)$ is the static saturation remanence. If j_b is considerably less than 1, then, for distortion-free recording, only a small fraction of the maximum possible signal is, in fact, useful.

The values of the initial slope s and of the ratio j_b may be discussed as follows: Although s is ideally infinite, it assumes finite values due to the action of internal demagnetization effects (Néel 1943, Wohlfarth 1957; see also Daniel and Levine 1960). These effects arise as a result of the interactions between the magnetic particles on the tape, the presence of non-magnetic cavities inside the particles (Osmond 1953, Wohlfarth 1959), and for other reasons. The magnetostatic problems raised by these effects are very complex (see, for example, Wohlfarth 1955, Brown and Morrish 1957), and it has been customary to analyse them formally in terms of an internal demagnetization coefficient N_i, such that $s=1/N_i$ (here external demagnetization effects are either assumed to be negligibly small, as with longitudinal magnetization in thin tape specimens, or to have been allowed for). However, if N_i were constant throughout the material, then the ratio j_b in relation (1) would equal 1 (Wohlfarth 1957). In order to interpret observed values $j_b<1$ it is thus necessary to introduce the idea of *internal demagnetization spectra*, such that $n(N_i)dN_i$ gives the relative volume of the

† Communicated by the Author.

magnetic material with internal demagnetization coefficients in the range dN_i. The form of this distribution function is determined by such properties of the tape as the dispersion and orientation of the magnetic particles, which in their turn determine other effects such as noise (Howling 1956). It is shown here that $n(N_i)$ may be estimated for a magnetic tape (or, indeed, for any other heterogeneous magnetic material) from accurate measurements of the anhysteretic remanence curve over a wide range of the direct field strength.

§ 2. Calculation of the Internal Demagnetization Spectrum

Let
$$\left.\begin{aligned} j_{ar}(h) &= I_{ar}(H)/I_{ar}(\infty), \\ h &= H/I_{ar}(\infty), \end{aligned}\right\} \quad \text{where} \quad \ldots\ldots \quad (2)$$
and where $I_{ar}(H)$ is the anhysteretic remanent moment per unit volume of the magnetic material of the tape. Then, in terms of the distribution function $n(N_i)$,

$$j_{ar}(h) = \int_0^h n(N_i)dN_i + h\int_h^\infty n(N_i)d(\ln N_i), \quad \ldots\ldots \quad (3)$$

so that
$$n(h) = -hd^2j_{ar}(h)/dh^2, \quad \ldots\ldots \quad (4)$$

satisfying the normalization condition

$$\int_0^\infty n(N_i)dN_i = 1. \quad \ldots\ldots \quad (5)$$

Fig. 1

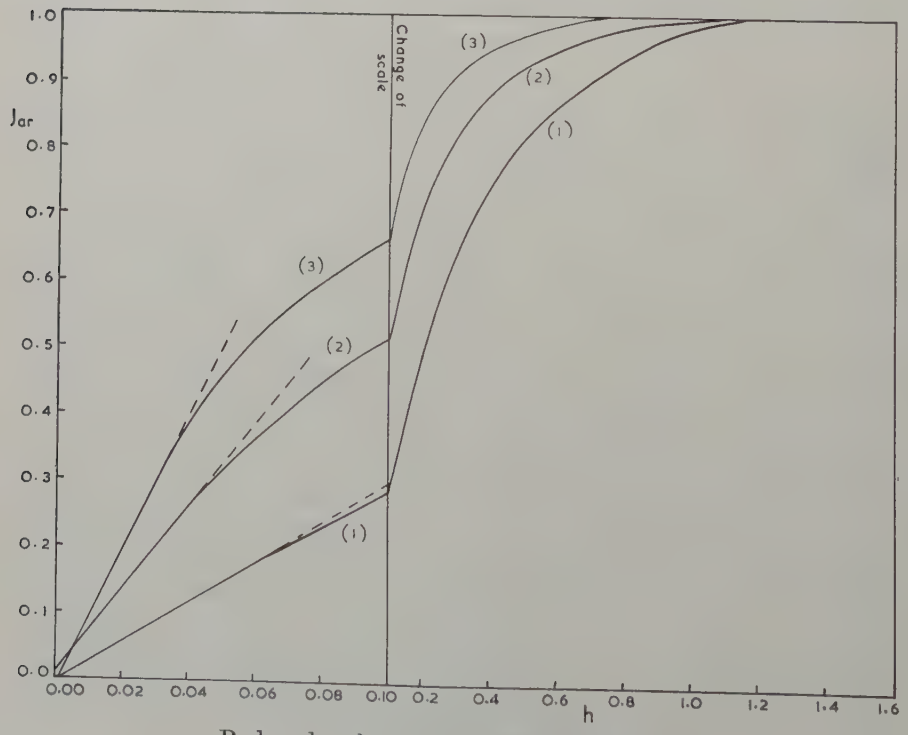

Reduced anhysteretic remanence curves.

Figure 1 shows $j_{ar}(h)$ curves for three distinct types of tape, and the table summarizes their relevant properties. Here s is the initial slope of the anhysteretic remanence curve $(dj_{ar}/dh)_{h\to 0}$ and $1/s$ gives the value of N_i which would have been calculated as the *unique* internal demagnetization coefficient in the absence of this analysis. Also N_0 gives the reduced field $H_0/I_{ar}(\infty)$ up to which the $j_{ar}(h)$ curve is linear, and N_1 the reduced field $H_1/I_{ar}(\infty)$ beyond which $j_{ar}(h)$ is equal to 1. Hence, from relation (4),

$$n(N_i)=0 \text{ for } \left.\begin{matrix} N_i<N_0, \\ N_i>N_1. \end{matrix}\right\} \quad . \ . \ . \ . \ . \ . \ . \quad (6)$$

Also, in the table, $j_b=j_{ar}(N_0)=N_0 s$ gives the relative extent of the linear portion of the curve along the j_{ar} axis, defined by relation (1), and $d=(N_1-N_0)$ is the width of the internal demagnetization spectrum. The quantities sd and $(\beta+1)/(\alpha+1)$ are used in the following analysis. Finally, N_m gives the most probable value of N_i, defined as that where $n(N_i)$ is a maximum. It appears that N_m is quite different from $1/s$, so that this last quantity has no direct significance, although $N_m s=0{\cdot}58\pm 0{\cdot}05$ for all three tapes.

Properties of Magnetic Tapes

Tape	s	$1/s$	N_0 $=H_0/I_{ar}(\infty)$	N_1 $=H_1/I_{ar}(\infty)$	j_b $=N_0 s$	d $=(N_1-N_0)$	sd	$\frac{\beta+1}{\alpha+1}$ (calc.)	N_m
1	3·1	0·32	0·055	1·12	0·17	1·06	3·3	3·0	0·19
2	6·2	0·16	0·043	1·10	0·27	1·06	6·6	8·0	0·10
3	10·6	0·09	0·028	0·80	0·29	0·77	8·2	10·6	0·05

The various quantities in the table could all be obtained from the measurements with reasonable accuracy.

Figure 2 shows the $n(N_i)$ curves for the three tape specimens obtained from fig. 1 and relation (4). The calculations were carried out by a combination of graphical interpolation and numerical differentiation, and, although the results are necessarily not too accurate, the normalization condition (5) was easily satisfied to within about 5%. If this analysis is applied more widely it should be possible to develop more accurate methods of calculation or even of automation.

§ 3. Analysis of the Results

As there is no simple theoretical formula for the curves of fig. 2, and since direct numerical calculations based on those curves are not sufficiently accurate, the results described in § 2 were analysed on the basis of an approximate though general expression for the distribution function, of the form

$$n(N_i)=AN_i(N_i-N_0)^{\alpha}(N_1-N_i)^{\beta}\geqslant 0, \quad . \ . \ . \ . \quad (7)$$

where A is the normalizing constant. Relation (7) satisfies (6), and, with

$0 < \alpha \ll 1$, $\beta \gg 1$, describes the curves of fig. 2 qualitatively quite well. It then follows from (3) and (7) that

$$s = (\alpha+\beta+2)[N_0(\beta+1)+N_1(\alpha+1)]^{-1}, \quad . \quad . \quad . \quad . \quad . \quad (8)$$

so that

$$j_b = 1 - sd[1+(\beta+1)/(\alpha+1)]^{-1} \geqslant 0. \quad . \quad . \quad . \quad . \quad . \quad (9)$$

Fig. 2

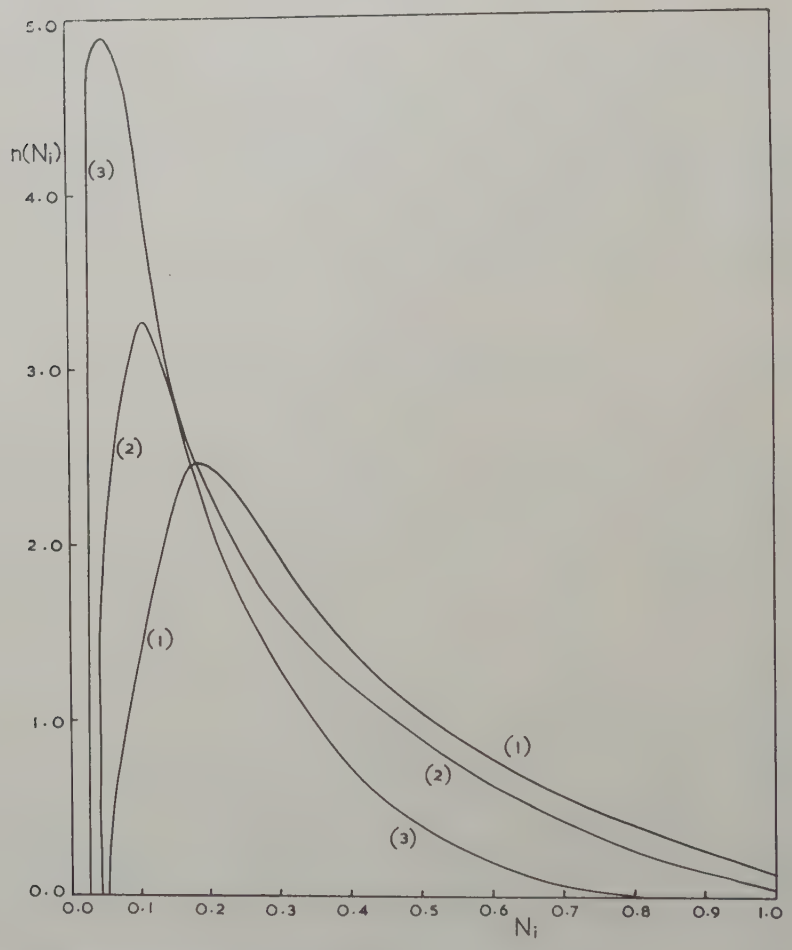

Internal demagnetization spectra. N_i, internal demagnetization coefficient; $n(N_i)$, distribution function, referred to the volume of the magnetic material.

Other approximations to $n(N_i)$ were also investigated; in all cases j_b depends only on the product sd and a form factor. Relation (9) shows that for large values of j_b, which are desirable, it is necessary to have a tape material with the following properties,

(1) Low anhysteretic slope s; this is unfortunate as it implies that high j_b, i.e. high signal, and high sensitivity are difficult to obtain simultaneously.

(2) A low value of the width, d, of the internal demagnetization spectrum; this result is to be expected on general grounds and could be brought about by good dispersion, orientation, etc. of the tape particles.

(3) A high value of the form factor $(\beta+1)/(\alpha+1)$, i.e. a rapid rise followed by a rapid decay of the distribution function $n(N_i)$; this state of affairs could again be brought about by good dispersion. Using relation (9) and the observed values of s, $d=(N_1-N_0)$ and $j_b=N_0 s$, all of which characterize the *extreme regions* of the anhysteretic remanence curve, it is now possible to calculate the values of the form factor, and the results are also shown in the table. They may then be compared with the actual form of the distribution function, obtained from the anhysteretic remanence curve over the *whole range* of the direct field strength from relation (4).

Although *specimen* 1 has a low anhysteretic slope s, it has nevertheless also a very low value of j_b. The calculated value of the form factor $(\beta+1)/(\alpha+1)$ is thus also low, as given in the table, and fig. 2 shows that the form of the $n(N_i)$ curve over the whole range agrees qualitatively with this result.

Specimen 2 has the same value of the width d as specimen 1 but a much higher slope s. In order to interpret the observed value of j_b it is thus found that the calculated form factor is much higher than for specimen 1, agreeing with the much peakier appearance of the $n(N_i)$ curve of fig. 2.

Finally, *specimen* 3 has the largest s and j_b and the smallest d, and thus, in agreement with fig. 2, the largest corresponding value of $(\beta+1)/(\alpha+1)$.

§ 4. Discussion

The results for the three tape specimens can be correlated qualitatively by means of an analysis based on the idea of internal demagnetization spectra. Some correlation is also possible with the actual dispersion and orientation of the tape particles.

This method should also be useful for other magnetic materials such as sintered cubic (Brož and Šternberk 1959) and hexagonal ferrites (Stuijts and Wijn 1958), permanent magnet alloys (Gould and McCaig 1954), other heterogeneous alloys (Kranz 1956) and anisotropic thin magnetic films, for which a structural orientation of imperfections has been tentatively suggested (Wohlfarth 1959, unpublished) to account, in part, for the magnetic annealing mechanism.

Acknowledgments

I am indebted to Dr. R. R. Pearce and Dr. P. M. Griffiths of the Research Laboratories of Electric and Musical Industries Ltd. for supplying the experimental data on which this analysis is based, and to them and Dr. A. N. Gordon for helpful discussions.

References

Brown, W. F., and Morrish, A. H., 1957, *Phys. Rev.*, **105,** 1198.

Brož, J., and Šternberk, J., 1959, *Czech. J. Phys.*, **9,** 666.

Daniel, E. D., and Levine, I., 1960, *J. acoust. Soc. Amer.*, **32,** 1, 258.

Gould, J. E., and McCaig, M., 1954, *Proc. phys. Soc. Lond.* B, **67,** 584.

Greiner, J., 1953, *Der Aufzeichnungsvorgang beim Magnettonverfahren mit Wechselstromvormagnetisierung* (Berlin: VEB).

Howling, D. H., 1956, *J. acoust. Soc. Amer.*, **28,** 977.

Kranz, J., 1956, *Beiträge zur Theorie des Ferromagnetismus und der Magnetisierungskurve* (Berlin: Springer), p. 180.

Néel, L., 1943, *Cahiers Phys.*, **17,** 47.

Osmond, W. P., 1953, *Proc. phys. Soc. Lond.* B, **66,** 265.

Schwantke, G., 1958, *Frequenz*, **12,** 355, 383.

Stuijts, A. L., and Wijn, H. P. J., 1958, *Philips tech. Rev.*, **19,** 209.

Westmijze, W. K., 1953, *Philips res. Rep.*, **8,** 245.

Wohlfarth, E. P., 1955, *Proc. roy. Soc.* A, **232,** 208; 1957, *Phil. Mag.*, **2,** 719; 1959, *J. appl. Phys.*, **30,** 1465; 1960, *Symposium on Solid State Physics*, **3,** 223 (Brussels, 1958).

Woodward, J. G., and Della Torre, E., 1960, *J. appl. Phys.*, **31,** 56.

An Electron Spin Resonance Investigation of Photographic Processes in Crystals of AgCl containing Traces of CuCl†

By I. S. Ciccarello, M. B. Palma-Vittorelli, and M. U. Palma
Istituto di Fisica dell'Università di Palermo

[Received March 7, 1960]

Abstract

An electron spin resonance spectrum, due to the formation of cupric ions during illumination, has been observed in crystals of silver chloride containing 0·1 mol % of cuprous chloride, which have been quenched to −183°c immediately following irradiation. The spectrum fades rapidly if the crystals are kept at any temperature above −140°c after the end of illumination. An interpretation of this behaviour is given which is based upon the Mitchell theory of the photochemical process in crystals of silver halides.

§ 1. Introduction

Experimental work on crystals of silver halides containing traces of cuprous halides (Clark and Mitchell 1956, Moser *et al.*, 1957) has given results of considerable interest in connection with the mechanism of the formation of photolytic silver and has revealed new dislocation phenomena of great interest for the physics of solids (Parasnis and Mitchell 1959).

The observations which have been made, particularly: (*a*) the enhancement of the photochemical sensitivity, (*b*) the appearance of a transient coloration upon illumination, and (*c*) the regression of the silver nuclei upon storage or appropriate heat treatment (Parasnis and Mitchell 1959), indicate that an experimental study of the behaviour of the positive holes which are liberated during illumination and involved in regression would be of great interest.

Such an experimental study may be carried out with Electron Spin Resonance (E.S.R.) techniques and a preliminary account of experiments on the behaviour of crystals of silver chloride containing traces of CuCl will be presented in this paper.

§ 2. Experimental Methods and Results

Silver chloride single crystals of high purity containing about 0·1 mol % of cuprous chloride have been used for the present investigation. They have been generously supplied by Professor J. W. Mitchell‡ and Dr. E. A.

† Partially supported by the Comitato Regionale Ricerche Nucleari, Palermo. Communicated by J. W. Mitchell.

‡ Now at the Department of Physics, University of Virginia, Charlottesville, Virginia.

Braun of the University of Bristol. The methods used for the preparation of the specimens have been described by Clark and Mitchell (1956) and by Parasnis and Mitchell (1959). Specimens in the form of rectangular parallelepipeds were cut from single crystals. Their surfaces were carefully polished on soft cloth soaked in a 5% solution of potassium cyanide and then, after thorough washing, they were annealed at a temperature of 420°C in an atmosphere of nitrogen.

The E.S.R. measurements were made in the 3 cm band, using the spectrometer which has been previously described; in this spectrometer a high sensitivity is achieved by the accurate stabilization of both the magnetic field and the microwave frequency (Palma-Vittorelli and Palma 1958). The use of the rotatable magnet, and of a rotatable sample holder inside the microwave cavity permit the steady magnetic field to be oriented along any direction in the crystal, for any initial orientation of the crystal in the holder. All the measurements in any plane of the crystal may thus be performed without removing the crystal from the microwave cavity, which is maintained at a constant and controlled temperature.

The crystals were irradiated for 10 to 20 sec at a distance of about 10 cm from a 500 w Hanau mercury vapour lamp with quartz envelope (S 500/PL 324).

The most important experimental results are:

(*a*) No E.S.R. has been observed either at room temperature or at liquid oxygen temperature, with non-irradiated crystals of silver chloride containing 0·1 mol % of cuprous chloride.

(*b*) An E.S.R. signal has been observed in the same crystals when they have been irradiated at room temperature and then cooled rapidly to liquid air temperature. For these experiments, the microwave cavity was surrounded by a Dewar vessel filled with liquid oxygen, and the crystal (already fixed on its holder) was dropped into the cavity at the end of the period of irradiation, within an extremely short interval of time.

The E.S.R. spectra obtained under these conditions are similar to those obtained by Tucker (1958) with crystals of AgCl containing traces of CuCl which had been exposed to an atmosphere of chlorine. The figure shows the spectrum obtained at liquid oxygen temperature in the direction which gives the best resolution; it is assumed, by comparison with the results of Tucker (1958), that this is a ⟨100⟩ direction. The main lines (indicated by arrows) are attributed to cupric ions formed by the trapping of positive holes by cuprous ions occupying cation lattice sites and subjected to a crystalline electric field having a symmetry axis along a ⟨100⟩ direction. For such a symmetry, the E.S.R. spectrum is described (Bleaney, Bowers and Ingram 1955, Bleaney, Bowers and Pryce 1955, Tucker 1958) by the following spin Hamiltonian:

$$\mathscr{H} = g_{\parallel}\beta H_z S_z + g_{\perp}\beta(H_x S_x + H_y S_y) + A S_z I_z + B(S_x I_x + S_y I_y) + P\,[I_z^2 - \tfrac{1}{3}I(I+1)]$$

which in our case fits the experimental results with the following values: $S=\frac{1}{2}$, $I=\frac{3}{2}$ and

$$g_{\parallel}=2{\cdot}28\pm0{\cdot}01, \qquad A=115\pm10\,\text{gauss},$$
$$g_{\perp}=2{\cdot}066\pm0{\cdot}003, \qquad B=40\pm5\,\text{gauss},$$
$$P=8{\cdot}5\pm3\,\text{gauss}.$$

The two central lines of the four $\Delta M_I=\pm2$ lines, which are allowed on account of the nuclear quadrupole interaction, are almost coincident, and are not resolved. The other barely-resolved lines, which are not indicated by arrows, are attributable to cupric ions in different configurations (see, for instance, Tucker 1958).

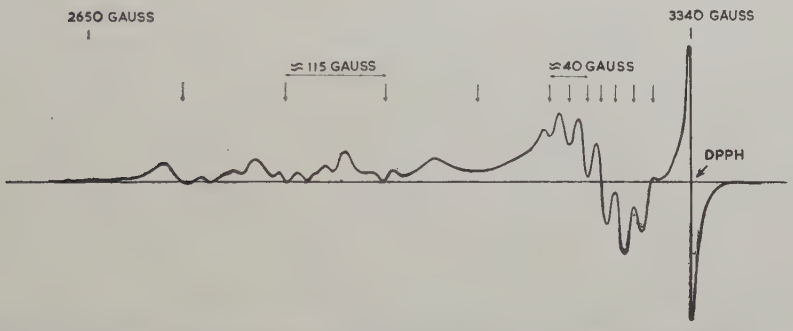

E.S.R. spectrum (derivative) of a silver chloride crystal containing about 0·1 mol % of CuCl, after illumination at room temperature and rapid cooling to liquid air temperature. The crystal is assumed to have had a ⟨100⟩ direction parallel to the steady magnetic field.

(*c*) No significant change in the spectrum is observed when the temperature of the cavity containing the specimen is raised to about -160°C for several hours. The same is true when the temperature is raised to -145°C for 30 min. If the temperature is, however, raised to -120°C for 30 min, the E.S.R. signal fades and is barely detectable. The fading is not reversible, and the spectrum shown in the figure cannot be obtained if the temperature is lowered again to -183°C.

If the specimen is not cooled rapidly immediately after irradiation, erratic and non-reproducible results (including the absence of an E.S.R. signal) are obtained.

§ 3. Discussion of the Results

The features of the hyperfine structure of the E.S.R. spectrum which is reproduced in the figure and the measured values of the parameters of the spin Hamiltonian leave little doubt that the spectrum is due to the formation of cupric ions during the exposure of the crystals at room temperature.

The striking observation is that the E.S.R. signal fades extremely rapidly at room temperature and this probably accounts for the negative results reported by Tucker (1958) in his study of similar crystals.

The absorption of light with a wavelength near the edge of the absorption band of the crystals results in the liberation of conduction electrons and positive holes. According to the Mitchell theory of photochemical processes in crystals of silver halides, the positive holes are trapped before the electrons, and the trapping of the positive hole is followed by the passage of a silver ion from a neighbouring site into an interstitial position and its diffusion away. The conduction electrons then combine with silver ions at sites on external and internal surfaces and along dislocation lines to form the groups of silver atoms of the surface and internal latent images and, ultimately, particles of photolytic silver (Mitchell 1957 a, b, 1958).

We believe that our experimental observations provide supporting evidence for the operation, in these crystals, of the two stages in the Mitchell theory which are concerned with the positive holes. In crystals of silver chloride containing cuprous chloride, the positive holes would be trapped by the substitutional cuprous ions, Cu^{+}, to form the cupric ions, Cu^{++}, which are responsible for the E.S.R. signal. This corresponds with the first stage in the Mitchell mechanism. The signal fades rapidly at temperatures down to about $-130°$C but does not fade at temperatures below $-145°$C. In accordance with the second stage of the Mitchell mechanism, we believe that this fading might be related to the passage of a silver ion from one of the twelve possible sites around the cupric ion into an interstitial position and to its diffusion away, which occurs with a lowering of the free energy. In the resulting association complex, consisting of the cupric ion and the adjacent vacant silver ion lattice site, the positive hole might be shared between the cuprous ion and the six chloride ions surrounding the vacant silver ion lattice site. It is of interest to remark that the temperature below which the signal does not fade corresponds with that at which silver ions on lattice sites adjacent to cupric ions might be expected to be unable to jump into interstitial positions to diffuse away.

Acknowledgments

We are deeply indebted to Professor J. W. Mitchell for his cooperation, for valuable discussions and suggestions, and for his communication of experimental and theoretical results. Dr. E. Braun and Professor J. W. Mitchell kindly supplied the crystals used for the present work.

We also wish to thank Professor F. G. Fumi† and Dr. M. P. Tosi of his group for many valuable discussions.

Finally, we wish to express our deep appreciation of all the friendly assistance which we have received from the Director of the Institute, Professor M. Santangelo.

---

† Now at Cornell University, Ithaca, New York.

References

Bleaney, B., Bowers, K. D., and Ingram, D. J. E., 1955, *Proc. roy. Soc.* A, **228,** 147.

Bleaney, B., Bowers, K. D., and Pryce, M. H. L., 1955, *Proc. roy. Soc.* A, **228,** 166.

Clark, P. V. McD., and Mitchell, J. W., 1956, *J. photogr. Sci.*, **4,** 1.

Mitchell, J. W., 1957 a, *Die Photographische Empfindlichkeit* (Darmstadt: Helwich); 1957 b, *Rep. Progr. Phys.*, **20,** 433 (London: Physical Society); 1958, *J. photogr. Sci.*, **6,** 57.

Moser, F., Nail, N. R., and Urbach, F., 1957, *J. Phys. Chem. Solids*, **3,** 153.

Palma-Vittorelli, M. B., and Palma, M. U., 1958, *Nuovo Cim.*, Suppl. **7,** 139.

Parasnis, A. S., and Mitchell, J. W., 1959, *Phil. Mag.*, **4,** 171.

Tucker, R. F., Jr., 1958, *Phys. Rev.*, **112,** 725.

Dislocation Nets in Bismuth and Antimony Tellurides†

By P. Delavignette and S. Amelinckx
Centre d'Etude de l'Energie Nucléaire, Mol-Donk, Belgium

[Received February 24, 1960]

Abstract

The electron microscopic examination of thin foils of bismuth and antimony telluride, prepared by repeated cleavage, reveals the presence of extended dislocation patterns. Since the *c*-plane is simultaneously glide and cleavage plane, the dislocation arrangements are preferentially situated in the plane of observation. This is a considerable advantage if one wishes to study the configurations due to glide, since one might hope that the typical thin foil behaviour would not apply to the glide planes parallel to the foil. Sets of concentric dislocation lines are often observed, but they invariably originate in some invisible source, outside the crystal.

In the *c*-plane very extended nets are often observed. The multiplication of dislocations and the resulting formation of networks, as well as the elimination of dislocations are observed whilst in progress. The latter phenomenon is due to a combination of glide and climb. Some contrast effects are also mentioned.

§ 1. Introduction

The electron microscopic examination in transmission of thin metal foils as developed by Hirsch *et al.* (1956, 1958), Whelan and Hirsch (1957 a, b), Bollmann (1956), and others has opened up a new field in making possible the direct observation of 'clean' dislocations.

Most of the work on thin foils so far has been confined to metals, although some work has been done on semiconductors (Geach *et al.* 1957). Networks of dislocations, as observed in these foils, have been described and analysed for the case of aluminium and stainless steel by Whelan and Hirsch (1957 a), It is however surprising that in general well-developed networks, containing large numbers of meshes, as e.g. observed by decoration techniques in the alkali halides (Amelinckx 1956, 1958) have not been found in the electron microscopic studies, as yet. The object of this paper is to describe observations of some very well-developed networks, which are fairly regularly found in the basal plane of bismuth and antimony telluride single crystal flakes. In these materials it was possible to observe the actual formation of networks whilst in progress.

We will describe in this paper features common to both substances; phenomena typical of Sb_2Te_3 not found in Bi_2Te_3 will be described in a later paper.

† Communicated by the Authors.

§ 2. Experimental

The tellurides used for these observations were prepared for semiconductor application. They consisted of small single crystal blocks and were made by melting together the elements in the stoichiometric proportions, in a quartz tube. Specimens, sufficiently thin to transmit electrons were prepared by repeated cleavage. In electron diffraction these cleavage flakes showed excellent hexagonal cross-grating patterns, typical of the basal plane. This allowed complete orientation of the foil. The specimens are very stable except for melting and they can be examined up to several days after their preparation.

A satisfactory method for preparing these cleavage flakes consisted in sticking a crystal flake with one face to 'palavit', a rapidly setting plastic, used in dental surgery, and pulling off flakes at the other side by means of scotch tape. Sufficiently thin flakes adhering to the palavit are then selected and thoroughly washed, mounted on grids and examined with a standard Philips microscope operated at 100 kv. By tilting the specimens with respect to the electron beam a suitable contrast can be obtained.

Burgers vectors of dislocations were determined by the use of selected diffracted beams to produce a dark field image. The procedure is as follows. A diffraction pattern is produced at zero magnification; by means of the 25 μ object diaphragm a particularly intense spot can be selected. The image due to this spot is then magnified without tilting the specimen so as to allow observation of the dislocation pattern. If the selected spot corresponds to a reflection against a set of crystal planes passing through the Burgers vector, the dislocation is not visible. It is clear that this procedure allows a determination of the direction of the Burgers vector. An example of such an image is visible in fig. 1† whilst fig. 2 shows a similar field in normal conditions. It is clear that one set of lines is lacking in fig. 1. This information combined with a knowledge of the structure is sufficient to asign plausible Burgers vectors to the different segments of the net.

Although the specimens were not intentionally deformed the way of preparing them certainly introduces large numbers of dislocations.

§ 3. The Crystal Structure of Bismuth and Antimony Telluride; Burgers Vectors

Bismuth telluride has a close-packed layer structure (Lange 1939), Francombe 1958); it can schematically be described by the layer sequence

$$\ldots.[\text{Te–Bi–Te–Bi–Te}]\text{Te–Bi–Te–Bi–Te}|\,\text{Te–Bi–Te–Bi–Te–}|\ldots.$$
$$\longleftarrow 10\,\text{Å}\longrightarrow$$

One-third of the hexagonal unit cell has been indicated by brackets; its total height is about 30 Å. Each of these layers is close-packed and the stacking of the layers is further cubic close-packed: i.e. (see fig. 3)

$$\text{Te Bi Te Bi Te Te Bi Te Bi Te Te Bi Te Bi Te}$$
$$A_1B_1C_1A_2B_2|\,C_2A_3B_3C_3A_4|\,B_4C_4A_5B_5C_5|\ldots.$$

† Figures 1, 2, 7–10, 13, 14, 16, 21, 22, 24, 25 are shown as plates.

The structure of Sb_2Te_3 is not described in the literature, but it is probably the same, antimony being substituted for bismuth (fig. 3).

The pronounced layer structure explains why there is an extremely perfect cleavage along the basal plane. Cleavage probably takes place between two tellurium layers, since the bonds are weakest there. The main glide plane is also the basal plane and specimens deform quite easily by glide along this plane. This could be observed directly in the microscope.

Fig. 3

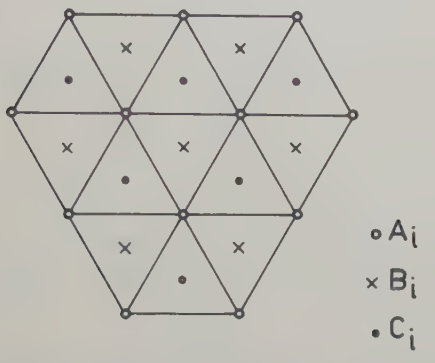

Schematic view of different sites in cubic close-packed structures to which is referred in the description on the structure of bismuth and antimony telluride.

Fig. 4

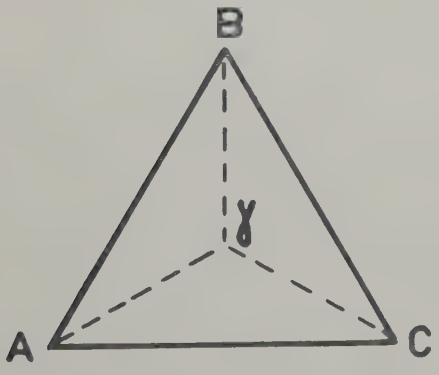

Notation used for Burgers vectors in the basal plane.

The location of the glide plane is probably the same as the one of the cleavage plane, i.e. between the two Te-layers. The fact that both cleavage plane and glide plane are parallel to the *c*-plane, makes Bi_2Te_3 and Sb_2Te_3 excellent materials for the preparation of foils that will have extensive dislocations arrangement in the plane of the foil.

The c-plane being the main glide plane, the distribution of Burgers vectors is similar to the one found in the hexagonal metals, i.e. there are six possible basal plane Burgers vectors which connect nearest neighbours in this plane. They can all be given a name by referring to fig. 4, e.g. AB, BC.... In principle the possibility of dissociated dislocations exists, e.g. AB may dissociate into Shockley partials according to the reaction:

$$\mathrm{AB} \rightarrow \mathrm{A}\gamma + \gamma\mathrm{B}.$$

With the microscope at our disposal it was difficult to decide unambiguously whether the dislocations were single or dissociated. There are indications that sometimes dissociation occurs.

The direction of these Burgers vectors agree with those found by using the selected beam method. This cannot be considered as a proof that glide is between the two tellurium layers.

§ 4. Possible Dislocation Arrangements

Practically only dislocations with Burgers vector in the basal plane are easily formed; they are presumably also the only ones that are observed over an appreciable length, since the plane of observation is in all cases the c-plane. The number of essentially different dislocation patterns is therefore rather restricted.

If glide on only one slip system has taken place the only possible arrangement is a set of parallel lines or concentric loops. If glide has taken place on several parallel glide planes of the same set, tilt boundaries in planes perpendicular to the Burgers vector might eventually form. The probability to observe them is however small in view of the small thickness of the foil.

If slip on two systems has taken place along the same or neighbouring glide planes, stable hexagonal nets form after some anneal.

Using the notation introduced in § 3, which is an adaptation of Thompson's notation (Thompson 1953), the lettering pattern becomes as shown in fig. 5. One could now distinguish a number of singularities which give rise to deviations from the normal hexagonal grid. They have been analysed by Amelinckx (1956) and Frank (1955) for the case of the face-centred cubic lattice, more specifically for the sodium chloride structure. Since in the present case we are restricted to co-planar Burgers vectors, very few observable singularities result. Some possibilities are nevertheless shown in fig. 6.

Since we have no dislocations with mutually perpendicular Burgers vectors, square grids are not to be expected.

§ 5. Results of Observations

5.1. *Sets of Parallel Lines (Straight or Curved)*

Sets of parallel curved lines apparently originating from some invisible centre are frequently observed. These centres are very probably the dislocation sources which operated during deformation. Sources situated

in the bulk material have however not been found. Invariably the origin is somewhere out of the foil or at its surface. Examples of sets of lines are visible in fig. 7.

When a dislocation with a different Burgers vector is present in the same or nearby glide plane, zig-zag lines result, as shown in fig. 8, A, B, C and D.

Fig. 5

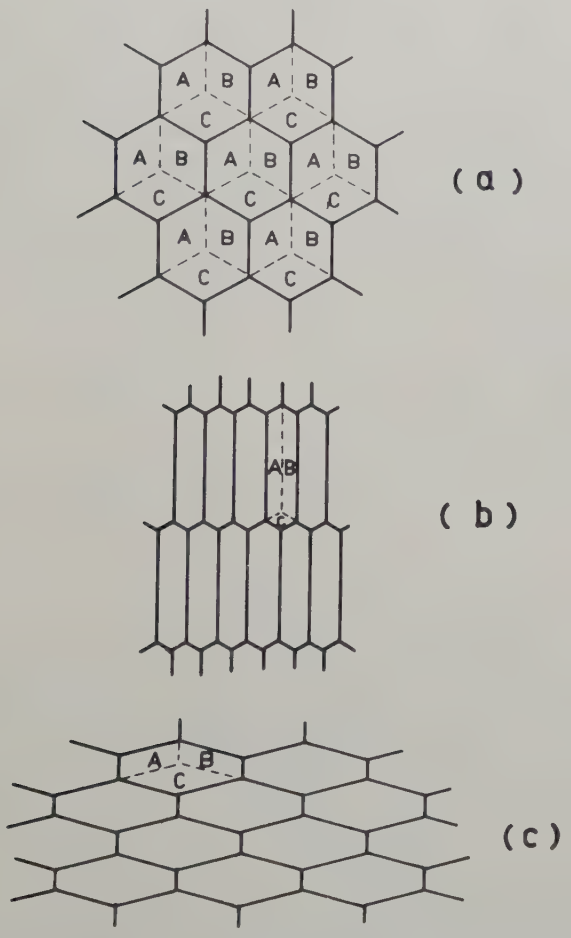

Differently shaped networks as observed in both tellurides.

In a few cases the dislocation lines seem to be interrupted; see e.g. fig. 9, arrows A. This is due to the fact that locally segments of dislocation lines left the crystal. It is clear that this is the combined effect of glide and climb. The argument is that if it were due to pure glide it would require cross slip of a dislocation in the screw orientation. In that case all missing segments would have to have well-defined screw orientations, i.e. parallel to Burgers vectors, which obviously is only approximately the case.

We have actually observed the process taking place. Figure 10 gives an example which could be photographed. It is obvious that the segment A has shortened in the interval of time, i.e. 20 sec between the two exposures.

Fig. 6

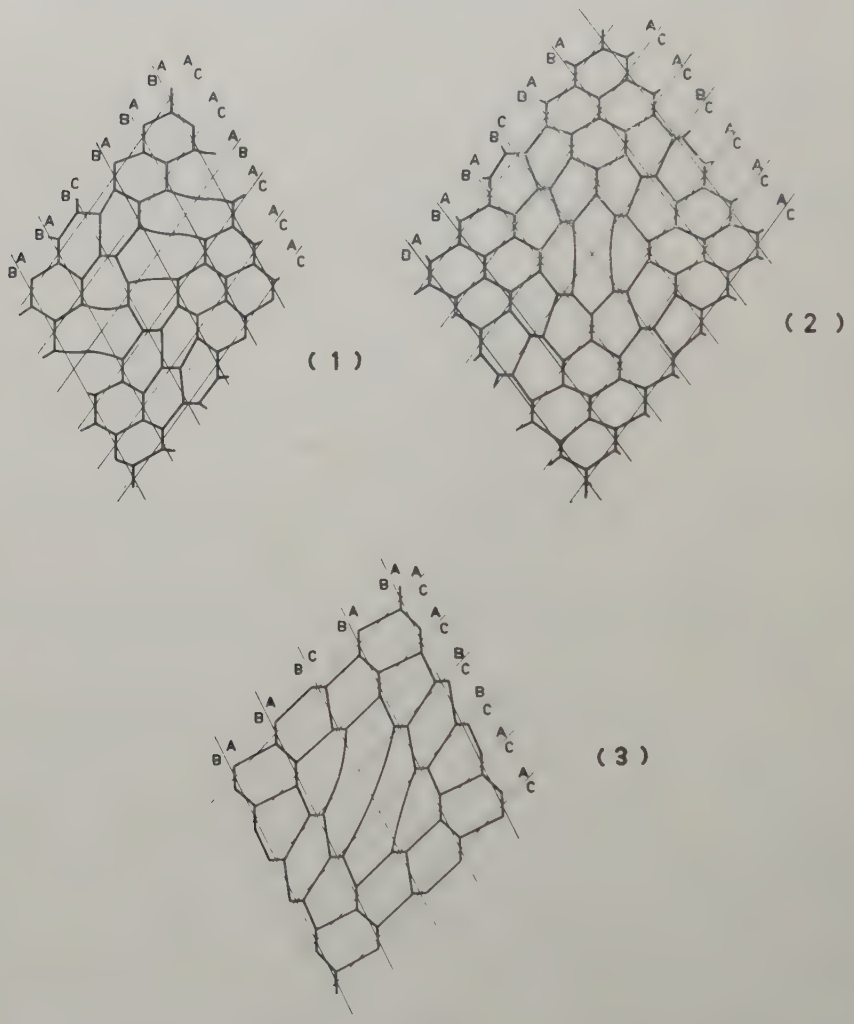

Possible singularities in networks consisting only of dislocations with a basal plane Burgers vector.

The geometry of the process can be pictured as in fig. 11. As driving forces one can consider the line tension of the dislocations and the image force on it; the first tends to shorten the line; the second tends to pull it out of the crystal. They both induce it to climb out of the crystal. The necessary activation for climb is provided by the heating of the sample with the

electron beam. This is supported by the observation that most of the movement takes place at the beginning of the irradiation with the beam, i.e. during the temperature rise. Extensive glide motions in the c-plane were observed also.

5.2. *Hexagonal Nets*

Very extended nets, of which examples are shown in fig. 2, have been observed with a surprisingly good contrast. The shape of the meshes ranges from perfectly hexagonal to very elongated. These different shapes are shown schematically in fig. 5. Very elongated hexagons are present between lines B and C in fig. 8; hexagons of the type (c) are visible in the left top region of fig. 9. The nets result from the intersection of two systems of glide loops in the same or neighbouring glide planes. It is known (Amelinckx 1956) that crossed sets of screw dislocations in parallel glide planes exert a pronounced attraction, one on the other, which, after interaction and rearrangement, results in the formation of the hexagonal grids.

Fig. 11

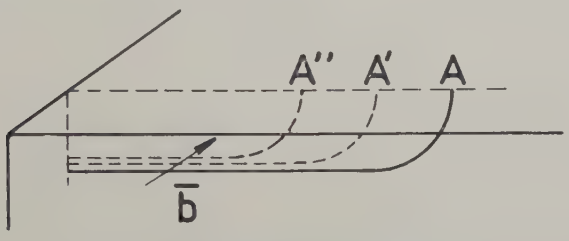

Movement of dislocations by climb.

The initial stage in the formation of such a grid is visible in fig. 9. The net with fine meshes is not yet formed, i.e. new segments have not yet been formed at the intersecting points. This can be deduced from the absence of certain sections of lines. We will present further successive stages in the formation of an hexagonal grid.

In a number of nets 'holes' are frequently observed. Such 'holes' could eventually result from intersecting singular lines in the net (Amelinckx 1958, Frank 1955). A careful analysis of all possibilities shows however that, if only co-planar Burgers vectors are available, which is the case here, such holes are not to be expected. The holes, in the present case, result from the fact that the foils are so thin that certain segments of dislocation line of the network are so near to the surface that they are pulled out of the crystal by the image force, in the way discussed previously. The remaining segments are then practically normal to the foil and their visibility is small. This process is schematized in fig. 12 for a single segment leaving the foil; observed examples are visible in fig. 13, as indicated by the arrows A. If a whole node leaves the foil, more complex holes may form as shown schematically in fig. 12 (b) and observed in fig. 13, arrows B and C. In a

few cases a complete net gradually left the foil. The high contrast is probably due to the proximity of the net to the foil surface, which in turn makes possible the described phenomena.

5.3. *Square Grids*

The photograph of fig. 14 shows what is apparently a square grid of dislocations. We know however that the plane of observation is the c-plane and hence that Burgers vectors of dislocations in that plane enclose

Fig. 12

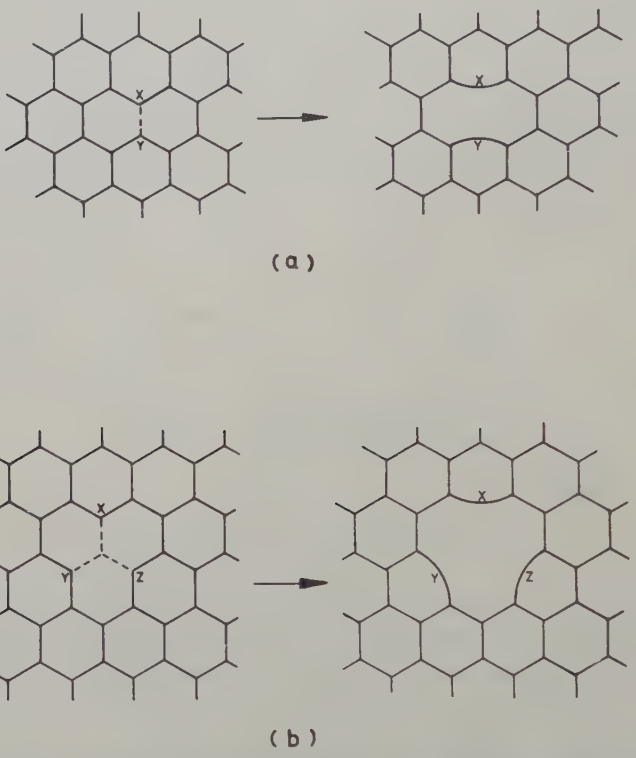

Holes in hexagonal nets resulting from the elimination of certain segments out of the foil. (a) segments XY left the foil ; (b) node XYZ left the foil.

angles of 60° or 120°. Therefore the square grid cannot be a stable arrangement. The observed pattern is therefore most probably composed of two roughly mutually perpendicular sets of dislocations in parallel glide planes. Such arrangements would, if climb should occur, give rise to hexagonal grids; they were therefore most probably introduced during deformation.

5.4. *Interactions between Dislocations in Parallel Glide Planes*

As pointed out by Read (1953) and shown experimentally by one of the present authors (Amelinckx 1956), dislocations in parallel glide planes exert at their crossing point large local forces which in general have a

component of attraction (or repulsion) and a torque. The torque tends to twist the dislocations into typical configurations of which examples are shown in fig. 15. Depending on the character of the dislocation lines the configuration may be symmetrical or asymmetrical. Observed examples can be found in fig. 16, at the points marked A. The same set of crossing lines may produce in different regions, different configurations; i.e. in one

Fig. 15

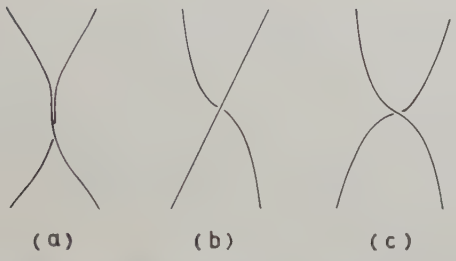

Twisting of dislocations at crossing points. Depending on the character of the dislocations the configuration is either symmetrical (*a*) and (*c*) or asymmetrical (*b*). Observed examples can be found in figs. 14 and 16.

Fig. 17

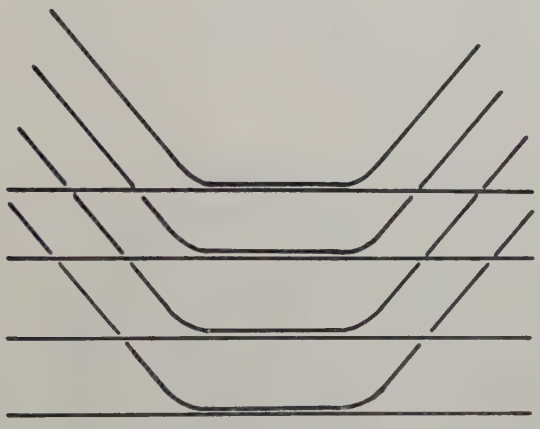

Lining up of dislocations as observed in the marked regions of fig. 16.

region it may be symmetrical, in the other asymmetrical. The reason for this is obviously that the direction of the lines, and hence their character, changes. Examples of asymmetrical twisting are visible in fig. 14 in the marked square.

In a few cases dislocations of apparently the same system of parallel lines, i.e. with the same Burgers vector, also show interactions, proving that they are not in the same but in parallel glide planes. Examples of this are visible in fig. 16 in the region indicated by the arrows A. Another striking feature is that equidistancy is conserved although the dislocations are not all in the same glide plane. This can of course be understood since

dislocations of the same sign and Burgers vector, but in parallel glide planes, repel one another unless they can line up in a plane perpendicular to the Burgers vector. Examples of lining up can be observed in fig. 16 in the region surrounded by a square, as is schematized in fig. 17.

Fig. 18

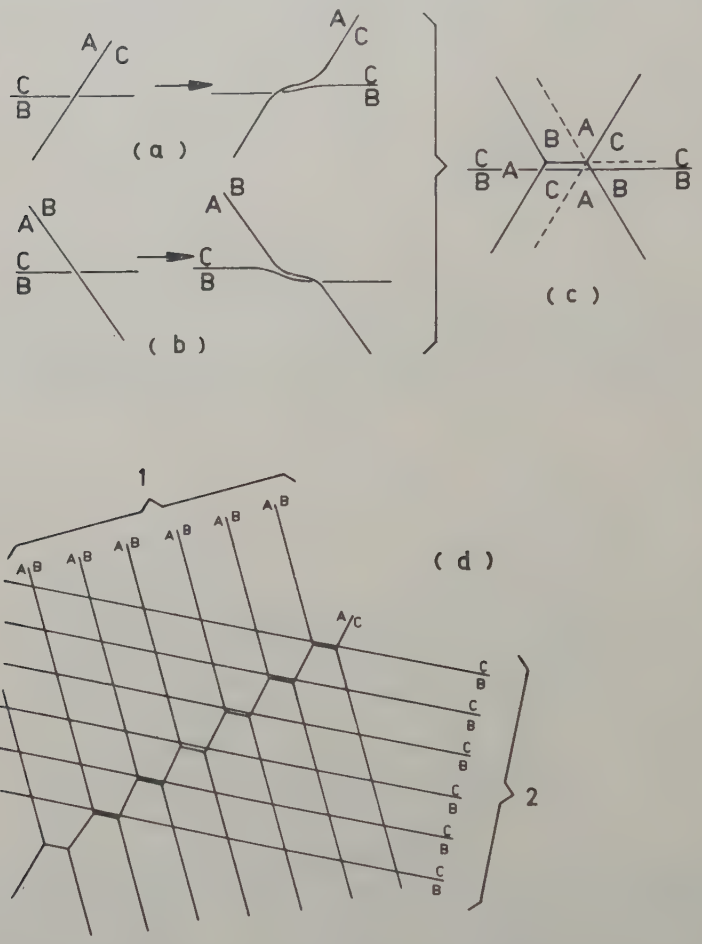

Interaction of segments of zig-zag lines A, B, C and D of fig. 8 with the dislocations of set (2). Figures (*a*), (*b*) and (*c*) show why the presence of the set (2) with Burgers vectors CB, catalyzes the formation of segments with Burgers vector BC at the crossing points of set (1) and the singular line (with Burgers vector AC).

We will now discuss in particular fig. 8 and the corresponding fig. 18. The field is covered by a lozenge-shaped network. As pointed out previously, this is most probably formed by two crossed sets of dislocations in parallel glide planes. One family of lines (1) is intersected by singular

lines, marked B, C and D on fig. 8. These singular lines formed zig-zag lines as a result of interaction. The remarkable feature is that one family of segments of the zig-zag line is invariably above a line of the set (2). By allocating suitable Burgers vectors, as shown, this behaviour can be completely understood. The distribution of Burgers vectors is such that the presence of the set (2) with Burgers vector CB catalyzes the formation of a segment of dislocations BC at the crossing point. This can be explained by referring to fig. 18.

Suppose for simplicity that a dislocation with Burgers vector AC is crossed by a dislocation with a Burgers vector CD (see fig. 18 (*a*)). At the crossing point dislocations will exert a torque one on the other in such a way that they tend to adopt the configuration shown in fig. 18 (*a*). If dislocations with a Burgers vector CB and AB cross, the torque at the crossing point is such that the configuration shown in fig. 18 (*b*) tends to develop. The result of the crossing of the three dislocations is now that *no* net torque is exerted on CB, but that the dislocations with Burgers vectors AB and AC develop parallel segments which will combine into a single segment with Burgers vector BC (fig. 18 (*c*)). Parallel to this segment are dislocations with Burgers vector CB, in a parallel glide plane. The equilibrium configuration of these two dislocations is one parallel to the other in such a way that the plane through both of them forms an angle of 45° with the slip plane (the *c*-plane). Since the dislocations are in nearby glide planes this effectively means that they will be observed one on top of the other (fig. 18 (*d*)).

§ 6. Dislocation Movements

As a result of the small thermal conductivity of the tellurides the specimens become rather hot, and in many cases, when thermal contact with the supporting grid is not good, they can be melted by means of the electron beam. At temperatures not too far from the melting point, extensive rearrangements of dislocations take place, especially in the neighbourhood of the contact with the grid, where thermal gradients are largest. The rearrangement goes in two ways: usually dislocations are eliminated, but in a number of cases dislocations are introduced and we were able to observe the actual formation of networks whilst in progress. We will now discuss the different types of rearrangements separately.

6.1. *Rearrangements by Glide in the Basal Plane*

The main glide plane is the *c*-plane; glide on it has usually jerky character. No evidence for Frank–Read sources was however found, although circumstances were almost ideal. In a number of cases segments lying in the foil over an appreciable length, and leaving the foil at their end points were observed. Such segments have the geometry of a Frank–Read source; they have however been observed to move as a whole, without multiplication.

6.2. *Elimination of Dislocations by Glide on other Glide Planes*

The glide planes different from the c-plane have traces along the close-packed directions of the basal plane; they are therefore very likely the traces of the octahedral planes of the pseudo cubic stacking. The second rearrangement process consists in a combination of glide on this system, using the same basal Burgers vectors, and climb, resulting in the elimination of the dislocation out of the foil. It proceeds in the way schematized in fig. 19. Once a small segment of dislocation has left the foil, the line tension of the dislocation tends to pull it completely out.

Fig. 19

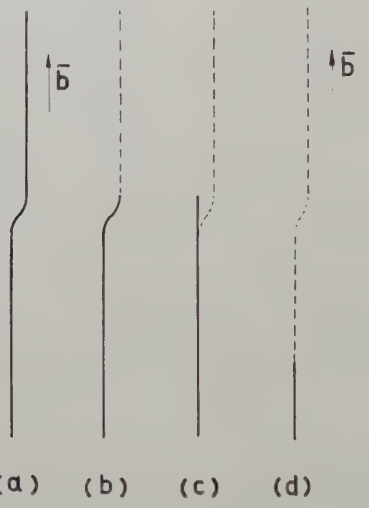

Illustrating the mechanism of elimination of dislocations out of a foil. The pure screw segments glide on non-basal slip planes: the edge sections slip on the basal plane or climb. Observed sequences can be found in figs. 10 and 21.

Two different cases arise. If the dislocations had, originally, both end points in the same face, it disappears completely, without leaving a trace, as opposed to the observations by Hirsch *et al.* (1956), in the case of aluminium. This is of course natural, if Hirsch's explanation based on the presence of an oxide film is right, since no surface step is raised in our case. If the dislocation had originally its two end points at opposite faces of the foil, it is reduced to a small segment of dislocation perpendicular to the foil.

The dislocations that are capable of this type of behaviour are those having large screw sections which can cross glide easily. Whilst gliding out of the foil some segments get stuck for a short while, as shown in fig. 19 (*b*), then glide further out. The stopping points are found to be small segments which are not pure screws and have therefore to climb a small distance or to cross glide on the c-plane, as represented in fig. 19 (*c*).

A process of elimination which was actually observed, but could not be photographed as yet, is summarized in fig. 20. Dislocation (3) of a set of parallel screws (1), (2), (3) was suddenly reduced by glide, to a dot dislocation, connecting upper and lower face. It then climbed slowly towards the next screw (2) of the set. On reaching it, the latter dislocation broke up into two parts (2′) and (2″) which suddenly disappeared by glide. This process is of course due to mutual annihilation at the intersection point, followed by the formation of two dislocation segments (2′) and (2″) connected to the surface of the foil. This is represented schematically in fig. 20 (*d*), (*e*).

Fig. 20

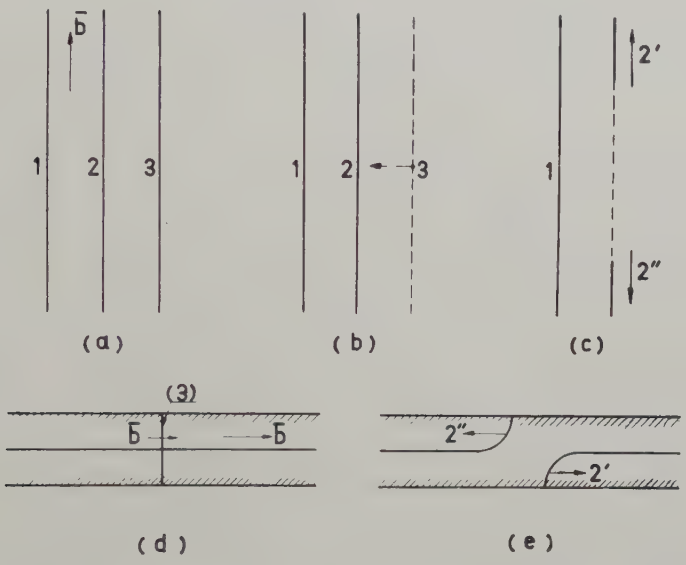

Illustrating a process of elimination of dislocations out of a foil. (*a*) dislocation (3) reduces to a segment perpendicular to the foil; (*b*) dislocation (3) climbs towards dislocation (2); (*c*) on intersecting dislocations (2), the two segments 2′ and 2″ are formed, they glide out of the foil; (*d*) and (*e*) illustrate in cross section the process happening in (*c*).

Sequences of pictures illustrating the elimination of dislocations by means of the described processes are reproduced as fig. 10 (*a*), (*b*), (*c*), (*d*). The sections of dislocations marked B and C disappeared between the exposures (*a*) and (*b*). The node X was at the same time displaced along the dislocation marked (3).

Between exposures (*b*) and (*c*) the dislocations D and E disappeared and the dislocation A shortened considerably.

In the interval of time between the exposures (*c*) and (*d*) dislocation A shortened further and a number of other dislocations disappeared. Many more changes apart from those described can be found. It is evident that the disappearing segments have a certain preferred orientation but are

not parallel to the same direction over the whole length, as is consistent with the process described.

A second series of pictures (fig. 21 (*a*), (*b*), (*c*), (*d*) and (*e*)) illustrates the elimination of dislocations out of a regular sequence of parallel dislocations. The larger part of the motions is here conservative, i.e. glide along a glide plane that intersects the basal plane along a line parallel to the general direction of the dislocations. The process is therefore very rapid; the dislocations retract suddenly.

6.3. *Movement of Dislocations Resulting in the Formation of Networks*

Some of the networks, observed in these single crystal foils, actually formed during the observation. A sequence of photographs of the same area illustrating this process is shown in fig. 22 (*a*), (*b*), (*c*) and (*d*). The time interval between successive pictures was only of the order of half a minute or one minute maximum. At the end of the observation period the area was completely filled with a dense network. The most striking feature is the absence of extensive glide in the *c*-plane, most glide being on planes intersecting the basal plane along directions enclosing roughly angles of 60°. No activity of sources was observed, every dislocation developing separately. In cases where the origin could be identified it turned out to be a dislocation segment connecting upper and lower face of the foil (see 1 and 2 of fig. 22). In most cases the origin was not obvious.

It can be seen clearly that the segments of dislocation 1 and 2 are lengthening at both ends between exposures (*a*) and (*b*). The three possible shapes of the features 1 and 2 are:

(1) a segment connecting top and bottom face,

(2) a half loop ending with both ends in top or bottom face,

(3) a loop inside the crystal and lying in a plane perpendicular to the observation plane.

The first possibility is the more likely one. A half loop, for example, would be rather unstable. Buckling of the foil under the thermal gradients now creates an inhomogeneous shear stress, i.e. a shear stress changing sign at the neutral plane. This type of stress distribution tends to move both ends of the dislocation in opposite senses. This movement results necessarily in intersection 1 with the transverse set of lines 3, 4, 5 and 6, already present in the foil, and hence in the formation of three-fold nodes as shown in fig. 23. The general directions of the dislocations are such that they have mainly screw character. This is in fact implied in the description of the movement; this then fixes their Burgers vector. The non-rectilinear character of the dislocations 1 and 2 is due to some cross slip on the basal plane.

§ 7. Contrast Effects

As pointed out by Whelan (1959) dislocations are pictured under certain conditions of observation as double lines. This occurs when two

different Bragg reflections collaborate to the contrast. A striking example of this is visible in fig. 7 where even a threefold contrast is visible in one area marked A. This photograph shows that the double contrast is depending on the Burgers vector, on the orientation of the line and of course on the orientation of the foil.

In a number of cases (see figs. 13 and 14) dislocations show banded contrast, as if they consisted of a ribbon of stacking faults. This is however not the case since no contracted or extended nodes are seen in fig. 13.

A remarkable contrast effect was found, which as far as we know, is not yet described. An example is shown in fig. 24. The dislocation lines AB and CD separate a dark and a light region. That the dividing line is indeed a dislocation is shown by the fact that such lines often glide in the basal plane; the contrast accompanies them during this process. Sometimes the dislocation line itself does not produce any contrast.

Fig. 23

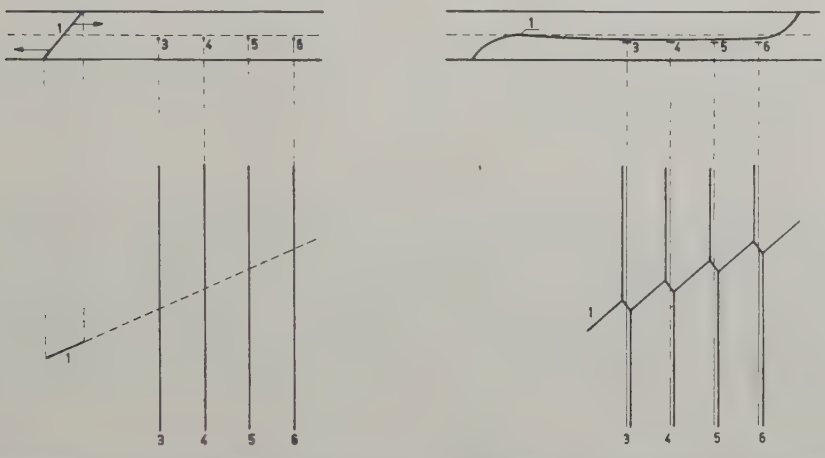

Illustrating the formation of networks. Dislocation 1 glides and intersects dislocations (3), (4), (5), (6). The observed sequence is shown in fig. 22.

In other cases only parts of the dividing line are formed by a visible dislocation line. This particular form of contrast is only seen near to a broad extinction contour. Overlapping regions produce different shades of contrast, as shown also in fig. 24.

The presence of a dislocation line producing this type of contrast may change the contrast of other dislocations intersecting it. In fig. 25, for example, the line AB is a dislocation line. In the region above AB dislocation lines are pictured as white lines, they exhibit so-called dark field contrast. In the region below AB they have normal contrast. The left part of the same photograph also exhibits the same type of contrast as shown in fig. 24. Different parts of the meshes of the network have a different shade, the shade changing discontinuously at dislocation lines.

Dislocation lines often change contrast discontinuously, a broad line may become suddenly fine, without changing direction (see, e.g., fig. 10 (*a*), arrows Y). The simplest explanation is to assume that this is due to a change in Burgers vector as a consequence of branching in a plane perpendicular to the *c*-plane. This is shown schematically in fig. 26.

Fig. 26

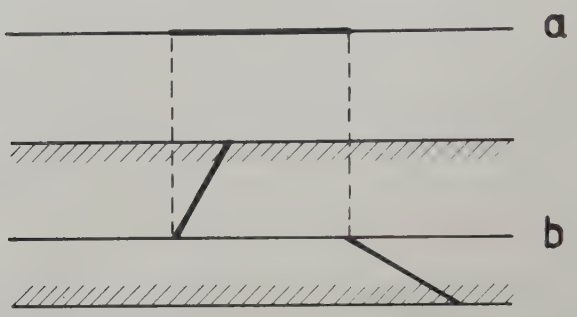

Illustrating the discontinuous change in contrast of certain dislocations: (*a*) top view as seen in microscope; (*b*) cross section of foil. Observed examples can be found in fig. 10.

Acknowledgments

We would like to express our thanks to Mr. Goens, director of the C.E.N. (Centre d'Etude de l'Energie Nucléaire), Mol, Belgium, for his permission to publish this paper.

We also thank Mr. Beyens for his careful photographic work, Mr. Nicasy for skilful preparation of specimens and Mr. Biermans for preparing the drawings.

References

Amelinckx, S., 1956, *Phil. Mag.*, **1**, 269; 1957, *Dislocations and Mechanical Properties of Crystals* (New York: Wiley and Sons), p. 3; 1958, *Acta Met.*, **6**, 34.

Bollmann, W., 1956, *Phys. Rev.*, **103**, 1588.

Francombe, M. H., 1958, *Brit. J. appl. Phys.*, **9**, 415.

Frank, F. C., 1955, *Rep. Bristol Conf. on Defects in Crystalline Solids* (London: The Physical Society), p. 159

Geach, G. A., Irving, B. A., and Philips, R., 1957, *Research*, **10**, 411.

Hirsch, P. B., Horne, R. W., and Whelan, M. J., 1956, *Phil. Mag.*, **1**, 677.

Hirsch, P. B., Silcox, J., Smallman, R. E., and Westmacott, K. H., 1958, *Phil. Mag.*, **3**, 897.

Lange, P. W., 1939, *Naturwissenschaften*, **27**, 133.

Read, W. T., 1953, *Dislocations in Crystals* (New York: McGraw-Hill).

Thompson, N., 1953, *Proc. phys. Soc. Lond.* B, **66**, 481.

Whelan, M. J., and Hirsch, P. B., 1957 a, *Phil. Mag.*, **2**, 1121; 1957 b, *Ibid.*, **2**, 1303.

Whelan, M. J., 1959, *J. Inst. Met.*, **12**, 392.

Effect of Temperature on Yield and Flow Stress of B.C.C. Metals†

By Hans Conrad
Metallurgy Department, Westinghouse Research Laboratories, Pittsburgh 35, Pennsylvania‡

[Received November 16, 1959]

Abstract

A comparison of data on yielding and flow of b.c.c. metals indicates that the proportional limit, the lower yield stress, the friction stress of Heslop and Petch, and the flow stress after some strain beyond the Lüders strain all exhibit the same strong temperature dependence. This suggests that they all represent the same deformation mechanism. Furthermore, in iron the temperature dependence of these parameters depends on the total interstitial content and on the presence of grain boundaries. Only when both are present does one observe the very strong temperature dependence normally associated with commercial irons and steels.

The strong temperature dependence of the lower yield stress, σ_{LY}, in b.c.c. metals has been attributed to the tearing of dislocations from their atmosphere of interstitial atoms (Cottrell and Bilby 1949, Fisher 1955). Subsequent deformation is then assumed to occur by the motion of free dislocations. If this is so, it is rather interesting that the proportional limit, σ_P, and the flow stress after some strain beyond the Lüders strain, σ_ϵ, show the same strong temperature dependence as the initial lower yield stress ; for example, see fig. 1 for molybdenum. Also Heslop and Petch (1956) have recently shown that the lattice friction stress§, σ_{00}, in iron shows a strong temperature dependence. Further, Conrad and Schoeck (1960) have found that the temperature dependence of the reversible flow stress ‖, σ_{fl} for strained electrolytic iron is independent of strain and is practically identical to that for the initial lower yield stress and for the lower yield stress after strain-ageing. This all suggests rather strongly that the proportional limit, the lower yield stress and subsequent plastic flow in b.c.c. metals are controlled by the same mechanism.

---

† Communicated by the Author.

‡ Present address : Research Laboratories, Atomics International, Canoga Park, California.

§ σ_{00} was obtained as follows : Plots of σ_{LY} versus (grain size)$^{-1/2}$ were extrapolated to infinite grain size to yield σ_0. Plots of σ_0 versus (C + N) content in solution were extrapolated to zero concentration to give σ_{00}.

‖ σ_{fl} was obtained by making a rapid change in temperature and noting the change in flow stress.

Fig. 1

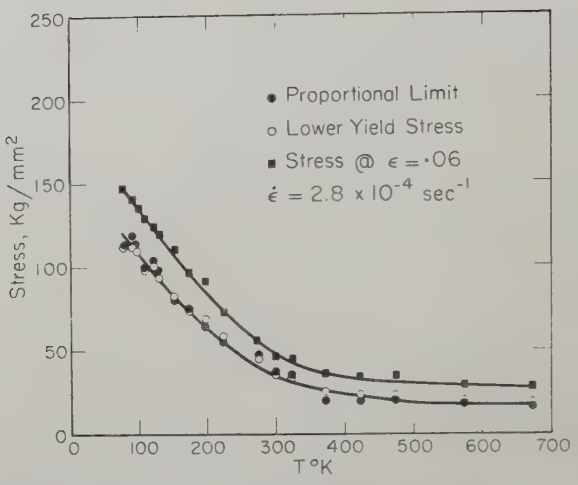

Effect of temperature on the proportional limit, yield stress and stress after strain of 0·06 for molybdenum in compression (data from Alers *et al.* 1958).

Fig. 2

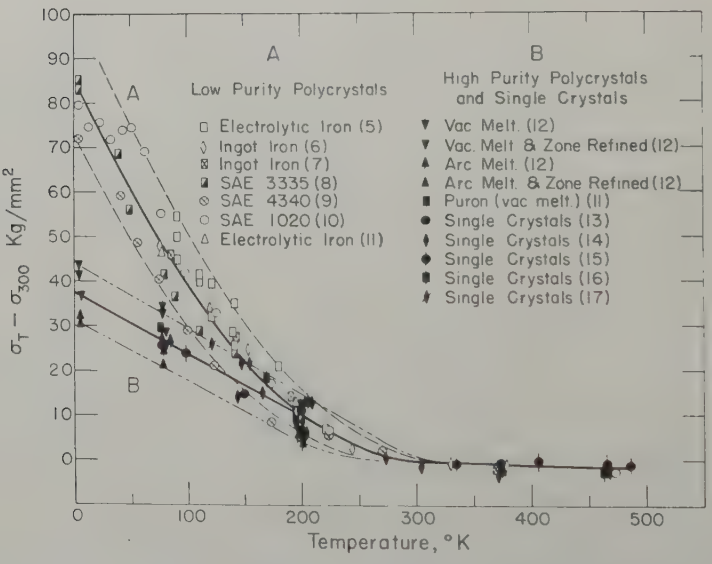

(5) Conrad and Schoeck (1960); (6) Geil and Carwile (1950); (7) McAdam and Mebs (1943); (8) Olleman (1955); (9) Wessel (1957); (10) Wessel (1956); (11) Wiener (unpublished research); (12) Smith and Rutherford (1957); (13) Allen *et al.* (1956); (14) Cox *et al.* (1957); (15) Paxton and Churchman (1953); (16) Vogel and Brick (1953); (17) Steijn and Brick (1954).

Effect of temperature on the lower yield stress of iron and several steels in tension.

When comparing the data in the literature for iron one finds that the temperature dependence of the yield stress is dependent on the purity and the form; i.e. whether it is single or polycrystalline. In the present note data for iron has been assembled to illustrate these effects and to point out certain features which have not been previously defined explicitly.

Figure 2 shows the effect of temperature on the lower yield stress of iron single and polycrystalline specimens of various impurity contents. The temperature independent component of the stress has been removed by plotting the difference between the yield stress at temperature T and the yield stress at 300°K versus the temperature. Pertinent data for the various materials are listed in the table. It is seen from fig. 2 that the data points lie in two scatter bands, one with the strong temperature dependence generally associated with b.c.c. metals (Band A), and the other with a somewhat weaker temperature dependence, especially at the low temperatures (Band B). The temperature dependence of Band B is, however, still greater than that generally observed for f.c.c. and c.p.h. metals. In Band A lie the data points for all polycrystalline materials of low purity, i.e. $(C+N) > 0{\cdot}01$ wt %. In Band B lie the data points for high purity polycrystals, $(C+N) < 0{\cdot}01$ wt %, and for single crystals of both low and high purity.

Fig. 3

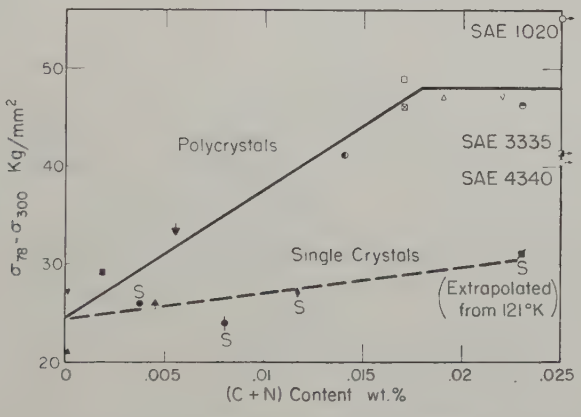

Effect of C+N content on the difference in yield stress at 78°K and 300°K for single (S) and polycrystalline specimens of iron (refer to table and fig. 2 for symbols).

The effect of interstitial content and grain boundaries on the temperature dependence of the yield stress is further shown in fig. 3, where the difference between the yield stress at 78°K and at 300°K is plotted versus the carbon plus nitrogen content. It is here seen that the temperature dependence of the yield stress for polycrystalline iron depends sensitively on the interstitial content up to ~0·015 wt %, while that for the single crystals shows only a very slight dependence. Above 0·015% there does not appear to be any further effect of interstitial content for the polycrystals. Thus the strong

Information Pertaining to Figs. 2 and 3

Symbol	Material	Reference	C (wt %)	N (wt %)	C(%)+N(%)	A.S.T.M. G.S.	Strain rate (sec^{-1})
		(*a*) Low purity polycrystals					
◇	Ingot iron	Geil and Carwile (1950)	0·02	0·002	0·022	2–3	Very low
⊠	Igot iron	McAdam and Mebs (1943)	0·015	—	~0·015	—	Very low
□	Electrolytic iron	Conrad and Schoeck (1960)	0·014	0·003	0·017	3–8	$1·7 \times 10^{-3}$
△	Electrolytic iron	Wiener (unpublished research)	0·012	0·007	0·019	5	$2·7 \times 10^{-4}$
◓	Electrolytic iron deoxidized with C	Steijn and Brick (1954)	0·023	—	~0·023	5	$1·7 \times 10^{-4}$
◐	Carbonized pure iron	Hall (1953)	0·014	0·0002	0·014	2	—
◪	SAE 3335	Olleman (1955)	0·34	—	~0·34	9	$2·8 \times 10^{-4}$
⊗	SAE 4340	Wessel (1957)	0·30	—	~0·30	1	$2·8 \times 10^{-4}$
○	SAE 1020	Wessel (1956)	0·24	—	~0·24	5	$2·1 \times 10^{-3}$

Information Pertaining to Figs. 2 and 3 (*continued*)

Symbol	Material	Reference	C (%)	N (%)	C (%) + N (%)	A.S.T.M. G.S.	Strain rate (sec^{-1})
		(*b*) High purity polycrystals					
▼	Vac melt iron	Smith and Rutherford (1957)	0·005	0·0005	0·0055	8	1×10^{-5}
▼	Vac melt and zone ref.	Smith and Rutherford (1957)	0·00009	No trace	0·0001	5–6	1×10^{-5}
▲	Arc melt iron	Smith and Rutherford (1957)	0·004	0·00009	0·004	3–5	1×10^{-5}
▲	Arc melt and zone ref.	Smith and Rutherford (1957)	0·00009	No trace	0·0001	3–5	1×10^{-5}
■	Puron	Wiener (unpublished research)	0·0008	0·001	0·0018	7·5	$2{\cdot}7 \times 10^{-4}$
		(*c*) Single crystals					
●	Vac melted iron	Allen *et al.* (1956)	0·0027	0·001	0·0037	—	—
◆	Decarb SAE 1008	Cox *et al.* (1957)	0·010	0·0018	0·0118	—	$8{\cdot}3 \times 10^{-5}$
●	Decarb Armco iron	Paxton and Churchman (1953)	0·003	0·005	0·008	—	$3{\cdot}3 \times 10^{-5}$
✚	Ingot iron	Vogel and Brick (1953)	—	—	~0·01	—	$1{\cdot}7 \times 10^{-4}$
■	Electrolytic Iron deoxidized with C	Steijn and Brick (1954)	0·023	—	~0·023	—	$1{\cdot}7 \times 10^{-4}$

temperature dependence of the lower yield stress (Band A) is associated with the combined effect of interstitial impurities and grain boundaries. If either is missing a lower temperature dependence results (Band B). It is noteworthy that the temperature dependence of the yield stress for C + N = 0% (Band B) is approximately linear.

Figure 4 compares the effect of temperature on the lower yield stress, σ_{LY}, taken from fig. 2 with the effect of temperature on the lattice friction stress, σ_{00}, derived by Heslop and Petch (1956) from material with a total C + N content† of 0·16%, and the reversible flow stress after a strain of 5%, σ_{f1}, determined by Conrad and Schoeck (1960) for electrolytic iron with C + N content of 0·017%. It is seen that the data points for σ_{00} and σ_{f1} fall (with one exception) into Band A, as might be expected in view of the

Fig. 4

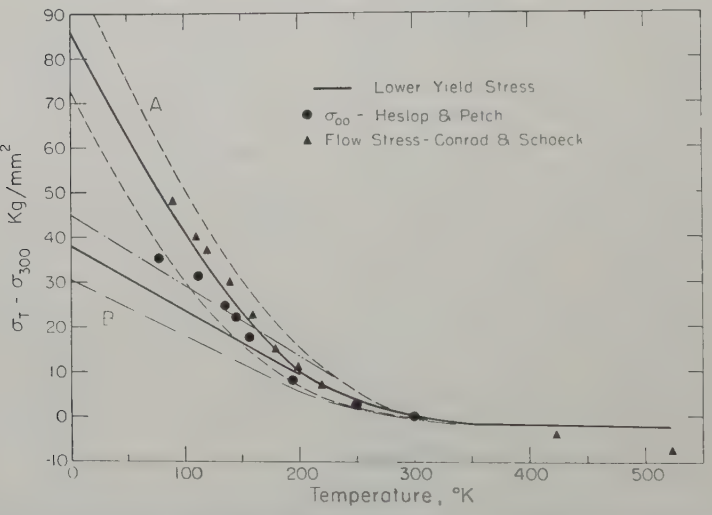

Effect of temperature on the lower yield stress σ_{LY}, the frictional stress σ_{00} and the flow strews σ_{f1} of iron in tension.

interstitial contents of the materials for which these quantities were determined. Since the values for σ_{00} were obtained by extrapolating σ_0 to (C + N) in solution = 0%, it appears that the total impurity content governs the temperature dependence of σ_{00} rather than the amount in solution. The value for σ_{00} at the lowest temperature, 77°K, falls outside Band A. This may be due to the occurrence of twinning which has been observed at this temperature (Deronja and Gensamer 1959, Hahn *et al.* 1959, Owen *et al.* 1958). It is anticipated that σ_{00} and σ_{f1} determined on high purity polycrystals or on single crystals of the purity listed in the table will fall into Band P.

† However, the amount in solution was only approximately 0·005 to 0·025%.

In conclusion, the available data on the effect of temperature on the deformation of b.c.c. metals indicate the following:

1. The proportional limit σ_P, the lattice friction stress σ_{00}, and the reversible flow stress σ_{fl} show a temperature dependence similar to that for the lower yield stress σ_{LY}.

2. The temperature dependence of the flow parameters σ_{LY}, σ_{fl}, σ_{00}, in polycrystalline iron is determined by the total interstitial content rather than that in solution.

3. In iron the presence of both grain boundaries and interstitial impurities are required to give the very strong temperature dependence of the stress normally attributed to b.c.c. metals.

References

Alers, G., Armstrong, R. W., and Bechtold, J. H., 1958, *Trans. Amer. Inst. min. (metall.) Engrs*, **212,** 523.

Allen, N. P., Hopkins, B. E., and McLennan, J. E., 1956, *Proc. roy. Soc.*, **234,** 221.

Conrad, H., and Schoeck, G., 1960, *Acta Met.* (to be published).

Cottrell, A. H., and Bilby, B. A., 1949, *Proc. phys. Soc. Lond.* A, **62,** 49.

Cox, J. J., Horne, G. T., and Mehl, R. E., 1957, *Trans. Amer. Soc. Metals*, **49,** 118.

Deronja, F. S., and Gensamer, M., 1959, *Trans. Amer. Soc. Metals*, **51,** 667.

Fisher, J. C., 1955, *Trans. Amer. Soc. Metals*, **47,** 451.

Geil, G. W., and Carwile, N. L., 1950, *J. Res. nat. Bur. Stand.*, **54,** 129.

Hahn, G. T., Averbach, B. L., Owen, W. S., and Cohen, M., 1959, Swampsott Conference on Fracture, N.A.S.

Hall, L. D., 1953, *A.S.T.M. Stand.*, No. 158, p. 374.

Heslop, J., and Petch, N. J., 1956, *Phil. Mag.*, **1,** 866.

McAdam, D. J., and Mebs, R. W., 1943, *Proc. Amer. Soc. Test. Mater.*, **32,** 661.

Olleman, R., 1955, Ph.D. Thesis, University of Pittsburgh.

Owen, W. S., Cohen, M., and Averbach, B. L., 1958, *Trans. Amer. Soc. Metals*, **50,** 517.

Paxton, H. W., and Churchman, A. T., 1953, *Acta Met.*, **1,** 473.

Smith, R. L., and Rutherford, J. L., 1957, *Trans. Amer. Inst. min. (metall.) Engrs*, **209,** 857.

Steijn, R. P., and Brick, R. M., 1954, *Trans. Amer. Soc. Metals*, **46,** 1406.

Vogel, F. L., and Brick, R. M., 1953, *Trans. Amer. Inst. min. (metall.) Engrs*, **197,** 700.

Wessel, E. T., 1956, *Proc. Amer. Soc. Test. Mater.*, **56,** 540; 1957, *Trans. Amer. Soc. Metals*, **49,** 149.

Wiener, G. W. (unpublished research, Westinghouse Research Laboratories).

CORRESPONDENCE

On the Residual Resistance of Binary Alloys

By E. Verboven†
Instituut voor theoretische fysica der Rijksuniversiteit, Utrecht, Netherland‡

[Received May 23, 1960]

It is well known that the electrical resistance of binary alloys may be divided into two parts: the thermal resistance and the residual resistance. This letter will be devoted to the residual resistance of disordered binary alloys. A first theoretical description of this property has been given by Nordheim (1931). His derivation is based on the quantum mechanical Boltzmann equation. He found the residual resistance ρ_0 to be proportional to the product of the concentrations m_A, m_B of the two metals ($m_A + m_B = 1$), so that

$$\rho_0 \sim m_A m_B (\Delta Z)^2 \qquad . \; . \; . \; . \; . \; . \; . \; (1)$$

where ΔZ is the difference in the effective charges of the two ions. Formula (1) is verified in practice to a high degree of accuracy for alloys of good conductors. A serious discrepancy is present for alloys of a good conductor and a transition metal. This effect was explained by Mott (1935) as an interband scattering of the s-electrons to the d-band. For a typical alloy such as Ag–Pd this scattering must be very important in order to explain the observed deviation from the parabolic law (1) in the region of high Pd-concentrations. However this mechanism cannot explain the deviation for lower Pd-concentrations.

Here we want to give another explanation for the deviation just discussed. The starting point is a simplified version of the Kubo-formula:

$$\sigma_{\mu\nu} = -\mathrm{Tr}_e \left\{ \frac{\partial f}{\partial H} \lim_{T\to\infty} \int_0^T dt \, \tfrac{1}{2} [j_\mu(t) j_\nu(0) + j_\mu(0) j_\nu(t)] \right\} \qquad . \; . \; (2)$$

which gives a closed expression for the conductivity tensor in terms of an equilibrium correlation between currents. This formula has been evaluated by perturbation theory to second order by Verboven (1960). The lowest order term reproduces the usual formula for the conductivity. In our case it gives the Nordheim result. The first higher order term in the conductivity introduces new effects. Its importance is governed by the dimensionless parameter $(\hbar/\tau(\eta)\eta)^{1/2}$, where $\tau(\eta)$ is the relaxation time taken at the Fermi surface and η the Fermi energy. Going over to the resistivity the additional term found there is

$$\rho_1 \sim m_A m_B (m_B - m_A)(\Delta Z)^3 \qquad . \; . \; . \; . \; (3)$$

† Aspirant of N.F.W.O., Belgium.
‡ On leave of absence from the University of Louvain.

Fig. 1

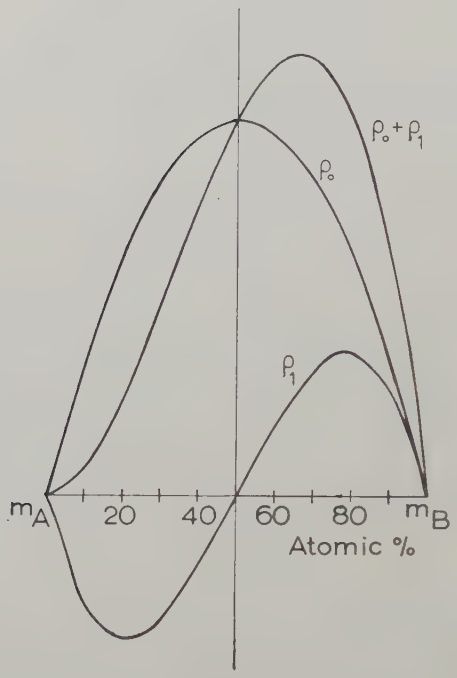

Theoretical curves.

Fig. 2

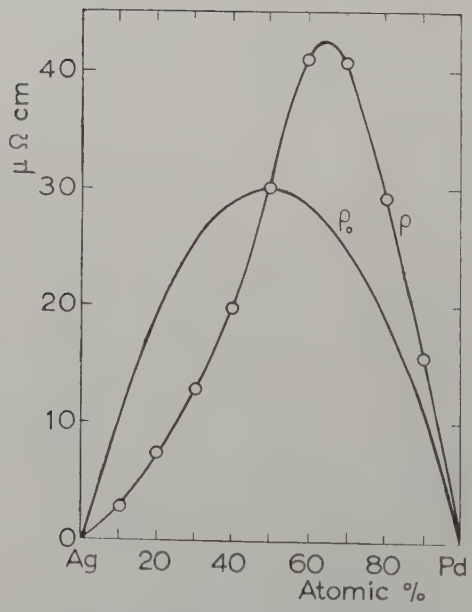

Residual resistance of Ag–Pd and ρ_0.

which contains the whole effect of ternary collisions. The sign depends on ΔZ. In the case of Ag–Pd this is negative. In fig. 1 we represent $m_A . m_B$, $m_A . m_B(m_A - m_B)$ and their sum in arbitrary units. In fig. 2 we plot the residual resistance ρ of Ag–Pd. The parabola ρ_0 is constructed

Fig. 3

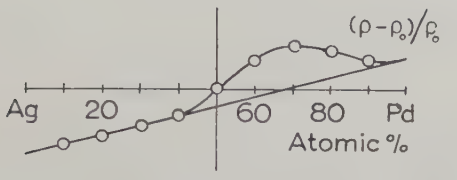

$(\rho - \rho_0)/\rho_0$ for Ag–Pd.

in such a way that it joins this curve in $m_A = \frac{1}{2}$. In fig. 3 we draw $(\rho - \rho_0)/\rho_0$ for Ag–Pd. It is seen that we have a deviation from the straight line predicted from (1) and (2) in the region of high Pd-concentrations. We interpret it as the additional part of the residual resistance due to the interband scattering. For alloys of good conductors the dimensionless parameter mentioned above is too small to give an important contribution.

References

Mott, N. F., 1935, *Proc. phys. Soc. Lond.*, **47**, 571.
Nordheim, L., 1931, *Ann. Phys., Lpz.*, **9**, 607.
Verboven, E., 1960, *Physica* (to be published).

A Note on the Selection Rules for Optical Transitions in Alloys

By J. M. Ziman
Cavendish Laboratory, University of Cambridge

[Received June 22, 1960]

It is well known (e.g. Mott and Jones 1936, p. 99) that direct optical transitions in solids are 'vertical', i.e. between states of nearly the same reduced $\mathbf{k}$-vector. Indirect transitions in which a phonon is emitted or absorbed with the photon, have also been studied (Bardeen *et al.* 1955). These depend on the temperature, but allow the initial and final states to differ by any $\mathbf{k}$-vector. The purpose of this note is to point out that one can also have indirect transitions involving the virtual scattering of the electron by *impurities*, and that in an alloy the transition probability for such processes may be comparable with the rate for direct transitions, so that an absorption edge may represent the minimum band gap, rather than the minimum energy difference between states lying directly 'above' each other in a reduced zone.

We use time-dependent perturbation theory, which tells us that in first order the transition probability is proportional to the square of the matrix element

$$\langle \mathbf{k}|P|\mathbf{k}'\rangle = \left(\frac{eE_0\hbar}{2\pi m\nu i}\right)\int \psi_{\mathbf{k}}^{*}\nabla\psi_{\mathbf{k}'}\,\mathbf{dr} \qquad . \quad . \quad . \quad . \quad (1)$$

between the states $|\mathbf{k}\rangle$ and $|\mathbf{k}'\rangle$. In second order (Schiff 1955, p. 202) this matrix element is replaced by the sum of two terms like

$$\frac{\langle \mathbf{k}|P|\mathbf{k}''\rangle\langle \mathbf{k}''|Q|\mathbf{k}'\rangle}{\Delta\mathscr{E}} \qquad . \quad . \quad . \quad . \quad . \quad . \quad (2)$$

where $\langle \mathbf{k}''|Q|\mathbf{k}'\rangle$ is the matrix element for the scattering of electrons by impurities, phonons, etc. Of course the intermediate state $|\mathbf{k}''\rangle$ must lie directly 'above' $|\mathbf{k}\rangle$ but the change of wave vector from $\mathbf{k}''$ to $\mathbf{k}'$ is not prescribed. Thus we may think of $|\mathbf{k}\rangle$ being the highest occupied state in one band, and $|\mathbf{k}'\rangle$ as the lowest empty state in the next band. We need not worry that the scattering from $|\mathbf{k}''\rangle$ to $|\mathbf{k}'\rangle$ is virtual with an energy change $\Delta\mathscr{E} = \mathscr{E}_{\mathbf{k}''} - \mathscr{E}_{\mathbf{k}'}$; the photon energy will be just the difference between the energies of initial and final states, i.e. the true band gap.

A typical model of an impurity is a screened coulomb potential, of charge Ze and screening constant q. In Born approximation this has the matrix element (e.g. Ziman 1960, p. 224)

$$\langle \mathbf{k}''|Q|\mathbf{k}'\rangle = 4\pi Ze^2/\{q^2 + |\mathbf{k}'' - \mathbf{k}'|^2\}. \qquad . \quad . \quad . \quad . \quad . \quad (3)$$

If we use the Thomas–Fermi approximation, we can write (Ziman 1960, p.161)

$$q^2 = 4\pi e^2 \mathcal{N}(\mathscr{E}) \quad . \quad . \quad . \quad . \quad . \quad . \quad . \quad . \quad (4)$$

in terms of the density of states at the Fermi level. This value of q^2 is large enough to make it the dominant term in (3) if the scattering is not through too large a distance in the zone. Putting (4) and (3) into (2), and supposing a relative concentration x of impurity atoms amongst the N atoms of the crystal, we have

$$\frac{\langle \mathbf{k}''|Q|\mathbf{k}'\rangle}{\Delta\mathscr{E}} \sim \left(\frac{xZ}{\mathcal{N}(\mathscr{E})} \cdot \frac{N}{\Delta\mathscr{E}}\right). \quad . \quad . \quad . \quad . \quad (5)$$

For a monovalent free-electron system this simplifies because $\mathcal{N}(\mathscr{E}) = 3N/2\mathscr{E}_F$ where $\mathscr{E}_F$ is the Fermi energy. Other things being equal, the ratio of indirect transitions to direct transitions should be the square of (5), i.e.

$$\left(\frac{2}{3}\frac{\mathscr{E}_F}{\Delta\mathscr{E}} xZ\right)^2. \quad . \quad . \quad . \quad . \quad . \quad (6)$$

In alloys of the noble metals, where xZ can be 0·3 or more before we reach the α-phase boundary, and where $\mathscr{E}_F$ is, say, 6 ev we can allow $\Delta\mathscr{E}$ to be as much as 1 ev and still have this ratio near unity. Of course there are a number of complicated correction factors, but these would not alter the general conclusion that we may really be watching indirect transitions across the band gap when we see absorption edges in alloys. This is important in the interpretation of experiments like those of Biondi and Rayne (1959) where the rigid-band model is being tested.

References

Bardeen, J., Blatt, F. J., and Hall, L. M., 1955, *Photoconductivity Conference* (New York), p. 146.

Biondi, M. A., and Rayne, J. A., 1959, *Phys. Rev.*, **115**, 1522.

Mott, N. F., and Jones, H., 1936, *The Theory of the Properties of Metals and Alloys* (Oxford).

Schiff, L. I., 1955, *Quantum Mechanics* (New York).

Ziman, J. M., 1960, *Electrons and Phonons* (Oxford).

The Shear Component of Ductile Fracture

By K. E. Puttick

Davy Faraday Research Laboratory, The Royal Institution,
21 Albemarle Street, London, W.1

[Received June 13, 1960]

There are two well-defined stages in the fracture of a cylindrical test piece of a ductile metal. The first stage begins on the axis in the centre of the necked region, and the general directions of propagation of the crack lie in a plane normal to the tensile axis; this is usually called the ' tensile ' part of the break, although it does not obey a simple tensile stress criterion. In the second and final stage the directions of propagation lie on the surface of a cone. It is generally supposed that this cone fracture represents slipping-off by intense local shear on a surface of maximum shear stress, but the details of the process are not at all well understood; in particular, what determines the localization of flow, and the geometry of the actual process of separation ?

To answer these questions fully we need to know how the tensile stage of the fracture is propagated, and although it has been shown that the essential process is the coalescence of inclusion holes with the growing central fissure, the distribution of stress and strain in the neck at this stage is obscure. However, experience with controlled cracks made to grow slowly indicates that the material in the neck only undergoes a very small increment of total strain during this period, so that the spring of the testing machine cannot relax much, and the applied load is probably sensibly constant during this period in a normal test. The stress on the uncracked material ahead of the fracture is thus rising during its lateral spread. Also, metallographic examination of the crack shows that it is wide in the centre and narrow at the tip, so that it is an internal notch whose effect must become progressively more severe as it approaches the surface. No theoretical solution of this problem for a cylindrical specimen is possible at present; the most one can do, as Zener (1948) has suggested, is to use known solutions in analogous plane strain problems as a guide in interpreting observations.

Consider, then, the case of a sheet specimen in plane strain containing a prismatic crack whose tip is approximately wedge-shaped. The incipient zone of deformation is the region of maximum stress ahead of the crack bounded by two planes passing through its edge and intersecting the free surface at 45° (fig. 1). When the specimen is stressed in tension, plastic deformation is initially confined to shearing along these planes of maximum shear stress. If the crack propagates toward the surface,

finite plastic deformation can occur without large discontinuities in displacement, as is shown in fig. 2. At any instant deformation is taking place only along planes OA, OB, O′A′, O′B′; the material which has already undergone deformation is contained within the shaded regions, having suffered a shear the magnitude of which is a function of the angle at the tip of the crack. The two ends of the specimen move outwards exerting little constraint on the wedges of material OAB, O′A′B′, which move inwards as rigid bodies. The pattern of flow is, in fact, essentially that described by Hill (1953) for the final stage of separation during the cutting of thin sheets by wedge-shaped tools.

Fig. 1

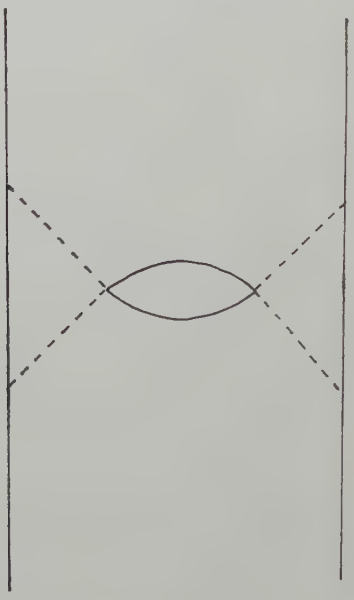

In the case of a cylindrical specimen containing a lens-shaped crack the deformation must be more complex than this, because the surfaces of maximum shear stress are cones, not planes, and the region bounded by them is a ring. In order to allow local shear deformation some plastic flow must take place within this ring to allow it to contract. However, deformation in the region is constrained by the material outside it, so that yielding develops radial and circumferential stresses in addition to the axial tension. Nevertheless, these diminish in intensity as the crack approaches the surface, and it seems reasonable to suppose that the crack initiates narrow zones of shear when it attains some critical size.

We now have to consider the actual process of separation. The usual hypothesis is that put forward by Zener (1948) that, at the high strain rate prevailing, adiabatic heating reduces the slope of the stress–strain curve of the material in the neighbourhood of the crack to a negative

value. The resulting instability localizes the shear strain to such an extent that the two halves of the specimen slip off along a shear surface. The main difficulty in accepting this explanation is that bodies in contact along conical surfaces cannot slide rigidly on each other; complete slipping off would require considerable plastic distortions outside the shear zone which are not, in fact, observed.

Fig. 2

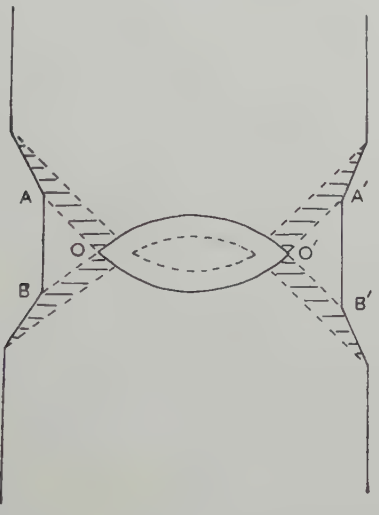

Direct observation of the actual process is hampered by the fact that the fracture is normally very fast in this stage and difficult to control. However, one occasionally finds a fractured specimen in which can be observed the zone of shear complementary to that along which the separation has occurred (that this complementary zone is not usually found is no doubt because a real crack is rarely ideally symmetrical). Figure 3 (*a*) (Pl. 101) shows such a specimen of copper sectioned and polished to reveal the inclusion holes, fig. 3 (*b*) (Pl. 101) the same section etched to show the grain flow. The local shear is clearly visible and is about 20°; along the shear zone the inclusion holes, which have been considerably elongated along the tensile axis by the previous deformation, have been reoriented. Such a reorientation, effectively producing a number of cracks inclined to the direction of the maximum principal tensile stress, must result in a considerable local magnification both of tensile and shear stresses, so that the zone represents a preferential path for the main fracture. It seems likely, in fact, that the final process of separation along the cone is essentially a tensile failure requiring little deformation elsewhere to accommodate it.

I suggest, therefore, that it is unnecessary to invoke adiabatic heating to explain the shear component of ductile fracture; as soon as the crack

grows to a sufficient size and sharpness to initiate far reaching zones of localized shear it will tend to follow them. In the absence of a detailed analysis of the strain around the growing crack it is impossible to make any quantitative estimate of 'sufficient size', but qualitatively, the simplest hypothesis is that localized shear is initiated when the shear stress ahead of the crack attains a critical value. If so, one might expect that by using a very hard machine so that the crack grows slowly under decreasing load, maintaining a constant stress on the uncracked material around it, the shear cone could be eliminated. I have, in fact, found that it is possible to do this; a specimen of ductile Armco iron tested in such a way broke with a tensile fracture right across the minimum section of the neck, while the same material in a normal test developed ordinary cup-and-cone fracture.

Acknowledgment

I wish to thank Mr. A. P. Green and Professor R. King for valuable discussions on this subject.

References

Hill, R., 1953, *J. Mech. phys. Solids*, **1**, 265.
Zener, C., 1948, *Fracturing of Metals* (American Society of Metals), p. 3.

REVIEWS OF BOOKS

The Electric Arc. By J. M. Somerville. (London: Methuen & Co. Ltd., 1960.) [Pp. ix+150.] 12*s.* 6*d.*

The electric arc is one of the most common forms of electrical discharge. It can be regarded as the final phase of the transition from a state of insulation of a gas to that of conduction, the initial state being the electrical breakdown process which is followed by the, possibly transitory, glow discharge. Whether in a useful application, as in a mercury arc rectifier, or, in its undesirable aspects, when it occurs in electrical contacts, the arc is of interest to physicists and electrical engineers alike. Investigation of the mechanism of operation of an arc discharge must range over a variety of interesting branches of physics involving the evaporation of metals, thermionic and cold electron emission from metals, ionization of atoms, and the diffusion and recombination of ions in gases and vapours. A modern book on the subject is therefore to be welcomed. This monograph *The Electric Arc* by Professor Somerville is for the non-specialist, and aims to give a concise account of arc phenomena and to make clear the basic physical processes. It can be said at once that it succeeds in this aim and can be recommended to students.

The subject matter is confined to basic physical processes; discussion of numerous practical applications of interest to the electrical engineer is omitted. The treatment is in two parts: Part I, of 87 pages, on the stable arc is equally divided between a treatment of the long luminous column and electrode effects; while Part II, of 34 pages, on the approach to the stable arc, mainly deals with the formation of the spark channel, its early development and expansion, electrode phenomena in sparks, and ends with a brief qualitative summary of the glow to arc transition, the very short arc, the vacuum arc and the drawn arc. However, copious references are given to enable the interested reader to pursue further these aspects of the subject. Thus, the main treatment of the arc is to be found in Part I and the reader will find this a very helpful introduction to an account of the phenomena and basic physics of the steady state arc column. F. LL. J.

Fast Neutron Physics. Part I, Techniques. Edited by J. B. Marion and J. L. Fowler. (New York: Interscience Publishers, 1960.) [Pp. 983.] £10 18*s.*

Fast neutron measurements are among the most difficult facing the nuclear physicist. However, because of their obvious connection with nuclear weapons much effort has been expended upon them both during and since the last war. The development of reactors in which fast neutrons play an important part has also intensified the practical interest in such measurements. Their importance as a tool for studying basic nuclear structure is also very great since fast neutrons interact only through the nuclear forces uncomplicated by the electrostatic forces.

This book records in practical and useful form the accumulated technical experience of over 30 experts in the fast neutron field. It is interesting that in general the old techniques have been refined and that there has been no dramatic 'break through' in method. A second volume will review experiments and theory. In this volume neutron sources of all types, recoil detection methods and detection by neutron-induced methods are the subject of many individual contributions. In addition many special problems receive individual treatment

such as shielding, target preparation, radiation hazards and computing techniques associated with fast neutron measurements. In spite of the large number of individual contributors the overall style and method of presentation is remarkably uniform. Although the theoretical background to the various techniques receives adequate treatment, most of the material is severely practical making it a handbook in the literal sense of the term. It is thus most regrettable that the price will prevent it reaching many research workers' shelves. E. B. P.

Irreducible Tensorial Sets. Vol. 4, Pure and Applied Physics. By U. Fano and G. Racah. (New York : Academic Press Inc., 1959.) [Pp. vii+171.] $ 6.80.

The kind of group theory which is applied to physics is seldom more than organized common sense. Of recent years, however, advances have been made in several branches of physical theory which have been greatly helped by mathematical techniques, of which it can be said that the organization of common sense is of such a high order than it can well be dignified by the name of group theory. These techniques, originally developed for the study of atomic spectroscopy, have found applications in nuclear theory and solid state physics as well, and are likely to be increasingly useful in the future as theoretical physicists become familiar with them.

Whenever the behaviour of a physical system is invariant under the operation of transformations which form a group (e.g. rotations about the nucleus in the case of the electrons in an atom), the various physical characteristics of the system can be classified in terms of the *representations* of the group. That is to say, they fall into sets of quantities (irreducible tensorial sets) which transform according to standard patterns. Physical calculations involving algebraic manipulations of these quantities are made much easier if they can be related to standard prototypes. When they involve the products of three or more quantities, the saving in labour and the gain in physical insight can be considerable. This is the basic task of the book. The methods as developed are specifically applied to the group of rotations in three dimensions, but they are in fact quite general. The chapters are short and each is easily digested, so that a difficult and abstract subject is made easy to assimilate. These methods have been steadily gaining in importance, and this systematic exposition of them is welcome. M. H. L. P.

[*The Editors do not hold themselves responsible for the views expressed by their correspondents.*]

Fig. 1

Substructure in 70/30 brass annealed for 20 min at 550°c.

Fig. 13

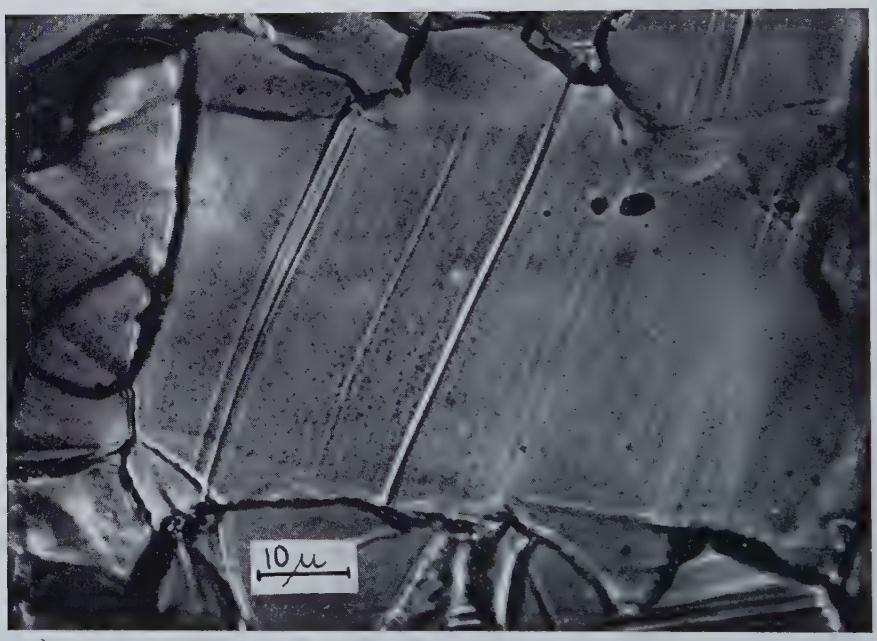

Transgranular slip bands developed during creep at 500°c at a stress of 500 kg/cm² in 70/30 brass. The specimen was examined after the initial extension had taken place, re-electropolished, and returned to the furnace. Bands were not observed after the initial extension. The immediate extension on re-loading was very small.

Fig. 2

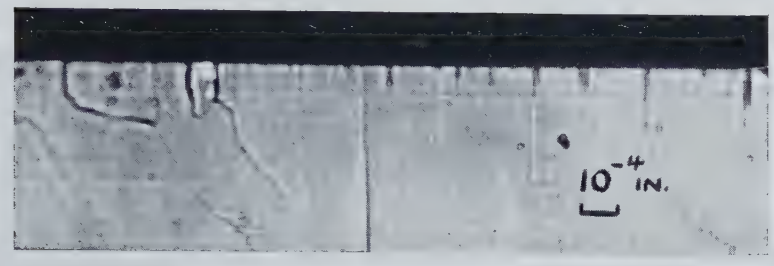

(*a*)

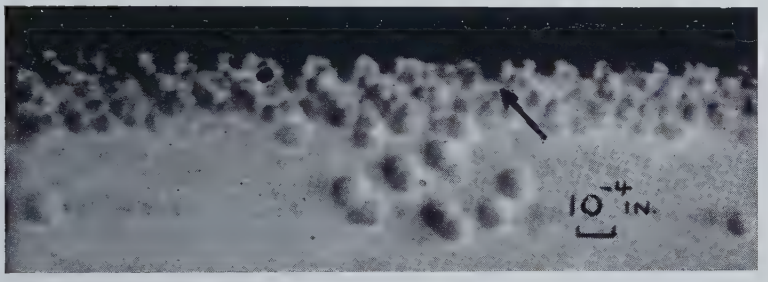

(*b*)

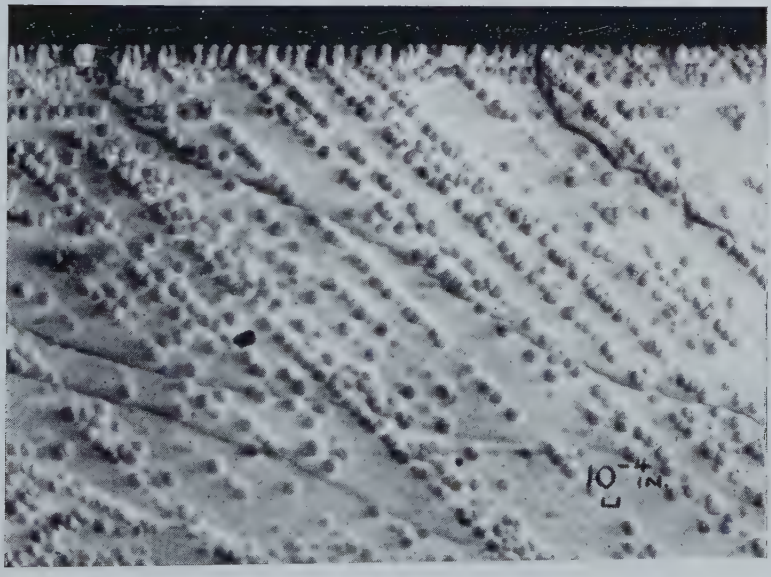

(*c*)

(*a*) Crystal edge prior to etching; (*b*) crystal edge after etching showing typical micro-cracks; (*c*) development of slip after stressing.

Fig. 3

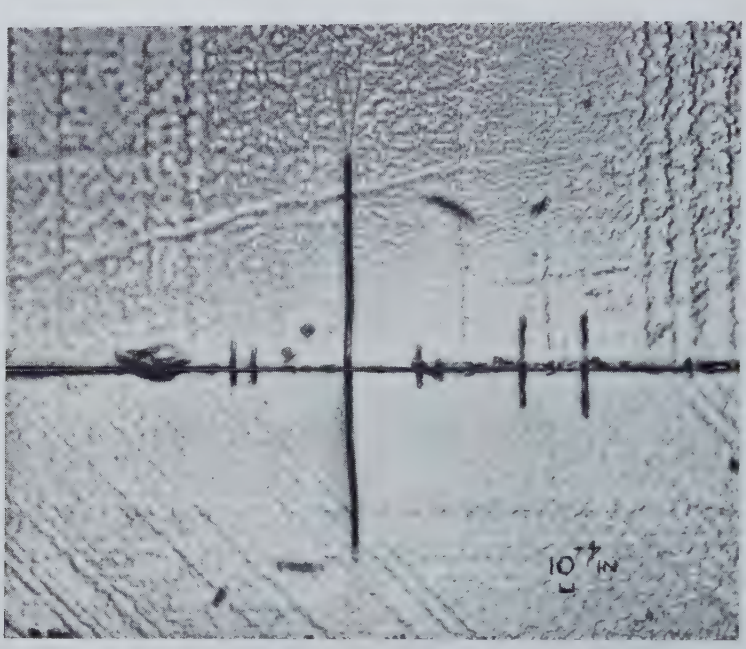

(*a*)

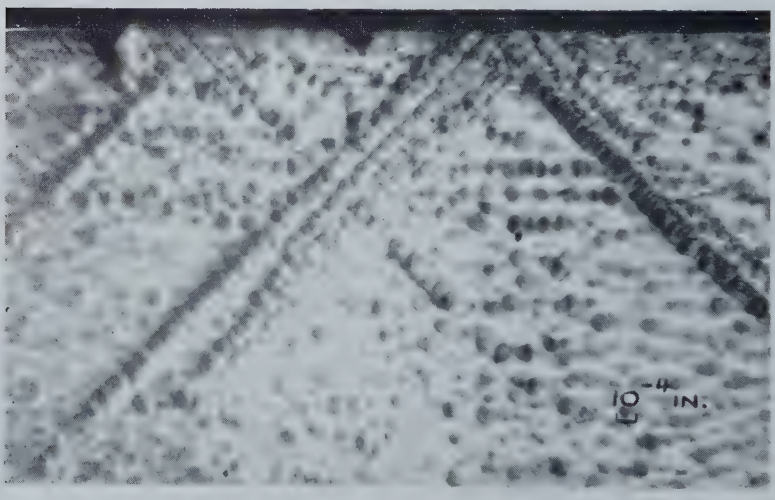

(*b*)

(*a*) Two adjacent faces are laid out flat to show the development of a micro-crack. All cracks are continuous—any appearance that this is not true is due to slightly different magnifications of the two photographs; (*b*) early stage in the development of orthogonal slip originating at a number of edge micro-cracks.

Fig. 4

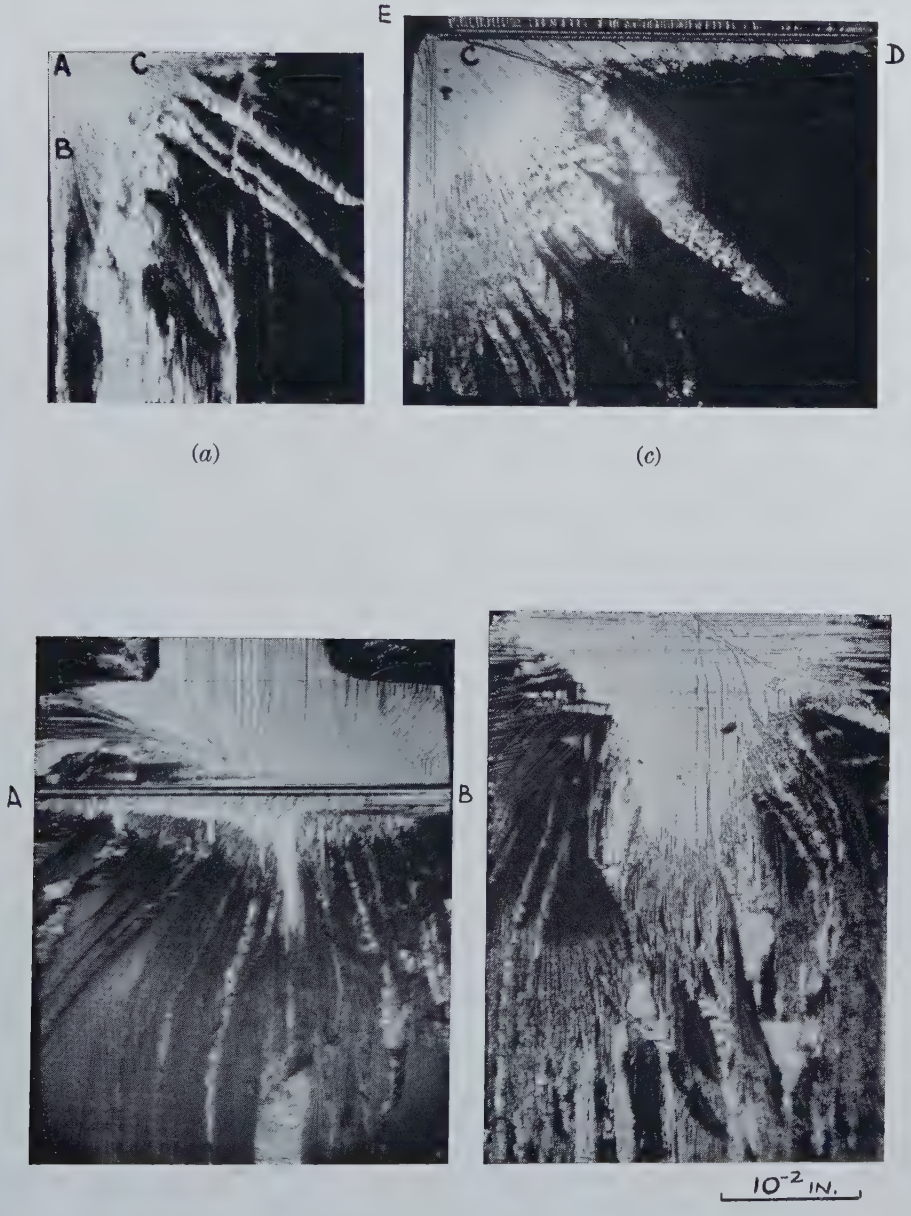

(*a*) (*c*)

(*b*) (*d*)

Various characteristic fracture faces.

(*a*) Corner originating fracture; (*b*) line originating fracture; (*c*) corner+line originating fracture; (*d*) fracture originating at a point on a face away from the edge.

Fig. 5

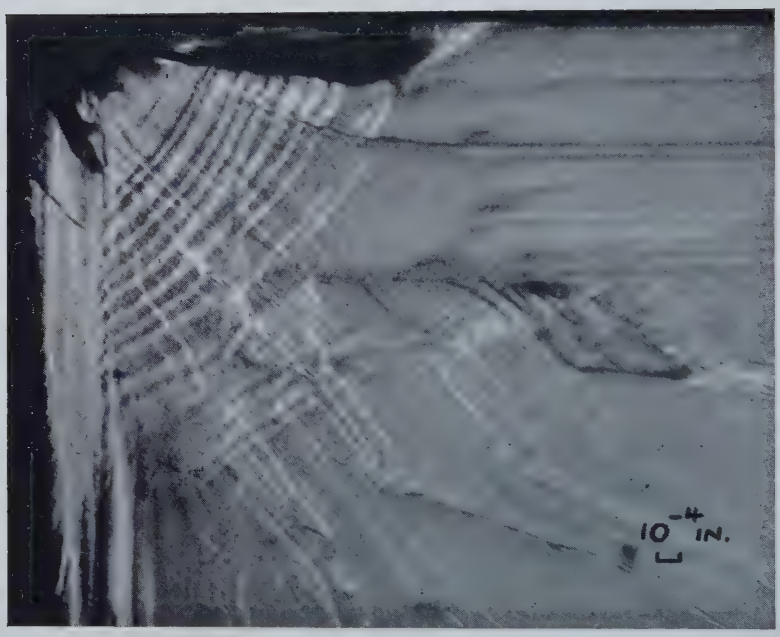

Slip configuration revealed by etching at the extreme corner (e.g. A in fig 4 (*a*)) of a crystal with fracture characteristics similar to fig. 4 (*a*).

Fig. 6

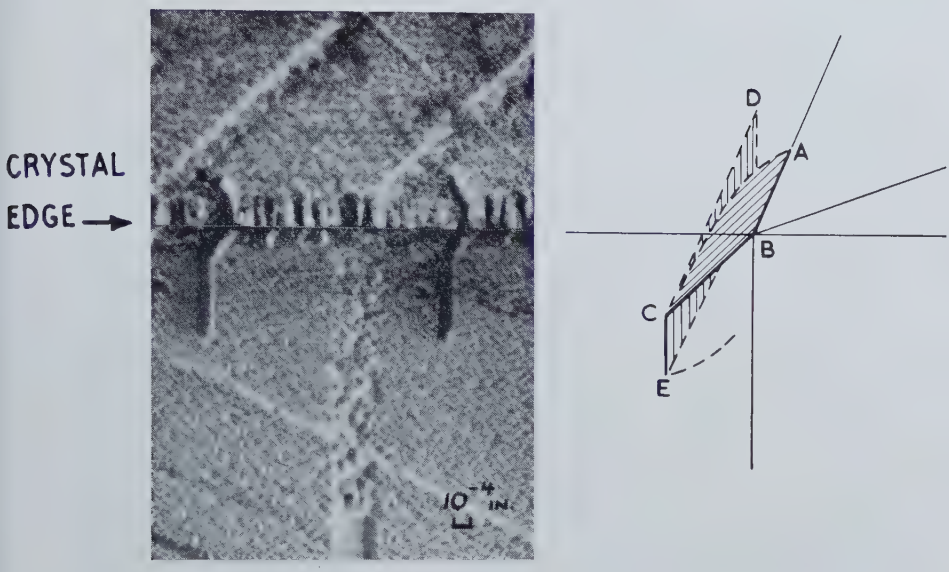

The photograph comprises those of two adjacent faces laid out flat to show the crack configuration. At the side is a schematic representation of the crack.

Fig. 8

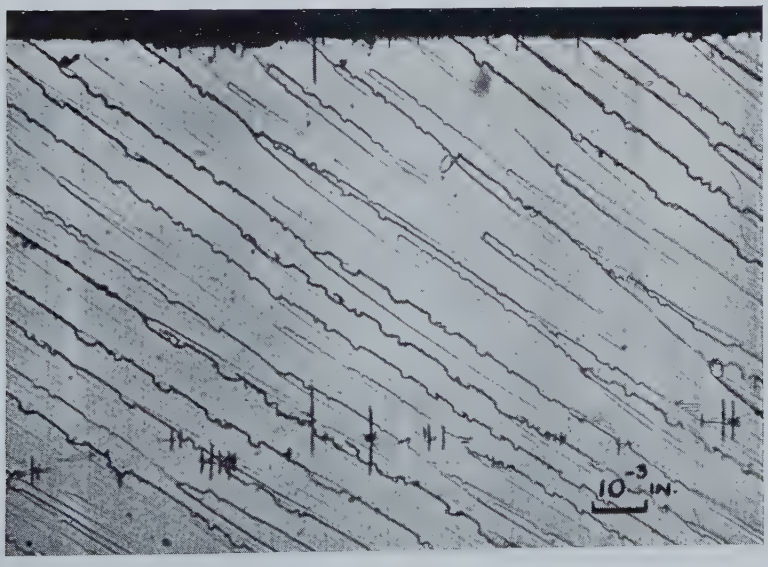

(100) cracks occurring away from crystal edge.

Fig. 1

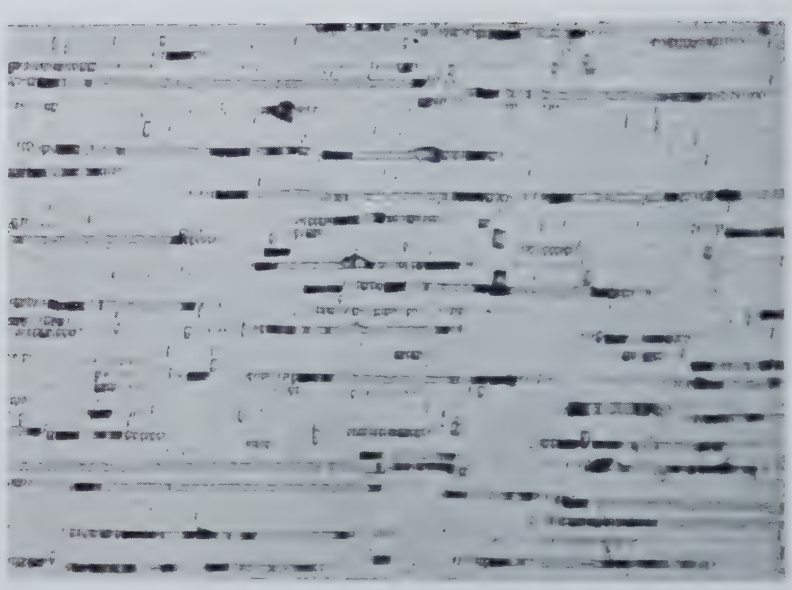

Etching pits on aluminium strained after electropolishing. ×600.

Fig. 2

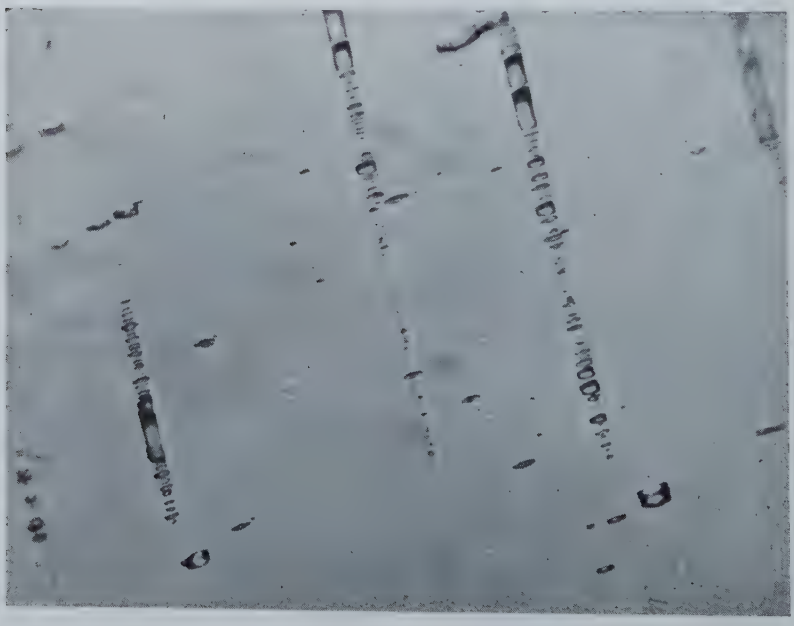

Bunching effect observable on specimen shown in fig. 1. ×1000.

Fig. 3

Pits formed along slip trace making no visible surface step.
Anodic film replica. ×6000.

Fig. 4

Absence of pits on slip trace making large surface step. ×16 000.

Fig. 5

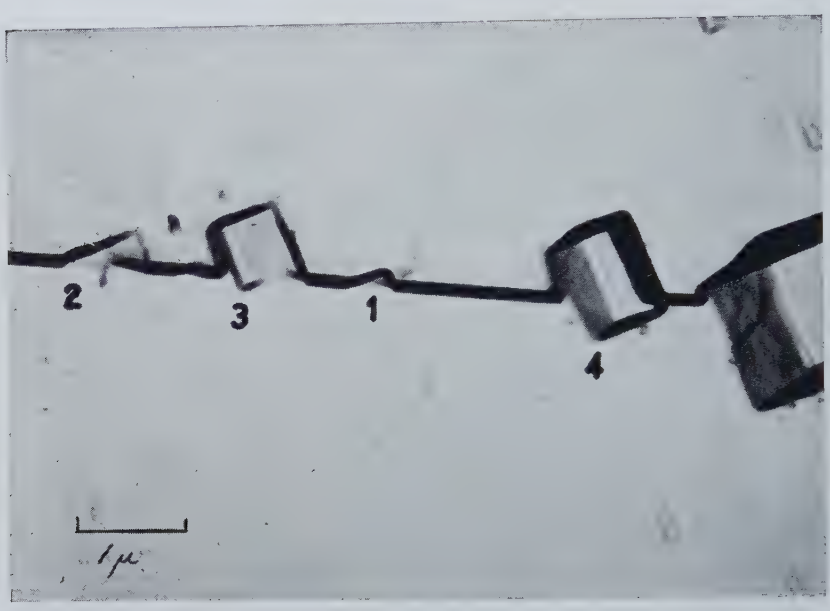

Stages in pit formation at compression slip step making acute angle with surface. × 16 000.

Fig. 6

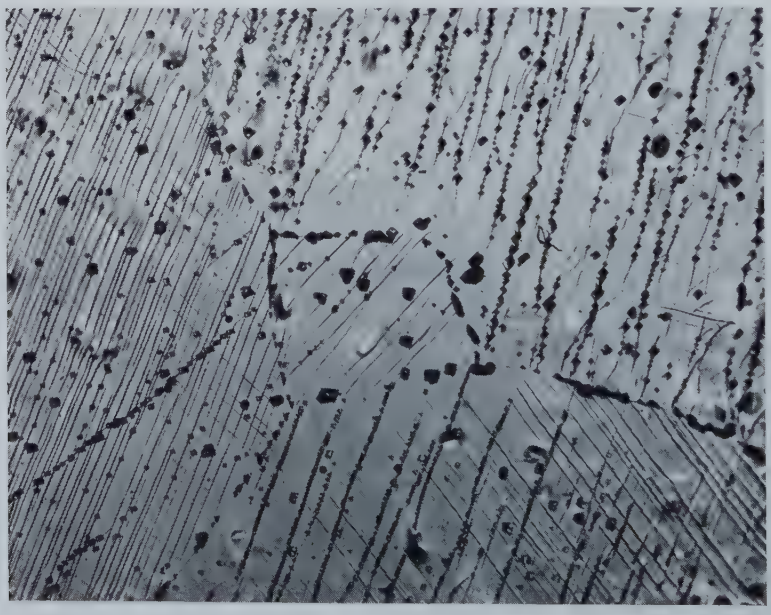

Pitting on both grain boundaries and at slip on specimen aged in vacuum for 32 days. Note that not all slip traces are etched. × 350.

Fig. 7

Cracks formed in heavy anodic film showing that there is no relation between cracks and structure and the manner in which etching pits are formed under the film. ×650.

Fig. 8

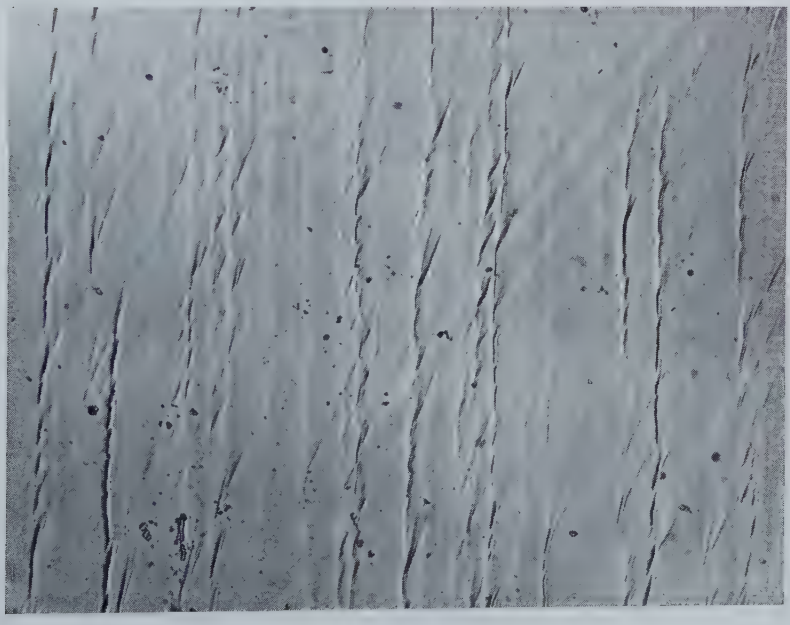

Cracking in thin anodic film showing relation with slip. ×650.

Fig. 9

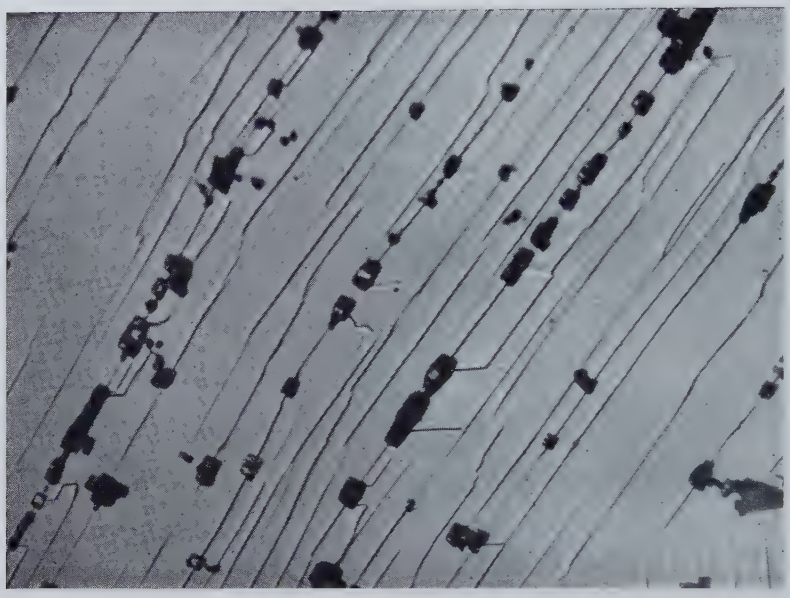

Pits formed by anodic attack in sodium chloride during bending the specimen. ×300.

Fig. 10

Transmission electron micrograph showing pits in thin foil containing many dislocations. ×16 000.

Fig. 11

Small pits in thin foil containing long dislocations roughly in the plane of the foil. ×60 000.

Fig. 12

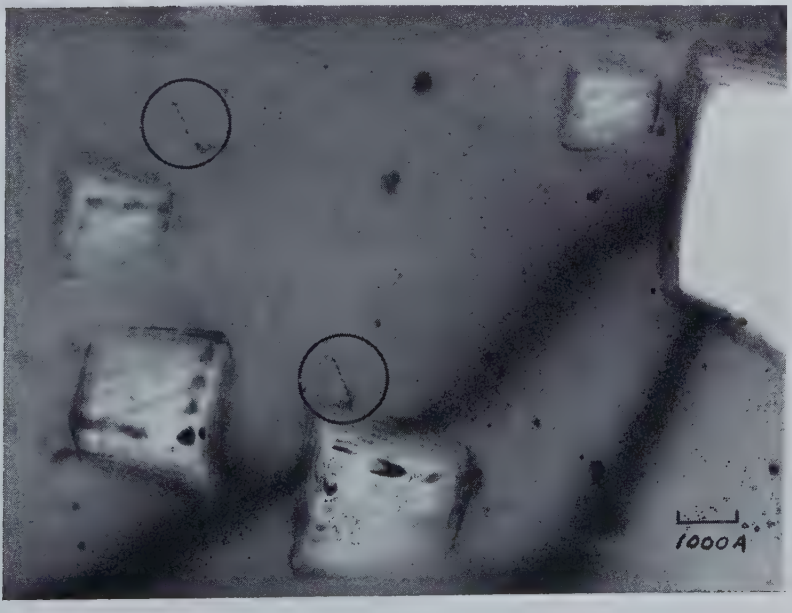

Pits in annealed aluminium showing two dislocations which have not been attacked. ×80 000.

Fig. 13

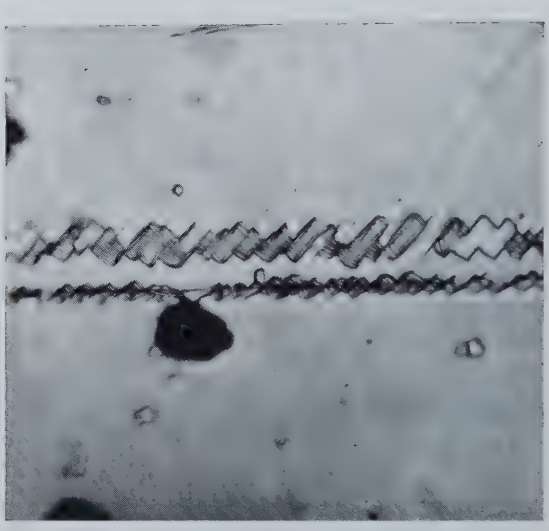

Mode of cracking of light tarnish film on brass. The interference effects are due to lifting of the film. ×2000.

Fig. 1

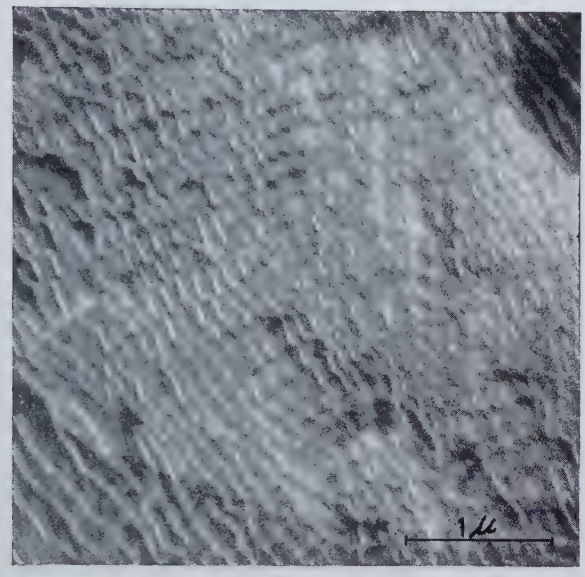

Dark field image of hexagonal network to show the disappearance of one set of lines.

Fig. 2

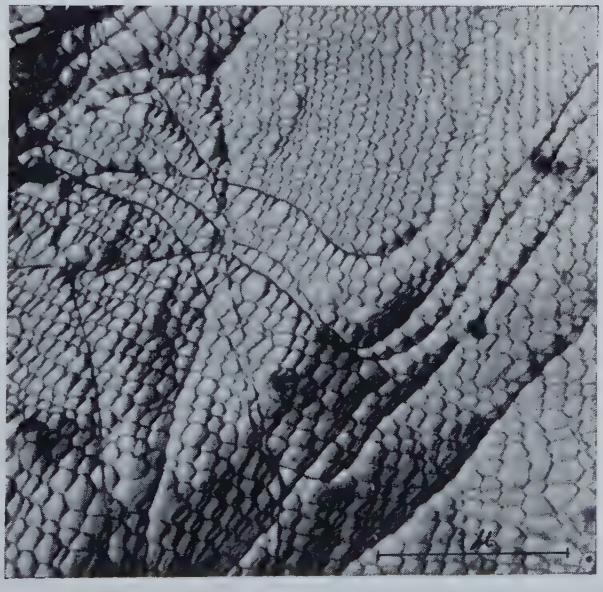

Hexagonal net in the basal plane of bismuth telluride. The net extended over an area equivalent to several times the field shown.

Fig. 7

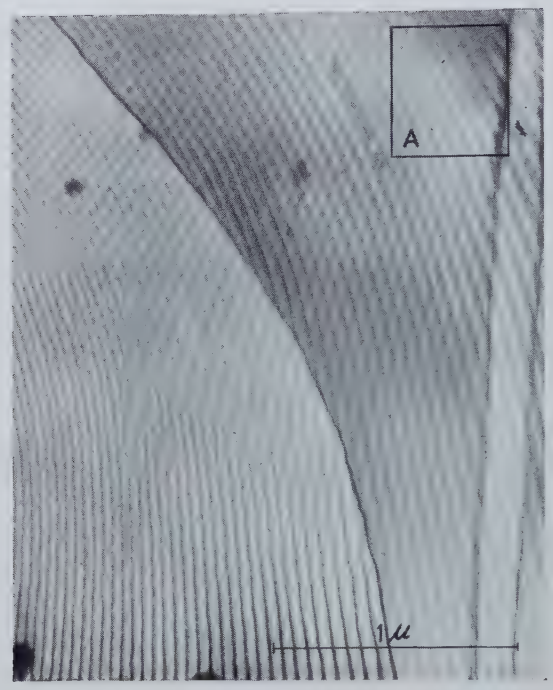

Set of parallel dislocation lines originating from some invisible source far to the left. Note that a number of dislocations have a double contrast in region A, a third line is faintly visible. It is believed that this is also an electron optical effect.

Fig. 8

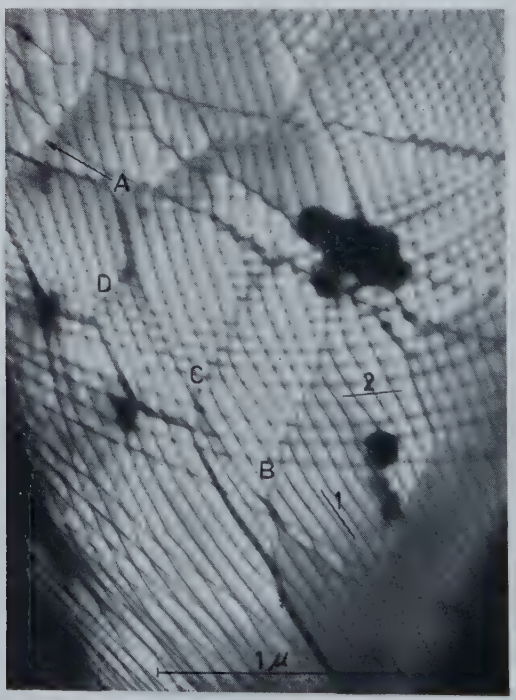

Networks with lozenge-shaped meshes resulting from the crossing of sets (1) and (2). Singular lines A, B, C and D interacted with (2) but not with set (1), and formed a zig-zag line. One family of segments of the zig-zag line lined up with lines of set (2). For detailed explanation see also fig. 18.

Fig. 9

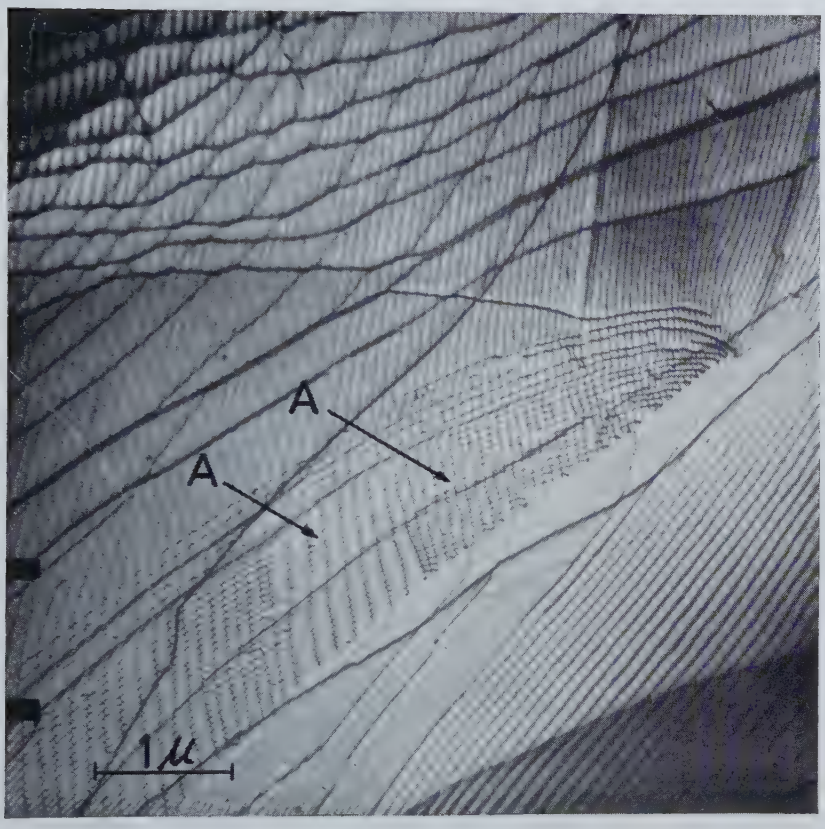

In the central region crossing sets of lines giving rise apparently to a network. Meshes have however not formed, as can be deduced from the absence of certain segments marked A. Segments are also lacking in the parallel set of lines ; the lacking segment left the foil.

Fig. 10

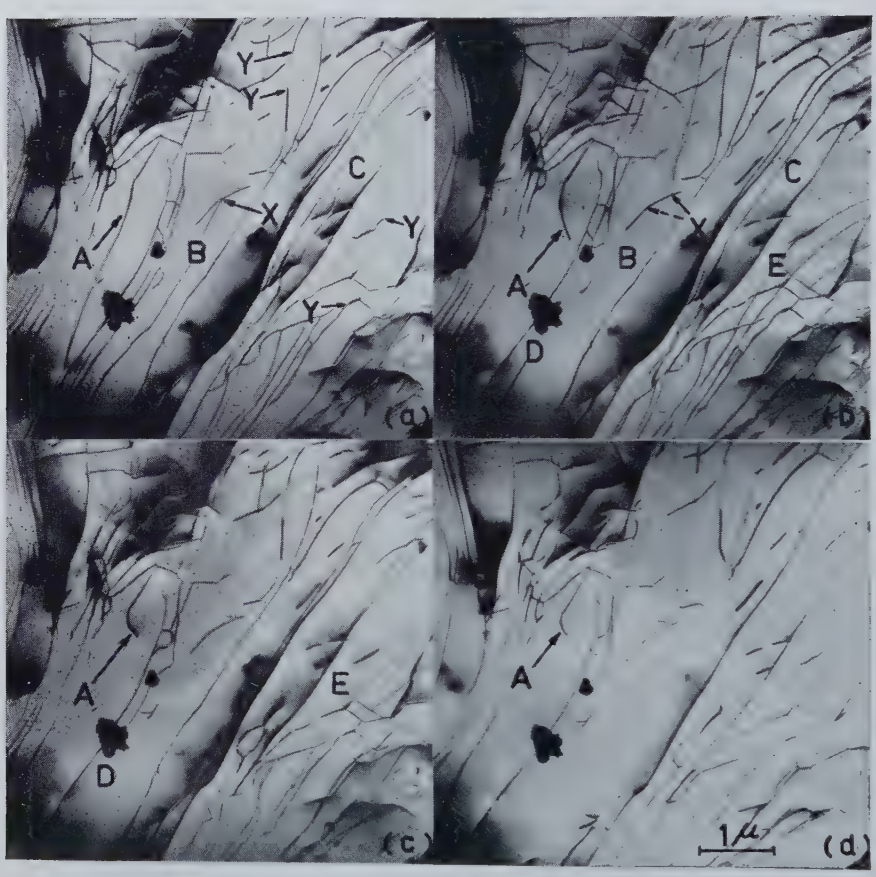

Successive stages in the elimination of dislocations out of the foil. Between exposures (*a*) and (*b*) the lines marked A, B and C disappeared; in further stages A shortens gradually. Between (*b*) and (*c*) the lines marked D and E left the foil. Note also the changing contrast along certain lines; compare with fig. 26.

Fig. 13

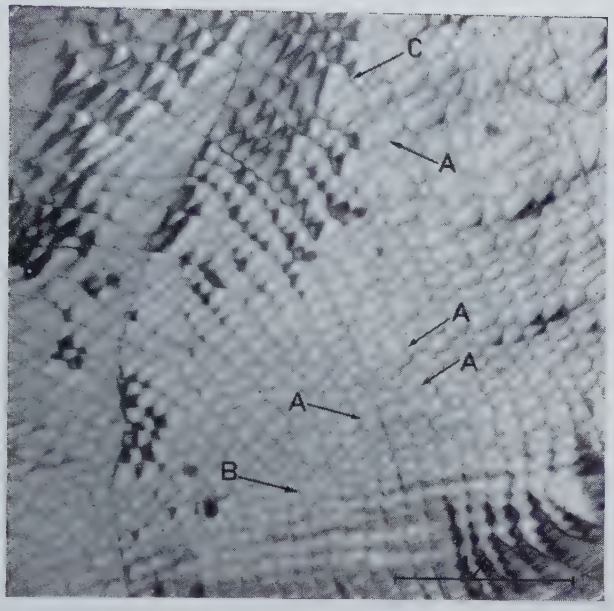

Hexagonal network in the basal plane of bismuth telluride. The dislocations all exhibit a banded contrast. A number of segments left the foil, as shown schematically in fig. 12, and gave rise to ' holes ' in the net. At the spots marked A a single segment left the foil, whilst at the spot B a node left the foil. A more complicated hole is visible in C.

Fig. 14

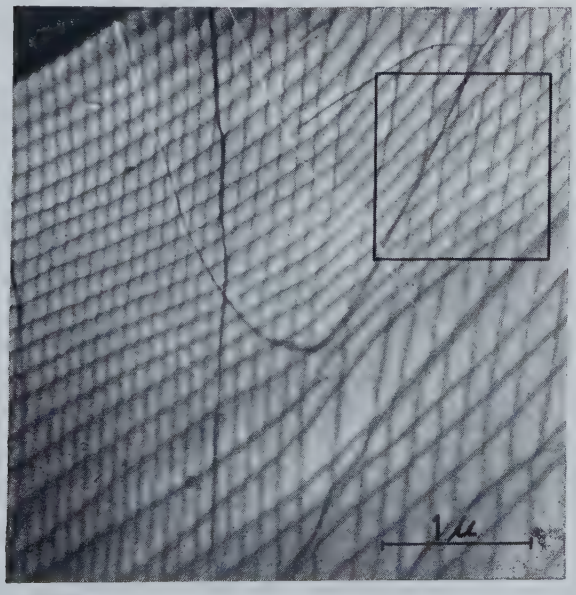

Two crossing sets of lines. Note in the square the asymmetrical twisting of dislocations at the crossing points. In the right bottom corner dislocations are pictured as wide bands resembling stacking-fault ribbons. It was however not possible to decide unambiguously whether splitting into partials really occurs or not.

Fig. 16

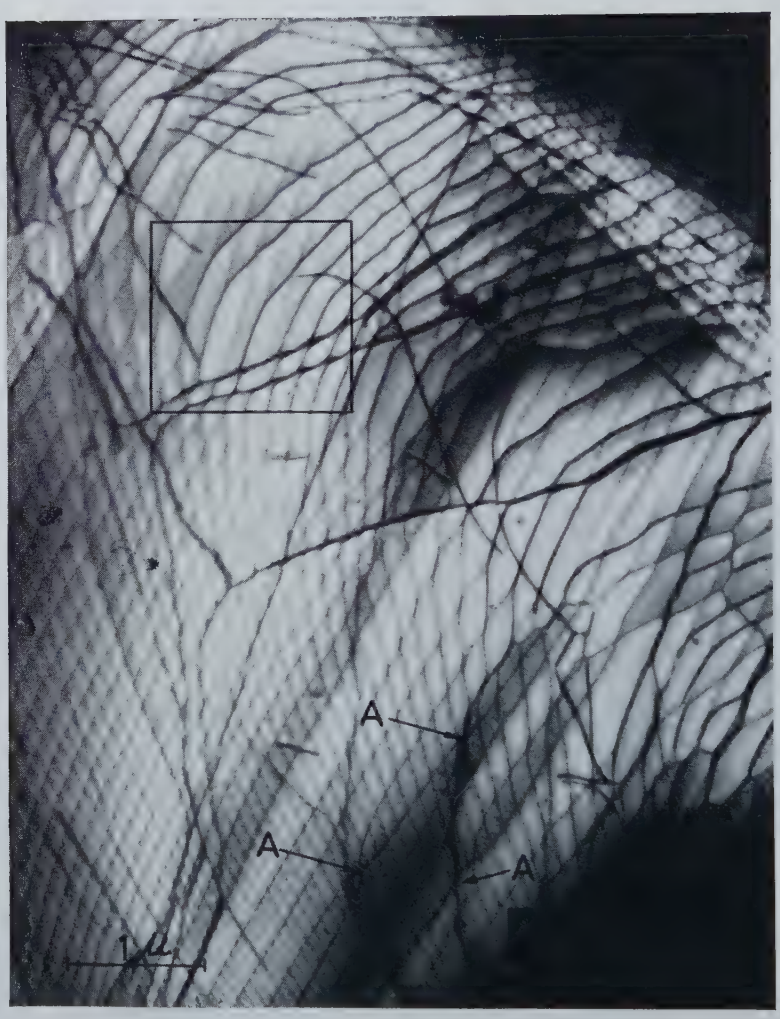

Crossing sets of dislocations showing elastic interactions. At the point marked A twisting at the crossing points is clearly visible. Note also lining up ' one on top of the other ' in the region marked by a square.

Fig. 21

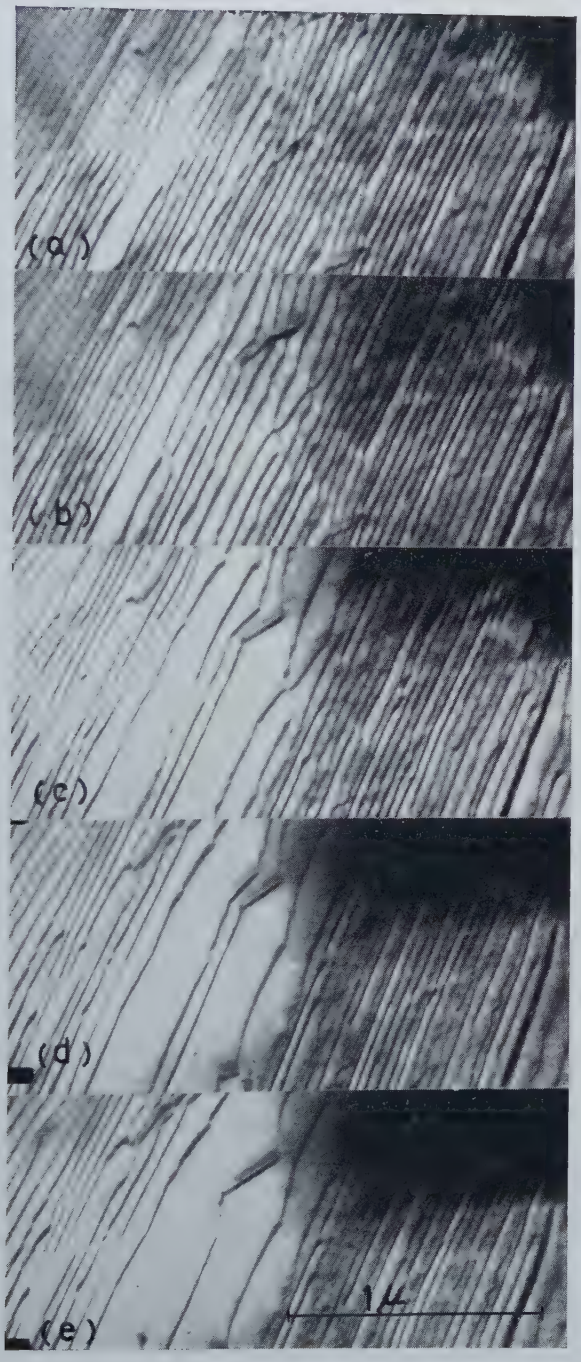

Elimination of dislocation lines by a combination of climb and glide, out of an antimony telluride foil. (*a*) 0 sec ; (*b*) 45 sec ; (*c*) 1 min, 30 sec ; (*d*) 2 min, 30 sec ; (*e*) 4 min.

Fig. 22

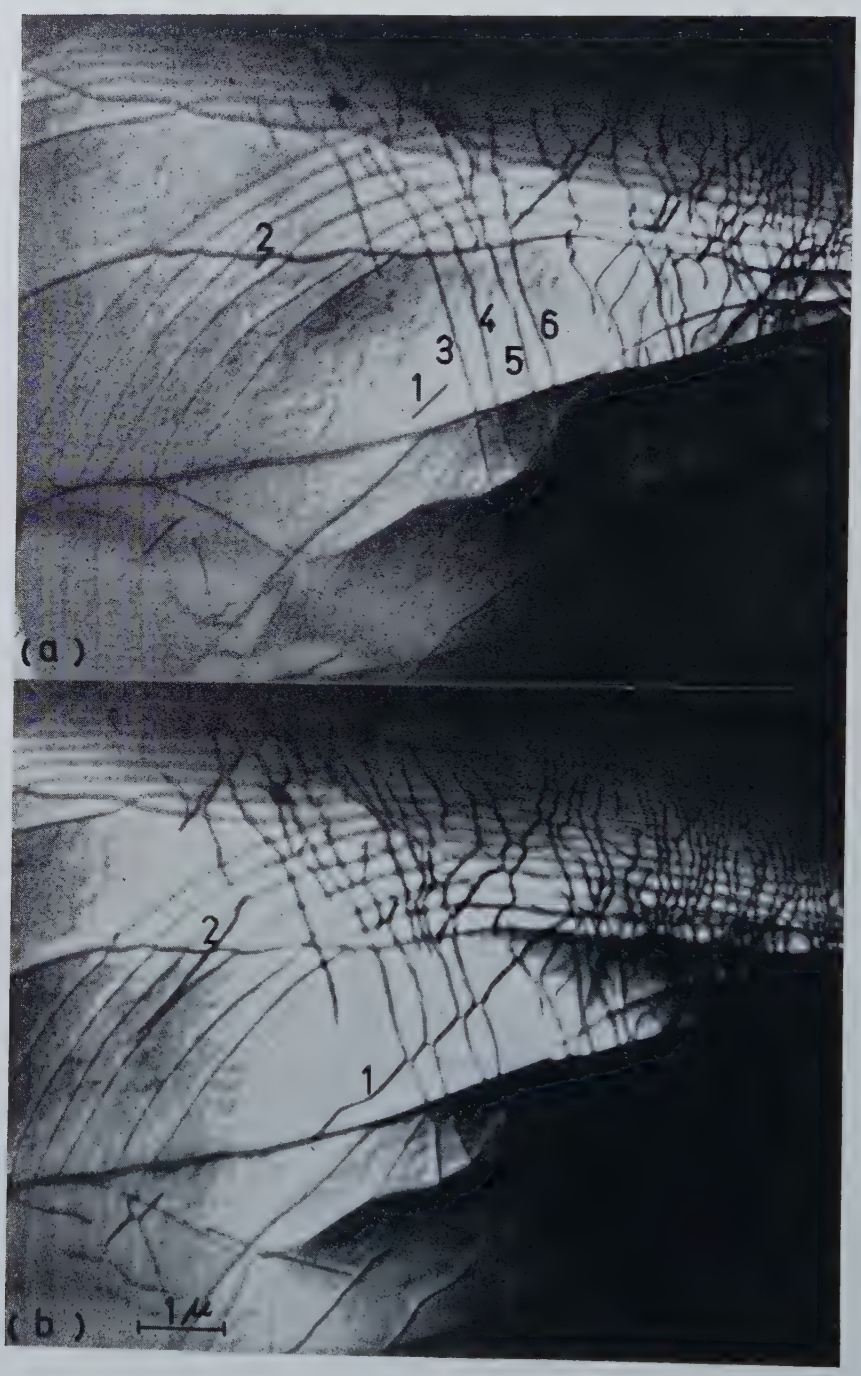

Fig. 22 (*continued*)

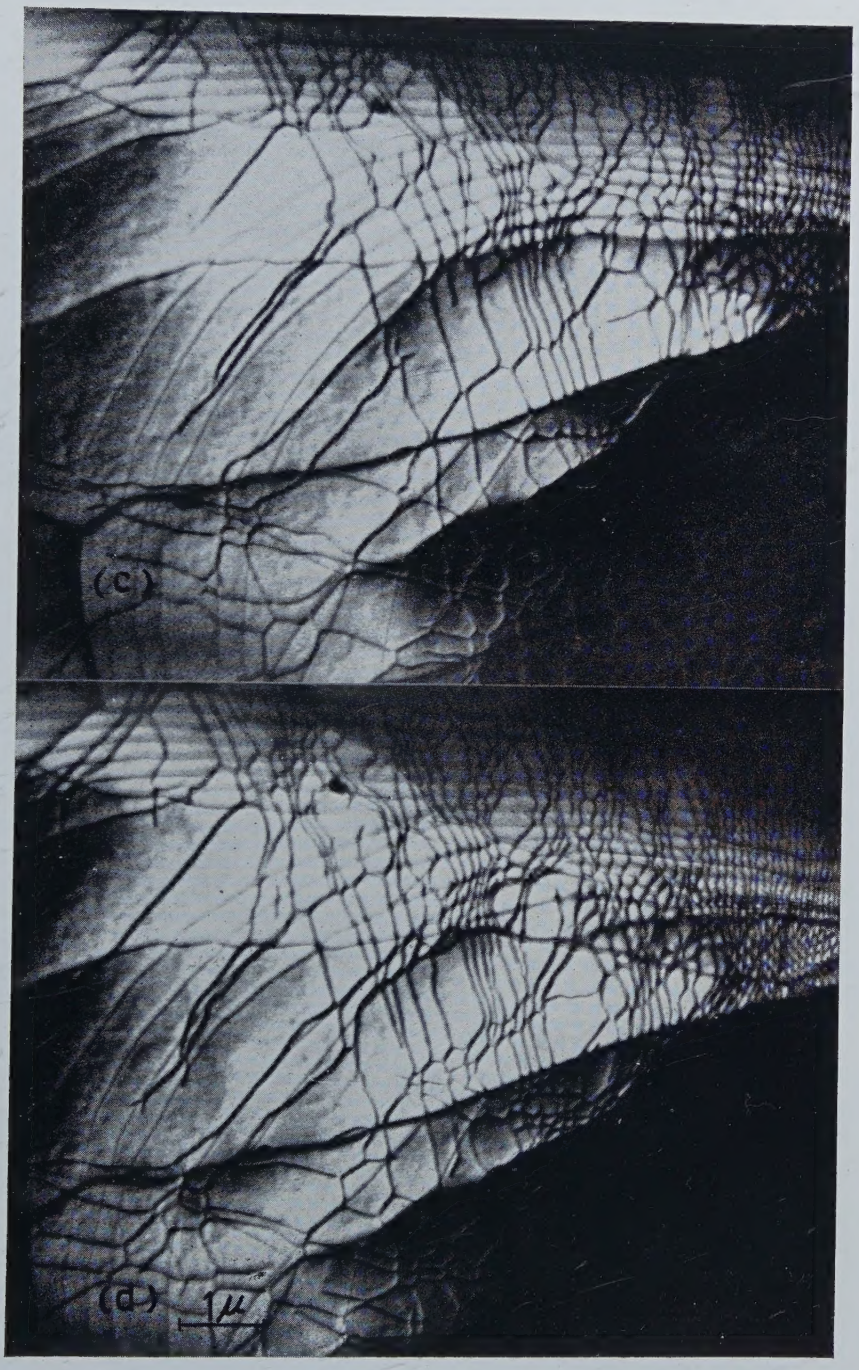

Formation of hexagonal networks in the basal plane of bismuth telluride. Note the lengthening of the segments (1) and (2) between stage (*a*) and (*b*). This results in the intersection of (1) with the set (3), (4), (5) and (6). The same process is repeated and the result is a network as shown in (*d*). In the final stage the whole area was covered with a network as dense as the area shown in the right top part of (*d*). The process is also illustrated schematically in fig. 23.

Fig. 24

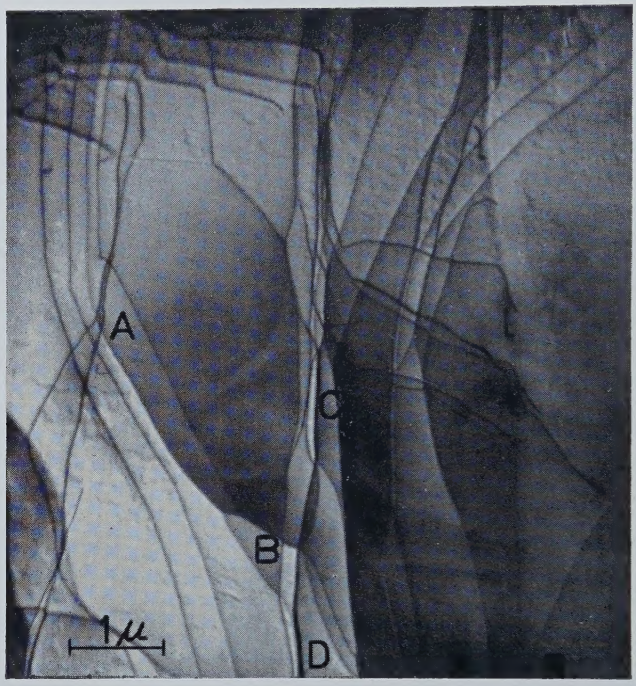

Discontinuous change in contrast at dislocation lines AB and CD. Overlapping regions show a different shade.

Fig. 25

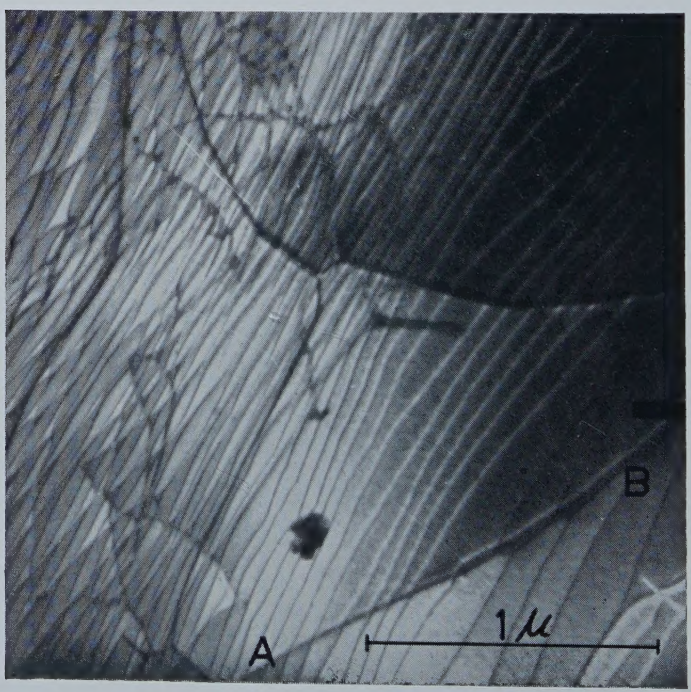

Illustrating contrast effects. Dislocations exhibiting a normal contrast acquire a dark field contrast on intersecting AB. In the left part of the photograph contrast effects similar to those illustrated in fig. 24 are visible.

Fig. 3

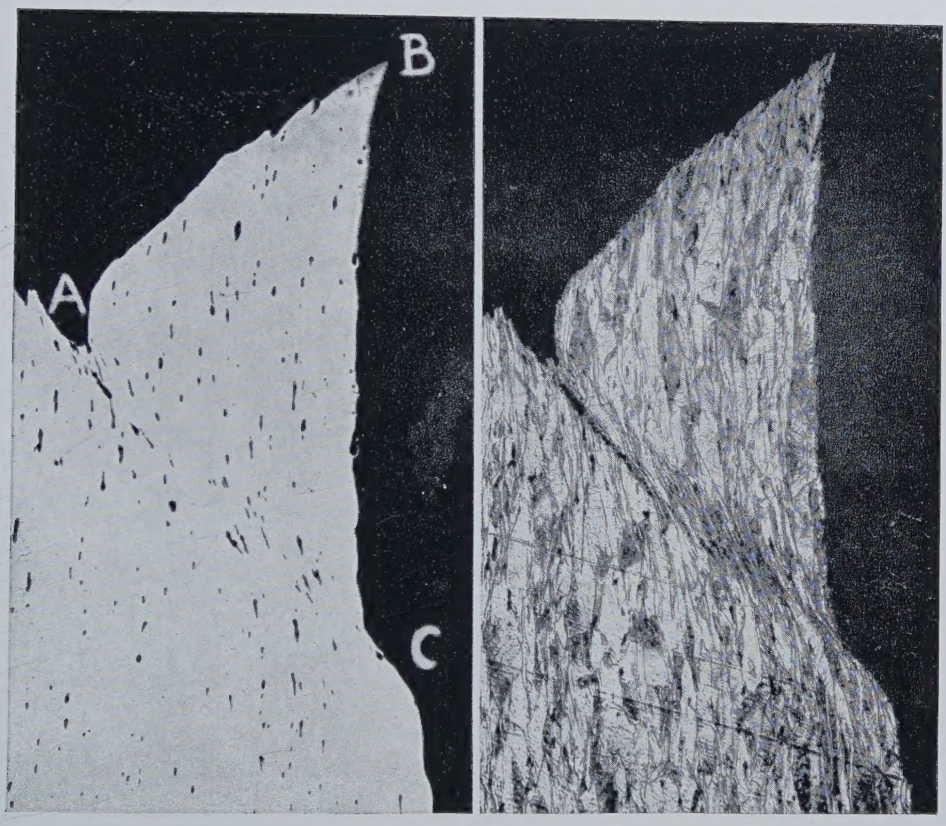

(*a*) (*b*)

Section of broken copper tensile test piece, showing ' cone ' fracture surface AB and complementary narrow zone of shear AC. Notice the surface step formed by the shear at C. ×70. (*a*) Polished, showing re-orientation of inclusion holes. (*b*) Etched, showing grain flow.